UNIVERSITY OF CALIFORNIA, SAN DIEGO

Topological States in Condensed Matter and Cold Atom Systems

A dissertation submitted in partial satisfaction of the
requirements for the degree
Doctor of Philosophy

in

Physics

by

Yi Li

Committee in charge:

Professor Congjun Wu, Chair
Professor Kenneth Intriligator, Co-Chair
Professor Daniel Arovas
Professor Mark Gross
Professor Jorge Hirsch
Professor Dragos Oprea

2013

The dissertation of Yi Li is approved, and it is acceptable in quality and form for publication on microfilm and electronically:

_____

_____

_____

_____

_____
Co-Chair

_____
Chair

University of California, San Diego

2013

DEDICATION

To my parents who cultivated me
with the love of sciences and the spirit of perseverance.

EPIGRAPH

Even if I knew that tomorrow the world would go to pieces,
I would still plant my apple tree.
—Martin Luther

Without proof the program remains incomplete,
but without the imaginative input it never gets started.
—Michael Atiyah

TABLE OF CONTENTS

LIST OF FIGURES

ACKNOWLEDGEMENTS

Firstly, I would like to thank my advisor, Professor Congjun Wu. His vivid understanding of condensed matter physics has fundamentally influenced my physics research and career. His boldness, delicateness and perseverance in the research set up the most important spirit for me to learn and emulate. As a great advisor, Congjun has never tired to carefully explain what to him is immediately obvious and delicate subtleties beyond projects at hand. He devoted immense time and energy patiently teaching and discussing with me. Without his nice guidance and intensive discussions, the work presented in this thesis would not be possible to accomplish. Besides, I would like to thank his great guidance on my career and support on my travels. Benefited from his support and open mind, my horizon has been greatly expanded. Discussions and collaborations with many other leading physicists around further inspired and stimulated my research.

I am grateful to Professor Ken Intriligator who kindly co-advised and guided me along with my difficult initial stage of research at UCSD. Besides devotedly helping me on demystifying many important concepts in high energy physics and mathematics with his graceful, clear and concise understanding, Ken greatly encouraged me on developing my research interests and always patiently helped me. His great encourage and trust on me gave me more confidence in front of difficulties and challenges.

I am also grateful to Professor Arovas, who kindly taught and guided me with his wide range of knowledge and insights in condensed matter and mathematics. From the fully written classroom blackboards a piece of tissue at the dinner, his devoted and fearless exploring spirit makes the discussions with him always learnful and enjoyable. Especially, I learned the importance of details at each step of research from him and Congjun. As greatly stimulated my study at UCSD, I can never forget episodes of him when he walked from his office straight way to the parking lot without eyes moving from the paper at his hands, when he flowing formulas on the whole blackboard with each step clear for first year students, when he humorously pretended a weightlifter with hands full of chalk dust after a devoted discussion session, when he encouraged me with the place to find the best

squirrels at Facebook feeds ...

I am indebt to my other collaborators Professors Jorge Hirsch at UCSD, Yue Yu at ITP of CAS, Shou-Cheng Zhang at Stanford and Xiangfa Zhou at USTC, who kindly guided and collaborated with me in my PhD years as partly presented in this thesis. Chapters 2 grew up from helpful discussions and collaborations with Professor Jorge Hirsch at the early stage. Chapters 2, 3, 5, 6 and 7, in parts, are reprints of the material as they appear in "High-Dimensional Topological Insulators with Quaternionic Analytic Landau Levels", by Yi Li and Congjun Wu, *Phys. Rev. Lett.*, 110, 216802 (2013); "Isotropic Landau levels of Dirac fermions in high dimensions", by Yi Li, Kenneth Intriligator, Yue Yu, and Congjun Wu, *Phys. Rev. B*, 85, 085132 (2012); "2D and 3D topological insulators with isotropic and parity-breaking Landau levels", by Yi Li, Xiangfa Zhou, and Congjun Wu, *Phys. Rev. B*, 85, 125122 (2012); "The J-triplet Cooper pairing with magnetic dipolar interactions", by Yi Li and Congjun Wu, *Scientific Report*, 2, 392 (2012); and "Spin-orbit coupled Fermi liquid theory with magnetic dipolar interaction", Yi Li and Congjun Wu, *Phys. Rev. B*, 85, 205126 (2012), respectively. Chapter 4, in part, has been submitted for publication of the material as it may appear in Physical Review series, "Topological insulators with SU(2) Landau levels" by Yi Li, Shou-Cheng Zhang, and Congjun Wu. The dissertation author was the author of these papers.

Further more, I would like to thank Professors Duncan Haldane, Nai Phuan Ong, Edward Rezayi and Donna Sheng for teaching me many important points for the future development of my reasearch, and many helpful advices and encourage from Professors Yosi Avron, Leon Balents, Andrei Bernevig, Ravindra Bhatt, Suk Bum Chung, Shankar Das Sarma, Xi Dai, Zhong Fang, Eduardo Fradkin , Steven Girvin, John McGreevy, Bertrand Halperin, Kazuki Hasebe, Jason Ho, Taylor Hughes, David Huse, Jainendra Jain, Alex Kitaev, Xiao-Liang Qi, Rahul Roy, Shinsei Ryu, Jay Sau, S. Sondhi, Yu-Peng Wang, Zhen-Han Wang, Zhong Wang, Yong-Shi Wu, Tao Xiang, Cenke Xu, and Kun Yang.

Besides great academic insights and advices that I luckily learned from leading physicists and mathematicians, I really appreciate the encourage and guidance I received at many key points of my life. I sincerely thank Professor Zhi Lu at

math department of Fudan University who is the first person taught me the way of initiating the research, Professor Shou-Cheng Zhang at Stanford University who encouraged me "being brave and pushing yourself" at my worst time, Jorge Hirsch who is the first person said "good job" to me when I started the research at UCSD. Without these precious words I may not luckily survive until now.

Finally, I would like to thank Aris Alexandradinata, Prarit Agarwal, Yang Bo, Meng Cheng, Zhe Fei, Siyuan Gu, Zheng-Cheng Gu, Zhoushen Huang, Hsiang-Hsuan Hung, Chao-Ming Jian, Hongchen Jiang, Hsin-Hua Lai, ChingHua Lee, Mengkun Liu, Da Wang, Jun Xiong, Yi-Jun Yao, Shilin Yu, Dong Zheng and many other friends for stimulating discussions and great help at many key points in my life.

VITA

2013	Doctor of Philosophy in Physics, University of California, San Diego
2012 Fall	Graduate Fellow, KITP at University of California, Santa Barbara
2010 - 2013	Research Assistant, Department of Physics, University of California, San Diego
2009 - 2010	Teaching Assistant, Department of Physics, University of California, San Diego
2009	Master of Sciences in Physics, Fudan University, Shanghai
2006 - 2009	Research Assistant, Department of Physics, Fudan University, Shanghai
2003 - 2006	Bachelor of Sciences in Physics, Fudan University, Shanghai

PUBLICATIONS

Yi Li, Congjun Wu, "High-Dimensional Topological Insulators with Quaternionic Analytic Landau Levels", *Phys. Rev. Lett.*, 110, 216802 (2013).

Yi Li, Congjun Wu, "Spin-orbit coupled Fermi liquid theory with magnetic dipolar interaction", *Phys. Rev. B*, 85, 205126 (2012).

Yi Li, Xiangfa Zhou, Congjun Wu, "2D and 3D topological insulators with isotropic and parity-breaking Landau levels", *Phys. Rev. B*, 85, 125122 (2012).

Yi Li, Kenneth Intriligator, Yue Yu, Congjun Wu, "Isotropic Landau levels of Dirac fermions in high dimensions", *Phys. Rev. B*, 85, 085132 (2012).

Yi Li, Congjun Wu, "The J-triplet Cooper pairing with magnetic dipolar interactions", *Scientific Report*, 2, 392 (2012).

Yue Yu, Yi Li, "Anyons emerging from fermions with conventional 2-body interactions", *J. Phys. A: Math. Theor.*, 43, 105306 (2010).

Yi Li, Tianxing Ma, Ruibao Tao, "Extra current and integer quantum Hall conductance in the spin-orbit coupling system", *Europhys. Lett.*, 83, 27002 (2008).

Yi Li, Ruibao Tao, "Current in a Spin-orbit-coupling system: Generalization of the Noether's theorem", *Phys. Rev. B*, 75, 075319 (2007).

Da Wang, Yi Li, Zi Cai, Congjun Wu, "Competing orders in the 2D half-filled SU(2N) Hubbard model through the pinning field quantum Monte-Carlo simulations", *arXiv:1305.3571*.

Yi Li, Da Wang, Congjun Wu, "Spontaneous time-reversal symmetry breaking in the boundary Majorana flat bands", *arXiv:1304.4268*.

Xiangfa Zhou, Yi Li, Zi Cai, Congjun Wu, "Unconventional states of bosons with synthetic spin-orbit coupling", *arXiv:1301.5403*.

Yi Li, Shou-Cheng Zhang, Congjun Wu, "Topological insulators with SU(2) Landau levels", *arXiv:1208.1562*.

Yi Li, Xiangfa Zhou, Congjun Wu, "3D quaternionic condensation and spin textures with Hopf invariants from synthetic spin-orbit coupling", *arXiv:1205.2162*.

ABSTRACT OF THE DISSERTATION

Topological States in Condensed Matter and Cold Atom Systems

by

Yi Li

Doctor of Philosophy in Physics

University of California, San Diego, 2013

Professor Congjun Wu, Chair
Professor Kenneth Intriligator, Co-Chair

The study of topological states has become a major research focus of contemporary physics. This thesis consists of several investigations on novel states of matter with non-trivial topological properties in both condensed matter and ultra-cold atom systems.

We have systematically generalized Landau levels (LL) from the two dimensions (2D) to 3D and above for both non-relativistic and relativistic fermions. LLs with the full 3D rotation symmetry and flat energy spectra are constructed by coupling fermions to the SU(2) Aharanov-Casher potential. Fermion spins are coupled to orbital motions with a helicity structure, and time-reversal symmetry is maintained. The lowest LL wavefunctions exhibit the quaternionic analyticity as a

generalization of the complex analyticity of the 2D cases. Each LL contributes one branch of gapless helical Dirac modes to the surface spectra. The elegant analytic properties together with the flat energy spectra are expected to facilitate future studies of high dimensional fractional topological states. LLs in the Landau-like gauge are also constructed in high dimensions, which exhibit spatial separations of 2D helical Dirac modes with opposite helicities or 3D Weyl modes with opposite chiralities. As a square root problem of the non-relativistic cases, LLs of Dirac electrons are constructed in 3D and above. The zeroth LL states are a branch of half-fermion Jackiw-Rebbi modes. We have also found parity breaking LL quantizations in harmonic traps in the presence of strong spin-orbit(SO) couplings.

We have studied topological properties in fermion systems with magnetic dipolar interactions. Different from electric dipoles which are classic vectors, atomic magnetic dipoles are quantum-like. Magnetic dipolar interactions are isotropic under simultaneous SO rotations. This feature gives rise to a novel p-wave spin triplet pairing symmetry with the total angular momentum $J = 1$ of the Cooper pair. Such a state is fundamentally different from both ^{3}He A and B-phases and exhibits Weyl type Bogoliubov excitations. In Fermi liquid theory, there exists a novel SO coupled zero-sound-like collective mode exhibiting non-trivial spin configurations over the Fermi surface.

Chapter 1

Introduction

1.1 Historical background

The mathematical concept of topology has played an essential role in modern physics. Topological properties are robust and invariant under continuous deformations, and thus are insensitive to the detailed system structures. The first application of topology in physics was by Lord Kelvin. He proposed that different types of atoms correspond to various knot patterns of ether and the chemical stability of atoms arises from the topological stability. Even though this knot theory of atoms turned out to be incorrect, the idea of exploring the topological stability of matter is ingenious and has ever-lasting impacts in modern physics.

In modern condensed matter physics, topological states and the associated topological invariant can be exhibited as various exotic observable phenomena. For example, quantized vortices in superfluids and superconductors are characterized by the winding number. Such an integer-valued topological invariant describes the number of times of the $U(1)$ superfluid phase winding around the real space S^1 circle enclosing the vortex core [1]. In the context of p-wave spin triplet pairing superfluids, such as ^{3}He-A and B phases [2], topological analysis has been widely used to classify various spin textures and superfluid phase vortices [3]. Furthermore, the concept of topological phase transition was developed. The celebrated example is the Kosterlitz-Thouless (KT) transitions for 2D systems with the $U(1)$ symmetry [4]. The novelty of the KT transition is that it does not fit the cele-

brated Landau-Ginzburg formalism. It is not triggered by spontaneous symmetry breaking but arises from the proliferation of topological defects of vortices and anti-vortices.

For the quantum electronic states, the 2D integer quantum Hall (QH) effect [5, 6] is among the earliest examples of states of matter characterized by topology rather than symmetry [7, 8]. It arises from the Landau level (LL) quantization of electron cyclotron motion in external magnetic fields. Their magnetic band structures possess topological Chern numbers defined in time-reversal (TR) symmetry breaking systems [7, 9, 10, 11, 12]. Near the edges of samples, gapless chiral edge modes arise which are responsible for the quantized charge transport [13, 14], a result from the chirality of Landau level wave functions.

Later on, as firstly pointed out by Haldane, LL quantization is not necessary for the integer quantum Hall effect [8]. The essential point is the non-trivial topology of band structures, which can even be achieved in Bloch wave functions in lattices with translation symmetry. The underlying topological quantization of Hall conductance is the Berry phase structure in the 2D Brillouin zone. The value of Chern number is just the number of the fictitious magnetic monoples enclosed by the Brillouin zone which has the geometry of a torus in momentum space. Such a Chern number can only be non-zero in time-reversal (TR) symmetry breaking systems, such as the celebrated Haldane's quantum anomalous Hall effect model defined in honeycomb lattice with complex valued next-nearest-neighbor hoppings [8].

The TR invariant generalization of Haldane honeycomb model gives rise to the Kane-Mele model of 2D topological insulators (TIs). Although the Chern number of the Kane-Mele model is zero, due to the property of $T^2 = -1$ for TR transformation of fermions, their band structures are characterized by the $\mathbb{Z}_2$-index. This $\mathbb{Z}_2$ topology was generalized into 3D TR invariant systems [15, 16, 17, 18, 19, 20, 21, 22, 23, 24, 25, 26]. Such an index is stable against TR invariant perturbations. On open boundaries, they exhibit odd numbers of gapless helical edge modes in 2D systems and surface Dirac modes in 3D systems. Current studies of TR invariant topological insulators (TIs) have made great success in both 2D and 3D. TIs have been experimentally observed through transport experiments

[27, 28, 29] and spectroscopic measurements [30, 31, 32, 33, 34, 35, 36].

So far, most of the current study of 3D TIs have been focused on systems with crystal lattice structures whose energy spectra are dispersive and Bloch wave functions are complicated. In comparison, Landau level (LL) wave functions are based on harmonic oscillator wave functions, which are simple and explicit. Furthermore, the LL energy spectra are flat such that interaction effects are non-perturbative. In the lowest Landau levels (LLL), wave functions exhibit the elegant complex analyticity. These two features have stimulated the study of fractional quantum Hall effect (FQHE), in particular, in constructing the Laughlin wavefunction and the study of fractional statistics of quasi-particles [37, 38]. However, LLs crucially rely on the 2D geometry, and it is not obvious how to generalize to high dimensions straightforwardly. In this thesis, we will provide a systematic construction of high dimensional LLs for both non-relativistic and relativistic fermions, and investigate their non-trivial topological properties.

Topological states of matter has also been generalized to Cooper pairing states [39, 40, 41, 2]. For example, the 2D $p_x + ip_y$ pairing chiral superfluids are also described the Chern number and exhibit chiral edge modes. Different from the QHE edge modes, these chiral edge modes are Majorana modes due to the particle-hole symmetry of the Bogoliubov-de Gennes equations of the pairing states. The ^{3}He-B phase is a topological pairing state in 3D, whose surface spectra are 2D helical Majorana modes. It would be interesting to further exploring pairing states with novel topological properties. In this thesis, we will present our study on topological properties of a novel experimental system of ultra-cold magnetic dipolar fermions. The magnetic dipolar interactions give rise to a novel mechanism leading to the p-wave spin triplet pairing. Different from the usual p-wave pairing states, such as ^{3}He-A and B phases [2], we have found a novel pairing symmetry with Weyl-type Bogolibov excitations. Topological effects from the magnetic dipolar interactions on the Fermi liquid collective excitations are also present in this thesis.

1.2 Motivations and Outline

In this thesis, we present novel topological states of condensed matter and ultra-cold atom systems in three and higher dimensions. In Chapters 2 - 5, novel topological Landau levels states for non-interacting spin-1/2 fermions are proposed in continuum three and higher dimensions. In Chapters 6 and 7, novel topological Weyl Cooper pairing and collective modes induced by magnetic dipolar interactions are analyzed at the particle-particle channel and the particle hole channel respectively. The motivations and main results in this thesis are explained as below.

As we have seen, the success of the prediction and discovery of topological insulator states in three dimensional Bloch-wave lattices greatly shifts the search for topological states from two dimensional to three dimensional systems. On another hand, two dimensional quantum Hall systems defined in the continuum possess flat and highly degenerate Landau levels with elegant analytic wave functions. Therefore, it would be interesting to develop their common counter part - Landau level states in continuum three and higher dimensions independent of the band inversion mechanism.

In Chapter 2, we construct SU(2) Landau level Hamiltonians in the isotropic symmetric-like gauge in three and higher dimensions. Spin-$\frac{1}{2}$ fermions are coupled to an Aharonov-Casher $SU(2)$ gauge field which is equivalent to the 3D harmonic potential with spin-orbit coupling. The orbital angular momentum and spin are coupled with a fixed helicity in the flat Landau levels which are dispersionless with respect to the total angular momentum J. The role of chirality in 2D Landau levels is replaced by helicity, and thus time-reversal symmetry is maintained. Each Landau level contributes one branch of gapless helical Dirac modes on open boundaries as characterized the $\mathbb{Z}_2$ topology. The magnetic translation for the highest weight states and the algebra structure have also been constructed. This scheme can also be generalized to 4D and arbitrary dimensions by combining harmonic potentials and spin-orbit coupling of fermions in the fundamental spinor representations.

Inspired by the complex analyticity of 2D lowest Landau levels, we have found an impressive result that the 3D and 4D LLL wave functions are quater-

nionic analytic. Since a two-component complex spinor can be mapped to a single component quaternion, we reformulate the SU(2) LLL wave functions in the quaternion representation. They satisfy the Fueter condition, the quaternionic generalization of the Cauchy-Riemann condition, and form the complete basis of quaternionic analytic polynomials. In addition, we have constructed the Laughlin-type wave functions for spontaneously spin polarized states at fractional fillings in 4D. The elegant analytic properties of 3D Landau level wave functions and the non-perturbative interaction effects in flat Landau level spectra can be expected leading richer results in 3D topological states.

In Chapter 3, to further exploit translational symmetries giving rise to more convenient description of topological properties, 3D and 4D Landau levels in the Landau-like $SU(2)$ gauge are constructed. They are spatially separated 2D helical modes and 3D Weyl modes along the 3rd and 4th directions, respectively. Modes with opposite helicities or chiralities are shifted in opposite directions. Just like that the 2D Landau level problem is equivalent to the quantization in the 2D phase space, the 3D (4D) Landau levels can be viewed as quantization in the 4D (6D) phase space. As a heuristic example of spatially separated (3+1)D chiral anomalies, we calculated the 4D quantum Hall effect in Landau level states which shows quantized non-linear electromagnetic responses.

In Chapter 4, nearly flat parity breaking Landau levels with high degeneracy on angular momentums are discussed. They have advantages in possible easier realizations in two and three dimensional harmonic traps with strong Rashba and $\vec{\sigma} \cdot \vec{p}$-type spin-orbit couplings respectively. On top of the gapped radial quantization provided by the harmonic trap, strong spin-orbit coupling plays an important double role. At one hand, it selects ground states with a fixed helicity, which leads topological nontrivial states at low fillings; on another hand, the angular momentum dependence in the energy dispersion is strongly suppressed by this spin-orbit coupling, which provides almost flat spectra with high degeneracy at the strong spin-orbit coupling regime.

In Chapter 5, as a relativistic square root problem of Chapters 2, three and higher dimensional isotropic Landau levels for Dirac fermions are discussed. It is constructed as a 3D quaternionic generalization of the 2D quantum Hall Hamil-

tonian in a single valley of graphene, whose square is a supersymmetric version of the non-relativistic 3D Landau level problem for non-relativistic fermions. It also shows a *non-minimal* Pauli coupling between 3+1 D Dirac fermions and the background field, which can also be considered as a generalization of the parity anomaly of the 2+1 D Dirac fermions. The zeroth 3D Landau level states are half-fermion Jackiw-Rebbi zero modes for all the values of angular momentum numbers (j, j_z).

Next, let us move to the novel topological states induced by magnetic dipolar interactions in ultra-cold atom system. Rare earth fermions ^{161}Dy and ^{163}Dy have been laser-cooled in B. Lev's group at Stanford. These are novel itinerant systems with magnetic dipolar interactions as an important energy scale. Unlike the more commonly studied electric dipoles which are non-quantized classic vectors, magnetic dipole moments, loosely speaking, are proportional to the total electron angular momentum up to a Lande factor, and thus are quantum mechanical operators. Magnetic dipolar interactions are invariant under the simultaneous rotations of both dipole orientations and the relative displacement between two dipoles, but not under neither of them. This is a feature of spin-orbit coupling. It is different from the usual single particle spin-orbit coupling, but an interaction effect.

In Chapters 6, we will find that this spin-orbit interaction gives rise to exotic Weyl Cooper pairing for spin-1/2 fermions.. The magnetic dipolar interaction induces a novel pairing symmetry: orbital p-wave $L = 1$, spin-triplet $S = 1$, and total angular momentum $J = 1$. Such a pairing symmetry is different from those in the ^{3}He-3 B phase which corresponds to $J = 0$, and the ^{A}He-3 A phase in which spin and orbit decouple. To our knowledge, this novel pairing with $J = 1$ has not been studied before. The resultant states can be either polar-like with $J_z = 0$ as a time-reversal invariant generalization of the ^{3}He-A phase, or, an axial-like time-reversal symmetry breaking state with $J_z = \pm 1$ which is a Cooper pairing version of the 3D Weyl fermions.

In Chapter 7, we study the spin-orbit coupled Fermi liquid properties with topological structures for spin-1/2 fermions. The spin-orbit coupled nature of magnetic dipolar interaction exhibits exotic Fermi liquid properties, such as spin-orbit coupled Pomeranchuk instabilities. In addition, we have identified a propagating

spin-orbit coupled collective mode with non-trivial topological configurations. A dynamic hedgehog type spin distribution appears on the Fermi surface, and oscillates over space and time.

In Chapter 8, conclusions and outlooks for future investigation are presented.

Chapter 2

Isotropic Landau levels of non-relativistic fermions in three and higher dimensions

2.1 Introduction

The current research of 3D topological insulators (TIs) has been focusing on the Bloch-wave band structures. Nevertheless, Landau levels (LLs) in two dimensional quantum Hall (2D QH) systems possess the advantages of the elegant analytic properties and flat spectra, both of which have played essential roles in the study of 2D integer and fractional QH effects [42, 43, 44, 45, 38, 46, 47, 48, 49, 50, 51, 52, 53, 54, 55, 56]. As pioneered by Zhang and Hu [57], LLs and QH effects have been generalized to various high dimensional manifolds [57, 58, 59, 60, 61, 62]. However, to our knowledge, TR invariant isotropic LLs have not been studied in 3D flat space before. It would be interesting to develop the LL counterpart of 3D TIs in the continuum independent of the band inversion mechanism. The analytic properties of 3D LL wavefunctions and the flatness of their spectra provide an opportunity for further investigation on non-trivial interaction effects in 3D topological states.

In this chapter, we construct 3D isotropic flat LLs in which spin-$\frac{1}{2}$ fermions are coupled to an $SU(2)$ Aharonov-Casher potential. When odd number LLs are

fully filled, the system is a 3D $\mathbb{Z}_2$ TI with TR symmetry. Each LL state has the same helicity structure, *i.e.*, the relative orientation between orbital angular momentum and spin. Just like that the 2D lowest LL (LLL) wavefunctions in the symmetric gauge are complex analytic functions, the 3D LLL ones are mapped into quaternionic analytic functions. Different from the 2D case, there is no magnetic translational symmetry for the 3D LL Hamiltonian due to the non-Abelian nature of the gauge field. Nevertheless, magnetic translations can be applied for the Gaussian pocket-like localized eigenstates in the LLL. The edge spectra exhibit gapless Dirac modes. Their stability against TR invariant perturbations indicates the $\mathbb{Z}_2$ nature. This scheme can be easily generalize to N dimensions. Interaction effects and the Laughlin-like wavefunctions for the 4D case are constructed. Realizations of the 3D LL system are discussed.

2.2 Three dimensional isotropic Landau levels from Aharonov-Casher potential

We begin with the 3D LL Hamiltonian for a spin-$\frac{1}{2}$ non-relativistic particle as

$$H^{3D,LL} = \frac{1}{2m}\sum_a \big\{ -i\hbar\nabla^a - \frac{q}{c}A^a(\vec{r})\big\}^2 + V(r), \tag{2.1}$$

where $A^a_{\alpha\beta} = \frac{1}{2}G\epsilon_{abc}\sigma^b_{\alpha\beta}r^c$ is a 3D isotropic $SU(2)$ gauge with Latin indices run over x, y, z and Greek indices denote spin components $\uparrow, \downarrow$; G is a coupling constant and σ's are Pauli matrices; $V(r) = -\frac{1}{2}m\omega_0^2 r^2$ is a harmonic potential with $\omega_0 = |qG|/(2mc)$ to maintain the flatness of LLs. $\vec{A}$ can be viewed as an Aharonov-Casher potential associated with a radial electric field linearly increasing with r as $\vec{E}(r)\times\vec{\sigma}$. $H^{3D,LL}$ preserves the TR symmetry in contrast to the 2D QH with TR symmetry broken. It also gives a 3D non-Abelian generalization of the 2D quantum spin Hall Hamiltonian based on Landau levels studied in Ref. [15]. More explicitly, $H^{3D,LL}$ can be further expanded as a harmonic oscillator with a constant spin-orbit (SO) coupling as

$$H^{3D,LL}_{\mp} = \frac{p^2}{2m} + \frac{1}{2}m\omega_0^2 r^2 \mp \omega_0\vec{\sigma}\cdot\vec{L}, \tag{2.2}$$

where $\mp$ apply to the cases of $qG > 0$ (< 0), respectively. The spectra of Eq. (2.2) were studied in the context of the supersymmetric quantum mechanics [63]. However, its connection with Landau levels was not noticed. Eq. (2.1) has also been proposed to describe the electrodynamic properties of superconductors [64, 65, 66].

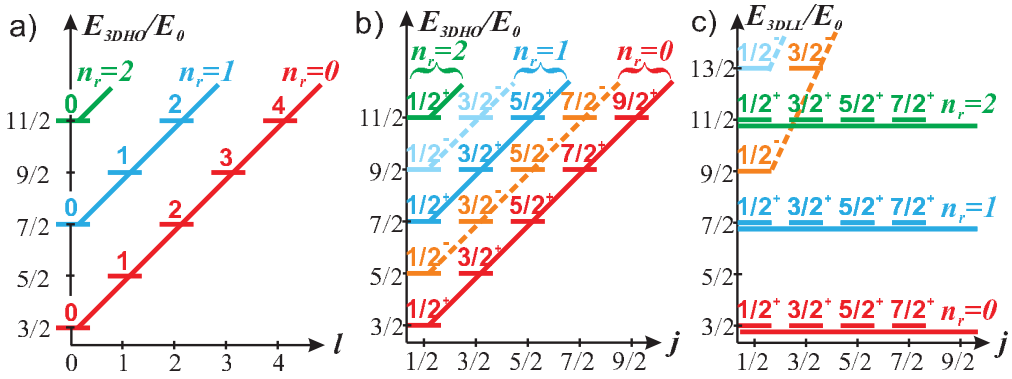

Figure 2.1: a) The eigenstates and energy spectrum of spinless 3D harmonic oscillators labeled by the orbital angular momentum l. States of different radial principle quantum numbers n_r are marked by different colors. b) For spin-$\frac{1}{2}$ 3D harmonic oscillators, their eigenstates and energy spectrum are labeled by the total angular momentum $j_\pm = l \pm \frac{1}{2}$. Following the solid (dashed) lines, the states with positive (negative) helicity are reorganized into 3D LLs. c) The reorganized eigenstates show high degeneracy over the total angular momentum for the branch of positive helicity and form the 3D Landau levels.

The spectra and eigenstates of Eq. 2.1 are explained as follows. We introduce the helicity number for the eigenstate of $\vec{L}\cdot\vec{\sigma}$, defined as the sign of its eigenvalue of the total angular momentum $\vec{J} = \vec{L} + \vec{S}$, which equals ± 1 for the sectors of $j_\pm = l \pm \frac{1}{2}$, respectively. At $qG > 0$, the eigenstates are denoted as $\psi_{n_r;j_\pm,j_z;l}(\vec{r}) = R_{n_r,l}(r)\mathcal{Y}_{j_\pm,j_z;l}(\hat{\Omega})$, where the radial function is $R_{n_r l}(r) = r^l e^{-\frac{r^2}{4l_G^2}} F(-n_r, l+\frac{3}{2}, \frac{r^2}{2l_G^2})$; F is the confluent hypergeometric function and $l_G = \sqrt{\frac{\hbar c}{qG}}$ is the analogy of the magnetic length; $\mathcal{Y}_{j_\pm,j_z;l}(\hat{\Omega})$'s are the spin-orbit coupled spheric harmonic with $j_\pm = l \pm \frac{1}{2}$, respectively. Flat spectra appear with infinite degeneracy in the sector of j_+, where the energy dispersion $E^+_{n_r,l} = (2n_r + \frac{3}{2})\hbar\omega_0$ is independent of l, and thus n_r serves as the LL index. For the sector of j_-, the energy disperses with l as $E^-_{n_r,l} = [2(n_r + l) + \frac{5}{2}]\hbar\omega_0$. Similar results apply to the case of $qG < 0$, where

the infinite degeneracy occurs in the sector of j_-. These LL wavefunctions are the same as those of the 3D harmonic oscillator but with different organizations. As illustrated in Fig. 2.1, these eigenstates along each diagonal line with the positive (negative) helicity fall into the flat LL states for the case of $qG > 0$ (< 0), respectively.

2.3 Ladder algebra for the spectra flatness

The degeneracy of the 3D LL over different values of angular momentum is not accidental, but protected by a ladder algebra constructed below. For example, we take the case of $qG > 0$ and consider the positive helicity Landau level states of H_+. The variable transformation for the radial eigenstates is applied as $\chi_{n_r,l}(r) = rR_{n_r,l}(r)$, and the corresponding radial Hamiltonians become

$$H_l = \hbar\omega_0\Big\{ -\frac{d^2}{dr^{*2}} + \frac{l(l+1)}{r^{*2}} - l + \frac{1}{4}r^{*2}\Big\}, \tag{2.3}$$

where the dimensionless radius is $r^* = \frac{r}{l_G}$. The ladder operators are defined as

$$\begin{aligned} A_+(l) &= \frac{d}{dr^*} - \frac{l+1}{r^*} - \frac{1}{2}r^*, \\ A_-(l) &= -\frac{d}{dr^*} - \frac{l}{r^*} - \frac{1}{2}r^*. \end{aligned} \tag{2.4}$$

They satisfy the relations

$$H_{l\pm1}A_\pm(l) = A_\pm(l)H_l. \tag{2.5}$$

Consequentially, $\chi_{n_r,l\pm1} = A_\pm(l)\chi_{n_r,l}$ with the same energy independent of l. All the states in the same LL can be reached by successively applying $A_\pm$ operators.

To connect different LLs, other two ladder operators are defined as

$$\begin{aligned} B_-(l) &= -\frac{d}{dr^*} - \frac{l}{r^*} + \frac{1}{2}r^*, \\ C_+(l) &= \frac{d}{dr^*} - \frac{l+1}{r^*} + \frac{1}{2}r^*, \end{aligned} \tag{2.6}$$

which satisfy

$$\begin{aligned} H_{l-1}B_-(l) &= B_-(l)(H_l + 2\hbar\omega_0), \\ H_{l+1}C_+(l) &= C_+(l)(H_l - 2\hbar\omega_0), \end{aligned} \tag{2.7}$$

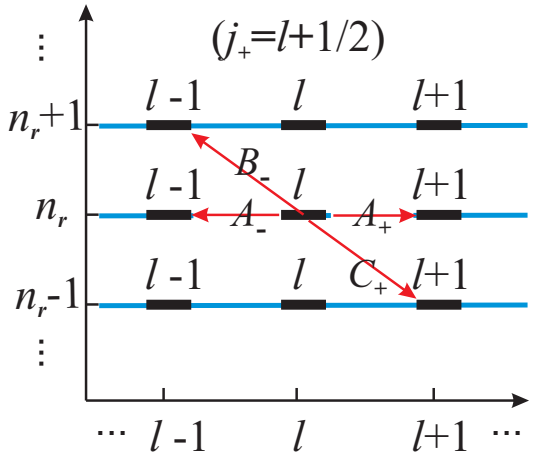

Figure 2.2: The algebra structure of the 3D Landau levels in the positive helicity sector. Operators $A_\pm(l)$ connect states with different l in the same Landau level, while $B_-(l)$ and $C_+(l)$ connect those between neighboring Landau levels.

respectively. By applying $B_-(l)$ ($C_+(l)$) to $\chi_{n_r,l}(r)$, we arrive at

$$\begin{aligned} \chi_{n_r+1,l-1} &= B_-(l)\chi_{n_r,l}, \\ \chi_{n_r-1,l+1} &= C_+(l)\chi_{n_r,l}, \end{aligned} \tag{2.8}$$

where the energy shifts $\pm 2\hbar\omega_0$, respectively, as illustrated in Fig. 2.2. Similar algebra can also be constructed for the case of $qG < 0$.

2.4 Magnetic translation for the highest weight state

Compared to the 2D case, a marked difference is that the 3D LL Hamiltonian has no magnetic translational symmetry. The non-Abelian field strength grows quadratically with r as $F_{ij}(\vec{r}) = \partial_i A_j - \partial_j A_i - \frac{iq}{\hbar c}[A_i, A_j] = g\epsilon_{ijk}\{\sigma^k + \frac{1}{4l_G^2} r^k(\vec{\sigma}\cdot\vec{r})\}$. Nevertheless, magnetic translations still apply to the highest weight states of the total angular momentum $\vec{J} = \vec{L} + \vec{S}$ in the LLL at $qG > 0$. For simplicity, we drop the normalization factors of wavefunctions below. For the positive helicity states with $j_z = j_+$, $\vec{L}$ and $\vec{S}$ are parallel to each other. Their wavefunctions are denoted by $\psi^{hw}_{\hat{z},l}(\vec{r}) = (x+iy)^l e^{-\frac{r^2}{4l_G^2}} \otimes \alpha_{\hat{\Omega}=\hat{z}}$, where $\alpha_{\hat{\Omega}}$ is the spin eigenstate of

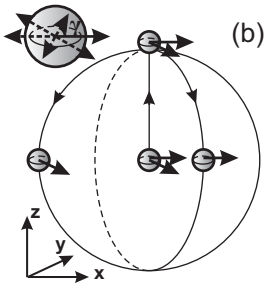

Figure 2.3: The magnetic translation for the LLL state ($l = 0$) localized at the origin in the case of $qG > 0$, whose spin is set along an arbitrary direction in the xy-plane. The displacement vector $\vec{\delta}$ lies in the plane perpendicular to spin orientation. The resultant state remains in the LLL as a localized Gaussian pocket.

$\hat{\Omega} \cdot \vec{\sigma}$ with eigenvalue 1. For these states, the magnetic translation is defined as usual $T_{\hat{z}}(\vec{\delta}) = \exp[-\vec{\delta} \cdot \vec{\nabla} + \frac{i}{4l_G^2} \vec{r}_{xy} \cdot (\hat{z} \times \vec{\delta})]$, where $\vec{\delta}$ is the displacement vector in the xy-plane and $\vec{r}_{xy}$ is the projection of $\vec{r}$ in the xy-plane. The resultant state, $T_{\hat{z}}(\vec{\delta})\psi^{hw}_{\hat{z},l}(\vec{r}) = e^{i\frac{\vec{r}_{xy}\cdot(\hat{z}\times\delta)}{4l_G^2}} \psi^{hw}_{\hat{z},l}(\vec{r} - \vec{\delta})$, remains in the LLL. Generally speaking, the highest weight states can be defined in a plane spanned by two orthogonal unit vectors $\hat{e}_{1,2}$ as $\psi^{hw}_{\hat{e}_3,l}(\vec{r}) = [(\hat{e}_1 + i\hat{e}_2) \cdot \vec{r}]^l e^{-\frac{r^2}{4l_G^2}} \otimes \alpha_{\hat{e}_3}$ with $\hat{e}_3 = \hat{e}_1 \times \hat{e}_2$. The magnetic translation for such states is defined as $T_{\hat{e}_3}(\vec{\delta}) = \exp[-\vec{\delta} \cdot \vec{\nabla} + \frac{i}{4l_G^2}\ \vec{r}_{12} \cdot (\hat{e}_3 \times \vec{\delta})]$, where $\vec{\delta}$ lies in the $\hat{e}_{1,2}$-plane and $\vec{r}_{12} = \vec{r} - \hat{e}_3(\vec{r} \cdot \hat{e}_3)$. As an example, let us translate the LLL state localized at the origin as illustrated in Fig. 2.3. We set the spin direction of $\psi^{LLL}_{\hat{e}_3,l=0}$ in the xy-plane parameterized by $\hat{e}_3(\gamma) = \hat{x}\cos\gamma + \hat{y}\sin\gamma$, *i.e.*, $\alpha_{\hat{e}_3}(\gamma) = \frac{1}{\sqrt{2}}(|\uparrow\rangle + e^{i\gamma}|\downarrow\rangle)$, and translate it along $\hat{e}_1 = \hat{z}$ at the distance R. The resultant states read as

$$\psi_{\gamma,R}(\rho, \phi, z) = e^{i\frac{g}{2}R\rho\sin(\phi-\gamma)} e^{-|\vec{r}-R\hat{z}|^2/4l_G^2} \otimes \alpha_{\hat{e}_3}(\gamma), \tag{2.9}$$

where $\rho = \sqrt{x^2 + y^2}$ and ϕ is the azimuthal angular of $\vec{r}$ in the xy-plane. Such a state remains in the LLL as an off-centered Gaussian wave packet.

The highest weight states and their descendent states from magnetic translations defined above have a clear classic picture. The classic equations of motion are derived as

$$\begin{aligned} \dot{\vec{r}} &= \frac{1}{m}\vec{p} + 2\omega_0(\vec{r} \times \frac{1}{\hbar}\vec{S}), \quad \dot{\vec{p}} = 2\omega_0\vec{p} \times \frac{1}{\hbar}\vec{S} - m\omega_0^2\vec{r}, \\ \dot{\vec{S}} &= \frac{2\omega_0}{\hbar}\vec{S} \times \vec{L}, \end{aligned} \tag{2.10}$$

where $\vec{p}$ is the canonical momentum, $\vec{L} = \vec{r} \times \vec{p}$ is the canonical orbital angular momentum, and $\vec{S}$ here is the expectation value of $\frac{\hbar}{2}\vec{\sigma}$. The first two describe the motion in a non-inertial frame subject to the angular velocity $\frac{2\omega_0}{\hbar}\vec{S}$, and the third equation is the Larmor precession. $\vec{L} \cdot \vec{S}$ is a constant of motion of Eq. 2.10. In the case of $\vec{S} \parallel \vec{L}$, it is easy to prove that both $\vec{S}$ and $\vec{L}$ are conserved. Then the cyclotron motions become coplanar within the equatorial plane perpendicular to $\vec{S}$. Centers of the circular orbitals can be located at any points in the plane.

The above off-centered LLL states break all the rotational symmetries. Nevertheless, we can recover the rotational symmetry around the axis determined by the origin and the packet center. Let us perform the Fourier transform of $\psi_{\gamma,R}(\rho, \phi, z)$ in Eq. 2.9 with respect to the azimuthal angle γ of spin polarization. The resultant state, $\psi_{j_z=m+\frac{1}{2},R}(\rho, \phi, z) = \int_0^{2\pi} \frac{d\gamma}{2\pi} e^{im\gamma}\psi_{\gamma,R}$, is a j_z-eigenstate as

$$e^{\frac{-|\vec{r}-R\hat{z}|^2}{4l_G^2}} e^{im\phi}\Big\{J_m(x)|\uparrow\rangle + J_{m+1}(x)e^{i\phi}|\downarrow\rangle\Big\}, \tag{2.11}$$

with $x = R\rho/(2l_G^2)$. At large distance of R, the spatial extension of $\psi_{j_z=m+\frac{1}{2},R}$ in the xy-plane is at the order of ml_G^2/R, which is suppressed at large values of R and scales linear with m. In particular, the narrowest states $\psi_{\pm\frac{1}{2},R}$ exhibit an ellipsoid shape with an aspect ratio decaying as l_G/R when R goes large.

2.5 Quaternionic analyticity in the 3D lowest Landau level wave functions

In analogy to the fact that the 2D LLL states are complex analytic functions due to chirality, we have found an impressive result that the helicity in 3D LL systems leads to the quaternionic analyticity. Quaternion is the first discovered non-commutative division algebra, which has three anti-commuting imaginary units i, j and k, satisfying $i^2 = j^2 = k^2 = -1$ and $ij = k$. It has been applied in quantum systems [67, 68] and SO coupled Bose-Einstein condensations [69]. Just like two real numbers forming a complex number, a two-component complex spinor $\psi = (\psi_\uparrow, \psi_\downarrow)^T$ can be viewed as a quaternion defined as $f = \psi_\uparrow + j\psi_\downarrow$. In the quaternion representation, the TR transformation $i\sigma_2\psi^*$ becomes $Tf = -fj$ satisfying

$T^2 = -1$; multiplying a U(1) phase factor $e^{i\phi}\psi$ corresponds to $fe^{i\phi}$; the SU(2) operations $e^{-i\frac{\sigma_x}{2}\phi}\psi$, $e^{-i\frac{\sigma_y}{2}\phi}\psi$, and $e^{-i\frac{\sigma_z}{2}\phi}\psi$ map to $e^{\frac{k}{2}\phi}f$, $e^{\frac{j}{2}\phi}f$, and $e^{-\frac{i}{2}\phi}f$, respectively. The quaternion version of $\psi^{LLL}_{j=j_+,j_z=m+\frac{1}{2}}$ is $f^{LLL}_{j_+,j_z}(x,y,z) = \Psi_{\uparrow,j_+,j_z} + j\Psi_{\downarrow,j_+,j_z}$, where $\Psi_{\uparrow,j_+,j_z} = \langle j_+, j_z | l, m; \frac{1}{2}, \frac{1}{2}\rangle r^l Y_{l,m}$, $\Psi_{\downarrow,j_+,j_z} = \langle j_+, j_z | l, m+1; \frac{1}{2}, -\frac{1}{2}\rangle r^l Y_{l,m+1}$. Please note that the Gaussian factor does not appear in $f^{LLL}_{j_+,j_z}$ which is a quaternionic polynomial.

As a generalization of the Cauchy-Riemann condition, a quaternionic analytic function $f(x,y,z,u)$ satisfies the Fueter condition [70] as

$$\frac{\partial f}{\partial x} + i\frac{\partial f}{\partial y} + j\frac{\partial f}{\partial z} + k\frac{\partial f}{\partial u} = 0, \tag{2.12}$$

where x, y, z and u are coordinates in the 4D space. In Eq. 2.12, imaginary units are multiplied from the left, thus it is the left-analyticity condition which works in our convention. Below, we prove the LLL function $f^{LLL}_{j_+,j_z}(x,y,z)$ satisfying Eq. 2.12. Since $f^{LLL}_{j_+,j_z}$ is defined in 3D space, it is a constant over u, and thus only the first three terms in Eq. 2.12 apply to it. Obviously the highest weight states with spin along the z-axis, $f^{LLL}_{j_+=j_z=l+\frac{1}{2}} = (x+iy)^l$, satisfy Eq. 2.12 which is reduced to complex analyticity. By applying an arbitrary SU(2) rotation g characterized by the Eulerian angles (α,β,γ), $f^{LLL}_{j_+=j_z}$ transforms to

$$f'^{,\,LLL}(x,y,z) = e^{-i\frac{\alpha}{2}}e^{j\frac{\beta}{2}}e^{-i\frac{\gamma}{2}} f^{LLL}_{j_+=j_z}(x',y',z'), \tag{2.13}$$

where $(x',y',\,z')$ are the coordinates by applying the inverse of g on (x,y,z). It can be checked that

$$\begin{aligned} & (\frac{\partial}{\partial x} + i\frac{\partial}{\partial y} + j\frac{\partial}{\partial z}) f'^{LLL}(x,y,z) \\ = \;& e^{i\frac{\alpha}{2}}e^{-j\frac{\beta}{2}}e^{i\frac{\gamma}{2}} \Big\{ \frac{\partial}{\partial x'} + i\frac{\partial}{\partial y'} + j\frac{\partial}{\partial z'} \Big\} f^{LLL}_{j_+,j_z}(x',y',z') = 0. \end{aligned} \tag{2.14}$$

Essentially, we have proved that Fueter condition is rotationally invariant. Since all the highest weight states are connected through SU(2) rotations, and they form an over-complete basis for the angular momentum representations, we conclude that all the 3D LLL states with the positive helicity are quaternionic analytic.

Next we prove that the set of quaternionic LLL states $f^{LLL}_{j_+=l+\frac{1}{2},j_z}$ form the complete basis for quaternionic valued analytic polynomials in 3D. Any linear superposition of the LLL states with j_+ can be represented as $f_l = \sum_{j_z=-j_+}^{j_+} f^{LLL}_{j_+,j_z}\, c_{j_z}$,

where c_{j_z} is a complex coefficient. Because of the TR relation $f^{LLL}_{j_+,-j_z} = -f^{LLL}_{j_+,-j_z} j$, f_l can be expressed in terms of $l+1$ linearly independent basis as

$$f_l(x,y,z) = \sum_{m=0}^{l} f^{LLL}_{j_+=l+\frac{1}{2},j_z=m+\frac{1}{2}} q_m, \tag{2.15}$$

where $q_m = c_{m+\frac{1}{2}} - jc_{-m-\frac{1}{2}}$ is a quaternion constant. On the other hand, it can be calculated that the rank of the linearly independent l-th order quaternionic polynomials satisfying Eq. 2.12 is just $C^2_{l+2} - C^2_{l+1} = l+1$, thus $f^{LLL}_{j_+,j_z}$'s with $j_z \geq \frac{1}{2}$ are complete.

For the case of the LLL with negative helicity, their quaternionic version $g^{LLL}_{j_-,j_z}(x,y,z)$ are not analytic any more. Nevertheless, since the wavefunctions of the negative helicity sector can be related to the positive one via $\mathcal{Y}_{j_-,j_z;l+1}(\hat{\Omega}) = -\vec{\sigma}\cdot\hat{\Omega}\mathcal{Y}_{j_+,j_z;l}(\hat{\Omega})$, where $\vec{\sigma}\cdot\hat{\Omega}$ has odd parity, their quaternionic version is related to the analytic one through $g^{LLL}_{j_-=(l+1)-\frac{1}{2},j_z} = (-\hat{x}k - \hat{y}j + \hat{z}i) f^{LLL}_{j_+=l+\frac{1}{2},j_z} i$. Here, the representation of quaternion imaginary units $\{i,j,k\}$ as Pauli matrices $\{i\sigma_z, -i\sigma_y, -i\sigma_x\}$ are used, as derived from the rotational properties of the spin-orbit coupled spheric harmonics.

2.6 Surface helical Dirac states

The topological nature of the 3D LL problem exhibits clearly in the gapless surface states. We have numerically calculated the spectra with the open boundary condition for the positive helicity states with $j_+ = l + \frac{1}{2}$. The results for the first four LLs are plotted in Fig. 2.4. At $qG > 0$, inside the bulk, LL spectra are flat with respect to $j_+ = l + \frac{1}{2}$. As l goes large, the classical orbital radius r_c approaches the open boundary with the radius R_0. For example, for a LLL state, $r_c = \sqrt{2l} l_G$. When the orbital angular momentum States with $l > l_c \approx \frac{1}{2}(R_0/l_G)^2$ become surface states. Their spectra become $E(l) \approx l(l+1)\frac{\hbar^2}{2mR_0^2} - l\hbar\omega_0$. When the chemical potential μ lies inside the gap, it cuts the surface states with the Fermi angular momentum denoted by l_f. These surface states satisfy $\vec{\sigma}\cdot\vec{L} = l\hbar$, thus the their spectra can be linearized around l_f as $H_{bd} = (v_f/R_0)\vec{\sigma}\cdot\vec{L} - \mu$. This is the Dirac equation defined on a sphere with the radius R_0. It can be expanded

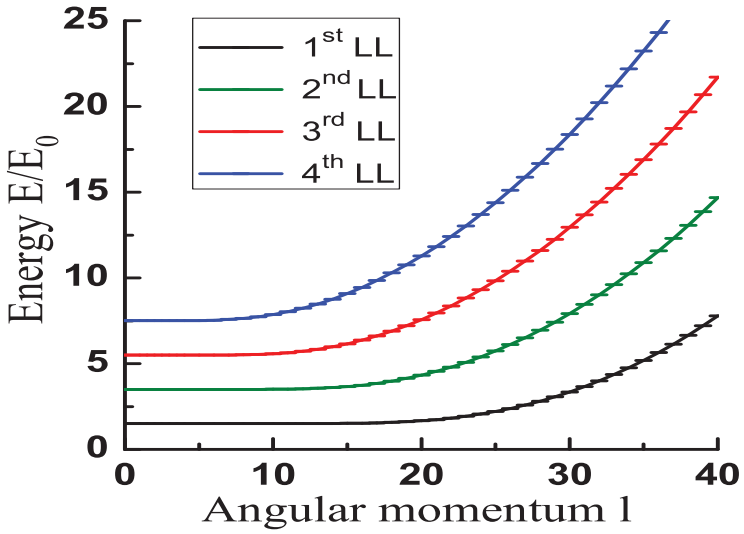

Figure 2.4: The energy dispersion of the first four Landau levels *v.s.* $l = j - \frac{1}{2}$. Open boundary condition is used for a ball with the radius $R_0/l_G = 8$. The edge states correspond to those with large values of l and develop linear dispersions with l.The most probable radius of the LLL state with l is $r = l_G\sqrt{l}$. l exceeds a characteristic value $l_c \approx 30$, the spectra become dispersive indicating the onset of surface states.

around $\vec{r} = R_0\hat{e}_r$ as $H_{bd} = \hbar v_f(\vec{k} \times \vec{\sigma}) \cdot \hat{e}_r - \mu$. Although the surface spectra look very similar to those of the 2D quantum Hall edges, a crucial difference is that each l in Fig. 2.4 does not represent a single chiral state but a set of helical states of $2j_+ + 1$ fold degeneracy with $j_+ = l + \frac{1}{2}$. Similar reasoning applies to other Landau levels which also give rise to Dirac spectra. Because of the lack of Bloch wave band structure, it remains a challenging problem to directly calculate the bulk topological index. Nevertheless, the $\mathbb{Z}_2$ structure manifests through the surface Dirac spectra. Since each fully occupied LL contributes one helical Dirac Fermi surface, the bulk is $\mathbb{Z}_2$-nontrivial (trivial) if odd (even) number of LLs are occupied. In the $\mathbb{Z}_2$-nontrivial case, the gapless helical surface states are protected by TR symmetry and are robust under TR invariant perturbations.

In Eq. 2, the harmonic frequency ω_T is set to be equal with the SO frequency ω_0 to maintain the flatness of LL spectra. However, the $\mathbb{Z}_2$ topology of the 3D LLs does not rely on this. Define $\Delta\omega = \omega_T - \omega_0$, and we set $\Delta\omega \geq 0$ to maintain the spectra bounded from below. $\Delta\omega > 0$ corresponds to imposing an external

potential $\Delta V(r) = \frac{1}{2}m(\omega_T^2 - \omega_0^2)r^2$ to the bulk Hamiltonian of Eq. 2. If $\Delta\omega \ll \omega_0$, $\Delta V(r)$ is soft. It results in energy dispersions of 3D LLs but does not affect their topology. For simplicity, let us check the case of $qG > 0$. The $\vec{\sigma}\cdot\vec{L}$ term commutes with the overall harmonic potential, thus the LL wavefunctions remain the same as those of Eq. 2 by replacing ω_0 with ω_T. Their dispersions become $E^+_{n_r,j_+} = (2n_r+1)\hbar\omega_T + \frac{1}{2}\hbar\omega_0 + j_+\hbar\Delta\omega$ which are very slow. In other words, $\Delta V(r)$ imposes a finite sample size with the radius of $R^2 < \hbar/(m\Delta\omega) = 2l_G\frac{\omega_0}{\Delta\omega}$ even without an explicit boundary. Inside this region, ΔV is smaller than the LL gap, and the LL states are bulk states. Their energies are within the LL gap and the angular momentum numbers $j_+ < \frac{2\omega_T}{\Delta\omega}$. LL states outside this region can be viewed as surface states with positive helicity. For a given Fermi energy, it also cuts a helical Fermi surface with the same form of effective surface Hamiltonian.

2.7 Generalization to N-dimensions

The above scheme can be easily generalized to arbitrary dimensions by combining the N-D harmonic oscillator potential and SO coupling. For example, in 4D, we have $H^{4D,LL} = \frac{p_{4D}^2}{2m} + \frac{1}{2}m\omega_0^2 r_{4D}^2 - \omega_0\sum_{1\le a<b\le 4}\Gamma^{ab}L_{ab}$, where $L_{ab} = r_a p_b - r_b p_a$ and the 4D spin operators are defined as $\Gamma^{ij} = -\frac{i}{2}[\sigma^i,\sigma^j]$, $\Gamma^{i4} = \pm\sigma^i$ with $1 \le i < j \le 3$. The $\pm$ signs of Γ^{i4} correspond to two complex conjugate irreducible fundamental spinor representations of $SO(4)$, and the + sign will be taken below. The spectra of the positive helicity states are flat as $E_{+,n_r} = (2n_r+2)\hbar\omega$. Following a similar method in 3D, we prove that the quaternionic version of the 4D LLL wavefunctions satisfy the full equation of Eq. 2.12. They form the complete basis for quaternionic left-analytic polynomials in 4D. For each l-th order, the rank can be calculated as $C^3_{l+3} - C^3_{l+2} = \frac{1}{2}(l+1)(l+2)$.

More generally, 3D and 4D LL systems can be generalized to N-D by replacing the vector and scalar potentials in Eq. 1 in the main text with the $SO(N)$ gauge field

$$A^a(\vec{r}) = gr^b S^{ab}, \quad V(r) = -\frac{N-2}{2}m\omega_0 r^2, \tag{2.16}$$

respectively, where S^{ab} are the $SO(N)$ spin operators constructed based on the

Clifford algebra. The rank-k Clifford algebra contains $2k+1$ matrices with the dimension $2^k \times 2^k$ which anti-commute with each other denoted as Γ^a $(1 \leq a \leq 2k+1)$. Their commutators generate

$$\Gamma^{ab} = -\frac{i}{2}[\Gamma^a, \Gamma^b], \tag{2.17}$$

for $1 \leq a < b \leq 2k+1$. For odd dimensions $N = 2k+1$, the $SO(N)$ spin operators in the fundamental spinor representation can be constructed by using the rank-k matrices as $S^{ab} = \frac{1}{2}\Gamma^{ab}$. For even dimensions $N = 2k+2$, we can select $2k+2$ ones among the $2k+3$ Γ-matrices of rank-$(k+1)$ to form $S^{ab} = \frac{1}{2}\Gamma^{ab}$, then all of S^{ab} commute with Γ^{2k+3}. This 2^{k+1}-D spinor representation of S^{ab} is thus reducible into the fundamental and anti-fundamental representations. Both of them are 2^k-D, which can be constructed from the rank-k Γ-matrices as $S^{a,2k+2} = \pm\frac{1}{2}\Gamma^a (1 \leq a \leq 2k+1)$ and $S^{ab} = \frac{1}{2}\Gamma^{ab} (1 \leq a < b < 2k+1)$, respectively.

As for TR properties, Γ^a's are TR even and odd at even and odd values of k, respectively. We conclude that at $N = 2k+1$, the N-D version of the LL Hamiltonian is TR invariant in the fundamental spinor representation. At $N = 4k$, it is also TR invariant in both the fundamental and anti-fundamental representations. However $N = 4k+2$, each one of the fundamental and anti-fundamental representations is not TR invariant, but transforms into each other under TR operation.

Similarly, the N-D LL Hamiltonian can be reorganized as the harmonic oscillator with SO coupling. For the case of $qG > 0$, it becomes

$$H_{N,+} = \frac{p^2}{2m} + \frac{1}{2}m\omega_0^2 r^2 - \hbar\omega_0 \Gamma_{ab} L_{ab}, \tag{2.18}$$

where $L_{ab} = r_a p_b - r_b p_a$ with $1 \leq a < b \leq N$. The l-th order N-D spherical harmonic functions are eigenstates of $L^2 = L_{ab}L_{ab}$ with the eigenvalue of $\hbar^2 l(l+D-2)$. The N-D harmonic oscillator has the energy spectra of $E_{n_r,l} = (2n_r + l + N/2)\hbar\omega$. When coupling to the fundamental spinors, the l-th spherical harmonics split into the positive helicity (j_+) and negative helicity (j_-) sectors, whose eigenvalues of the $\Gamma_{ab}L_{ab}$ are $\hbar l$ and $-\hbar(l+N-2)$, respectively. For the positive helicity sector, its spectra become independent of l as $E_+ = (2n_r + N/2)\hbar\omega$, with the radial wave

functions are

$$R_{n_r l}(r) = r^l e^{-r^2/4l_G^2} F(-n_r, l + N/2, r^2/2l_G^2). \tag{2.19}$$

The highest weight states in the LLL can be written as

$$\psi^{hw}_{ab,\pm l}(\vec{r}) = [(\hat{e}_a \pm i\hat{e}_b) \cdot \vec{r}]^l e^{-r^2/4l_G^2} \otimes \alpha_{\pm,ab}, \tag{2.20}$$

where $\alpha_{\pm,ab}$ is the eigenstate of Γ_{ab} with eigenvalue ± 1, respectively. The magnetic translation in the ab-plane by the displacement vector $\vec{\delta}$ takes the form

$$T_{ab}(\vec{\delta}) = \exp\big[-\vec{\delta} \cdot \vec{\nabla} + \frac{i}{2l_G^2} \Gamma_{ab}(r_a \delta_b - r_b \delta_a)\big]. \tag{2.21}$$

Similarly to the 3D case, staring from the LLL state localized around the origin with $l = 0$, we can perform the magnetic translation and Fourier transformation with respect to the transverse spin polarization. The resultant localized Gaussian pockets are LLL states of the eigenstates of the $SO(N-1)$ symmetry with respect to the translation direction $\vec{\delta}$. Again each LL contributes to one channel of surface Dirac modes on S^{N-1} described by $H_{bd} = (v_f/R_0)\Gamma_{ab}L_{ab} - \mu$.

2.8 Discussions of interaction effects in 3D Landau levels

We consider the interaction effects in the LLLs. For simplicity, let us consider the 4D system and the short-range interactions. Fermions can develop spontaneous spin polarization to minimize the interaction energy in the LLL flat band. Without loss of generality, we assume that spin takes the eigenstate of $\Gamma^{12} = \Gamma^{34} = \sigma^3$ with the eigenvalue 1. The LLL wavefunctions satisfying this spin polarization can be expressed as $\Psi^{LLL,4D}_{m,n} = (x + iy)^m (z + iu)^n e^{-\frac{r_{4D}^2}{4l_G^2}} \otimes |\alpha\rangle$ with $|\alpha\rangle = (1, 0)^T$. The 4D orbital angular momentum number for the orbital wavefunction is $l = m + n$ with $m \geq 0$ and $n \geq 0$. It is easy to check that $\Psi^{LLL,4D}_{m,n}$ is the eigenstate of $\sum_{ab} L_{ab}\Gamma^{ab}$ with the eigenvalue $(m + n)\hbar$. If all the $\Psi^{LLL,4D}_{m,n}$'s are filled with $0 \leq m < N_m$ and $0 \leq n < N_n$, we write down a Slater-determinant wavefunction as

$$\Psi(v_1, w_1; \cdots; v_N, w_N) = \det[v_i^\alpha w_i^\beta], \tag{2.22}$$

where the coordinates of the i-th particle form two pairs of complex numbers abbreviated as $v_i = x_i + iy_i$ and $w_i = z_i + iu_i$; α, β and i satisfy $0 \leq \alpha < N_m$, $0 \leq \beta < N_n$, and $1 \leq i \leq N = N_m N_n$. Such a state has a 4D uniform density as $\rho = \frac{1}{4\pi^4 l_G^4}$. We can write down a Laughlin-like wavefunction as the k-th power of Eq. 2.22 whose filling relative to ρ should be $1/k^2$. For the 3D case, we also consider the spin polarized interacting wavefunctions. However, it corresponds to that fermions concentrate to the highest weight states in the equatorial plane perpendicular to the spin polarization, and thus reduces to the 2D Laughlin states. In both 3D and 4D cases, fermion spin polarizations are spontaneous, thus low energy spin waves should appear as low energy excitations. Due to the SO coupled nature, spin fluctuations couple to orbital motions, which leads to SO coupled excitations and will be studied in a later publication.

2.9 Discussions of possible experimental realizations

One possible experimental realization for the 3D LL system is the strained semiconductors. The strain tensor $\epsilon_{ab} = \frac{1}{2}(\partial_a u_b + \partial_b u_a)$ generates SO coupling as $H_{SO} = \hbar\alpha[(\epsilon_{xy}k_y - \epsilon_{xz}k_z)\sigma_x + (\epsilon_{zy}k_z - \epsilon_{xy}k_x)\sigma_y + (\epsilon_{zx}k_x - \epsilon_{yz}k_y)\sigma_z]$ where $\alpha = 8\times10^5$m/s for GaAs. The 3D strain configuration with $\vec{u} = \frac{f}{2}(yz, zx, xy)$ combined with a suitable scalar potential gives rise to Eq. 2.1 with the correspondence $\omega_0 = \frac{1}{2}\alpha f$. A similar method was proposed in Ref. [15] to realize 2D quantum spin Hall LLs. A LL gap of 1mK corresponds to a strain gradient of the order of 1% over 60 μm, which is accessible in experiments. Another possible system is the ultra-cold atom system. For example, recently evidence of fractionally filled 2D LLs with bosons has been reported in rotating systems [71].

Furthermore, synthetic SO coupling generated through atom-light interactions has become a major research direction in ultra-cold atom system [72, 73]. The SO coupling term in the 3D LL Hamiltonian $\omega\vec{\sigma}\cdot\vec{L}$ is equivalent to the spin-dependent Coriolis forces from spin-dependent rotations, i.e., different spin eigenstates along $\pm x$, $\pm y$ and $\pm z$ axes feel angular velocities parallel to these axes,

respectively. An experimental proposal to realize such an SO coupling has been designed and will be reported in a later publication [74].

2.10 Summary

We have generalized the flat LLs to 3D and 4D flat spaces, which are high dimensional topological insulators in the continuum without Bloch-wave band structures. The 3D and 4D LLL wavefunctions in the quaternionic version form the complete bases of the quaternionic analytic polynomials. Each filled LL contributes one helical Dirac Fermi surface on the open boundary. The spin polarized Laughlin-like wavefunction is constructed for the 4D case. Interaction effects and topological excitations inside the LLLs in high dimensions would be interesting for further investigation. In particular, we expect that the quaternionic analyticity would greatly facilitate this study.

Acknowledgements: This work grew out of early collaborations with Professor J. E. Hirsch, to whom we are especially grateful. We thank S. C. Zhang and J. P. Hu for helpful discussions. Near the completion of this manuscript, we learned that the 3D Landau level problem is also studied by Zhang [75]. This chapter is in part a reprint of the paper "High-Dimensional Topological Insulators with Quaternionic Analytic Landau Levels", by Yi Li and Congjun Wu, *Phys. Rev. Lett.*, 110, 216802 (2013).

Chapter 3

Topological insulators with SU(2) Landau levels

3.1 Introduction

Time-reversal (TR) invariant topological insulators (TI) have become a major research focus in condensed matter physics[76, 25, 26]. Different from the 2D quantum Hall (QH) and quantum anomalous Hall systems which are topologically characterized by the first Chern number [5, 7, 14, 11, 8], time-reversal invariant TIs are characterized by the second Chern number in 4D [57, 22] and the Z_2 index in 2D and 3D [16, 15, 21, 22, 18, 20, 24]. Various 2D and 3D TIs are predicted theoretically and identified experimentally exhibiting stable gapless 1D helical edge and 2D surface modes against TR invariant perturbations [21, 27, 31, 77, 33, 34]. Topological states have also been extended to systems with particle-hole symmetry and superconductors [78, 79, 41].

Most current studies of 2D and 3D TIs focus on Bloch-wave bands in lattice systems. The non-trivial band topology arises from spin-orbit (SO) coupling induced band inversions [21]. However, Landau levels (LL) are essential in the study of QH effects because their elegant analytical properties enable construction of fractional states. Generalizing LLs to high dimensions gives rise to TIs with explicit wavefunctions in the continuum, which would facilitate the study of the exotic fractional TIs. Efforts along this line were pioneered by Zhang and Hu

[57]. They constructed LLs on the compact S^4 sphere by coupling fermions with the SU(2) monopole gauge potential, and various further developments appeared [80, 59, 61, 62, 81]. 2D TIs based on TR invariant LLs have also been investigated [15]. LLs of Schrödinger fermions have been generalized to high-dimensional flat space [82] in Chapter 2 by combining the isotropic harmonic potential and SO coupling. Further development for parity-breaking systems and high dimensional Dirac fermions[83, 84] will be discussed in Chapter 4 and 5 respectively.

In all the above works, angular momentum is explicitly conserved, thus they can be considered as LLs in the symmetric-like gauge. In 2D, LL wavefunctions in the Landau gauge are particularly intuitive: they are 1d chiral plane-wave modes spatially separated along the transverse direction. The QH effect is just the 1d chiral anomaly in which the chiral current generated by the electric field becomes the transverse charge current. In this article, we develop high dimensional LLs with flat spectra as spatially separated helical Dirac or chiral Weyl fermion modes, i.e., the SU(2) Landau-like gauge. They are 3D and 4D TIs defined in the continuum possessing stable gapless boundary modes. For the 4D case, they exhibit the 4D quantum Hall effect[57, 22], which is a quantized non-linear electromagnetic response related to the spatially separated (3+1)D chiral anomaly. Our methods can be easily generalized to arbitrary dimensions and also to Dirac fermions.

3.2 Three dimensional Landau levels with a "Landau" gauge

We begin with the 3D TR invariant LL Hamiltonian for a spin-$\frac{1}{2}$ fermion as

$$H_{LL}^{3D,\nu=\pm} = \frac{\vec{p}^2}{2m} + \frac{1}{2}m\omega_{so}^2 z^2 - \nu\omega_{so} z(p_x\sigma_y - p_y\sigma_x), \tag{3.1}$$

which couples the 1D harmonic potential in the z direction and the 2D Rashba SO coupling through a z-dependent SO coupling strength. $H_{LL}^{3D,\nu}$ possess translation symmetry in the xy-plane, TR and parity symmetries. $H_{LL}^{3D,+}$ and $H_{LL}^{3D,-}$ share the same physics up to a $z \to -z$ transformation. For simplicity, unless explicitly

mentioned, we only consider $H_{LL}^{3D,+}$ and suppress the index ν. Eq. 3.1 can be reformulated in the form of an SU(2) background gauge potential as $H_{LL}^{3D} = \frac{1}{2m}(\vec{p} - \frac{e}{c}\vec{A})^2 - \frac{1}{2}m\omega_{so}^2 z^2$, where $\omega_{so} = |eG|/mc$, and $\vec{A}$ takes the Landau-like gauge as $A_x = G\sigma_y z, A_y = -G\sigma_x z$ and $A_z = 0$. In Chapter 2, a symmetric-like gauge with $\vec{A}' = G\vec{\sigma} \times \vec{r}$ is used, which explicitly preserves the 3D rotational symmetry. However, the SU(2) vector potentials $\vec{A}'$ and $\vec{A}$ are *not* gauge equivalent. As shown below, the physical quantities of Eq. 3.1, such as density of states (DOS), are not 3D rotationally symmetric. Nevertheless, these two Hamiltonians belong to the same topological class. A related Hamiltonian is also employed for studying electromagnetic properties in superconductors with cylindrical geometry [66].

Eq. (3.1) can be decomposed into a set of 1D harmonic oscillators along the z-axis exhibiting flat spectra, a key feature of LLs. We define a characteristic SO length scale $l_{so} = \sqrt{\frac{\hbar}{m\omega_{so}}}$. Each of the reduced 1d harmonic oscillator Hamiltonian is associated with a 2D helical plane-wave state as $H^z(\vec{k}_{2D}) = \frac{p_z^2}{2m} + \frac{1}{2}m\omega_{so}^2[z - l_{so}^2 k_{2D}\hat{\Sigma}_{2D}(\hat{k}_{2D})]^2$, where $k_{2D} = (k_x^2 + k_y^2)^{\frac{1}{2}}$ and $\vec{k}_{2D} = (k_x, k_y)$; the helicity operator is defined as $\hat{\Sigma}_{2D}(\hat{k}_{2D}) = \hat{k}_x\sigma_y - \hat{k}_y\sigma_x$. The n-th LL eigenstates are solved as

$$\Psi_{n,\vec{k}_{2D},\Sigma}(\vec{r}) = e^{i\vec{k}_{2D}\cdot\vec{r}_{2D}}\phi_n[z - z_0(k_{2D},\Sigma)] \otimes \chi_\Sigma(\hat{k}_{2D}), \tag{3.2}$$

where $\vec{r}_{2D} = (x, y)$; $\chi_\Sigma(\hat{k}_{2D})$ are eigenstates of the helicity satisfying $\hat{\Sigma}\chi_\Sigma(\hat{k}_{2D}) = \Sigma\chi_\Sigma(\hat{k}_{2D})$ with helicity eigenvalues $\Sigma = \pm 1$; $\phi_n[z - z_0]$ are the eigenstates of the n-th harmonic levels with the central positions located at z_0, and $z_0(k_{2D},\Sigma) = \Sigma l_{so}^2 k_{2D}$. The energy spectra of the n-th LL is $E_n = (n + \frac{1}{2})\hbar\omega_{so}$, independent of $\vec{k}_{2D}$ and Σ.

The classical equations of motion for H_{LL}^{3D} are derived as

$$\begin{aligned} \dot{\vec{r}} &= \frac{\vec{p} - \frac{e}{c}\vec{A}}{m},\ \dot{\vec{p}}_{2D} = 0,\ \dot{p}_z = 2\omega(\vec{p} \times \vec{S})_z - m\omega^2 z, \\ \dot{\vec{S}}_{2D} &= -\frac{2\omega}{\hbar} z S_z \vec{p}_{2D}, \qquad \dot{S}_z = \frac{2\omega}{\hbar} z \vec{S}_{2D} \cdot \vec{p}_{2D}, \end{aligned} \tag{3.3}$$

where $\vec{S}_{2D} = (\frac{1}{2}\sigma_x, \frac{1}{2}\sigma_y)$ and $S_z = \frac{1}{2}\sigma_z$. If we choose the initial condition of spin $\vec{S}$ such that $S_{z,0} = 0$ and $\vec{S}_{2D,0} \perp \vec{p}_{2D,0}$, then $\vec{S}$ is conserved and lies in the xy-plane. The motion is reduced to a coplanar cyclotron one in the vertical plane perpendicular to $\vec{S}$. In other words, the orbital angular momentum and spin are locked, a feature from SO coupling.

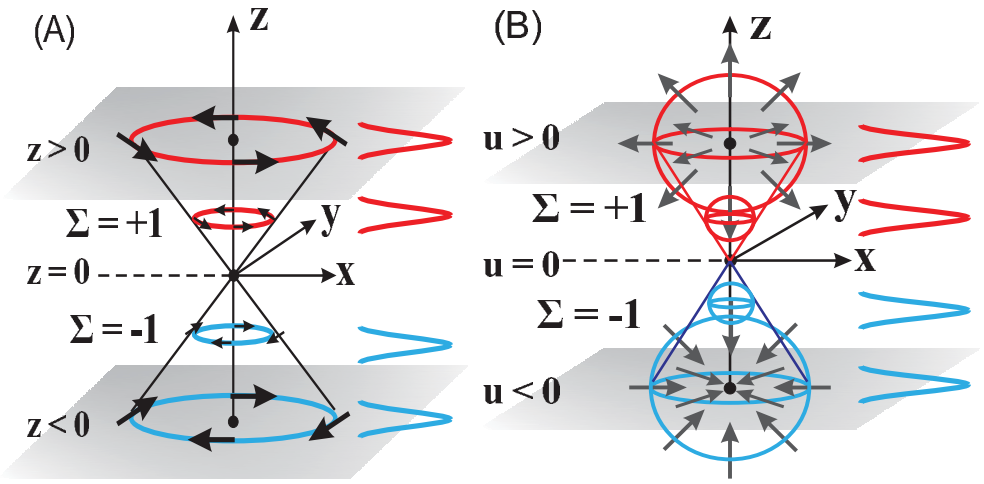

Figure 3.1: (Color online) 3D and 4D LLs for H_{LL}^{3D} and H_{LL}^{4D} as spatially separated 2D helical SO plane-wave modes localized along the z-axis (A), and 3D Weyl modes localized along the u-axis (B), respectively. Their central locations are $z_0(\vec{k}_{2D}, \Sigma) = \Sigma l_{so}^2 k_{2D}$ and $u_0(\vec{k}_{3D}, \Sigma) = \Sigma l_{so}^2 k_{3D}$, respectively. Note that 2D Dirac modes with opposite helicities and the 3D ones with opposite chiralities are located at opposite sides of $z = 0$ and $u = 0$ planes, respectively.

In the 2D LL case, the spatial coordinates x and y are non-commutative if projected to a given LL, say, the lowest LL (LLL). The LLL wavefunctions are chiral 1d plane-waves along the x-direction whose central y-position is $y_0 = l_B^2 k_x$, thus 1d chiral modes with opposite chiralities are spatially separated. Consequently, the xy-plane can be viewed as the 2D phase space of a 1d system, in which y plays the role of k_x. The momentum cut-off of the bulk states is determined by the system size along the y-direction as $|k_x| < \frac{L_y}{2l_B^2}$. Similarly, the 3D LL wavefunctions in Eq. 3.2 are spatially separated 2D helical plane-waves along the z-axis. As shown in Fig. 3.1 (A), for states with opposite helicity eigenvalues, their central positions are shifted in opposite directions. After the projection into the LLL, z is equivalent to $l_{so}^2(k_x\sigma_y - k_y\sigma_x)$, and thus

$$[x, z]_{LLL} = il_{so}^2\sigma_y, [y, z]_{LLL} = -il_{so}^2\sigma_x, [x, y]_{LLL} = 0. \tag{3.4}$$

Interestingly, the 3D LL states can be viewed as states in the 4D phase space of a 2D system (with x and y coordinates), in which $|z|$ plays the role of the magnitude of the 2D momentum. In fact, the momentum cut-off of the bulk states

is exactly determined by the spatial size L_z along the z direction as

$$k_{2D} < k_{2D}^B \equiv \frac{L_z}{2l_{so}^2}, \tag{3.5}$$

in which $-\frac{L_z}{2} < z < \frac{L_z}{2}$. Applying the open boundary condition along the z direction, and periodic boundary conditions in the x and y directions with spatial sizes L_x and L_y respectively, we can easily count the total number of states to be $\mathcal{N} = \frac{L_x L_y L_z^2}{8\pi l_{so}^4}$. The L_z^2 dependence of $\mathcal{N}$ may seem puzzling for a 3D system, but expressing L_z in terms of Eq. (3.5), we find $\mathcal{N} = \frac{1}{2\pi} L_x L_y (k_{2D}^B)^2$, which is the conventional state counting of a 2D system expressed in terms of the 4D phase space volume.

The topological property of this 3D LL system manifests through its helical surface spectra. Let us consider the upper boundary located at $z = z_B$ for H_{LL}^{3D}. For simplicity, we only consider the LLL as an example. If $z_B > 0$, the positive helicity states $\Psi_{0,\vec{k}_{2D},\Sigma=1}$ with $k_{2D} > k_{2D}^B = z_B l_{so}^{-2}$ are confined at the boundary. The 1d harmonic potential associated with $\vec{k}_{2D}$ and $\Sigma = 1$ is truncated at $z = z_B$, and thus the surface spectra acquire dispersion. If we neglect the zero-point energy, the surface mode dispersion is approximated by $\frac{1}{2} m\omega_{so}^2 (k - k_{2D}^B)^2 l_{so}^4$ with $k > k_{2D}^B$. If the chemical potential μ lies above the LLL, it cuts the spectra at surface states with a Fermi wavevector $k_f > k_{2D}^B$. The Fermi velocity is $v_f \approx m(k_f - k_{2D}^B)\omega_{so}^2 l_{so}^4$. The surface Hamiltonian is approximated as $H_{sf} \approx v_f(\vec{p} \times \vec{\sigma}) \cdot \hat{z} - \mu$ with an electron-like Fermi surface with $\Sigma = 1$. In another case, if the upper boundary is located at $z_B < 0$, then the negative helicity states $\Psi_{0,\vec{k}_{2D},\Sigma=-1}$ with $k_{2D} < k_{2D}^B$, and all the positive helicity states are pushed to the boundary as surface modes. Depending on the value of μ, we can have a hole-like Fermi surface with $\Sigma = -1$, a Dirac Fermi point, or, an electron-like Fermi surface with $\Sigma = 1$. Similarly, any other LL gives rise to a branch of gapless helical surface modes, and each filled bulk LL contributes one helical Fermi surface. For the lower boundary, the analysis is parallel to the above. Each filled LL gives rise to an electron-like helical Fermi surface with $\Sigma = -1$, or hole-like with $\Sigma = 1$.

3.3 Construction of four dimensional Landau levels with a "Landau" gauge

The above procedure can be straightforwardly generalized to any higher dimension. For example, the 4D LL Hamiltonian is denoted as

$$H_{LL}^{4D,\nu=\pm} = \frac{p_u^2}{2m} + \frac{1}{2}m\omega^2 u^2 + \frac{\vec{p}_{3D}^2}{2m} - \nu\omega u\vec{p}_{3D}\cdot\vec{\sigma}, \tag{3.6}$$

where u and p_u refer to the coordinate and momentum of the 4th dimension, respectively, and $\vec{p}_{3D}$ is the 3-momentum in the xyz-space. Without lose of the generality, let us focus on the case of $\nu = +$ and Eq. 3.6 can be represented as $H_{LL}^{4D} = \frac{1}{2m}\sum_{i=1}^{4}(p_i - \frac{e}{c}A_i)^2 - m\omega^2u^2$, where the SU(2) vector potential takes the Landau-like gauge with $A_i = G\sigma_i u$ for $i = x, y, z$ and $A_u = 0$. Eq. 3.6 preserves the translational and rotational symmetries in the xyz-space and TR symmetry. Similar to the 3D case, the 4D LL spectra and wavefunctions are solved by reducing Eq. 3.6 into a set of 1d harmonic oscillators along the u-axis as $H^u(\vec{k}_{3D}) = \frac{p_u^2}{2m} + \frac{1}{2}m\omega^2(u - l_{so}^2 k_{3D}\hat{\Sigma}_{3D})^2$ where $k_{3D} = (k_x^2 + k_y^2 + k_z^2)^{\frac{1}{2}}$ and $\hat{\Sigma}_{3D} = \hat{k}_{3D}\cdot\vec{\sigma}$. The LL wavefunctions are

$$\Psi_{n,\vec{k}_{3D},\Sigma}(\vec{r}, u) = e^{i\vec{k}_{3D}\cdot\vec{r}}\phi_n[u - u_0(k_{3D}, \Sigma)] \otimes \chi_\Sigma(\vec{k}_{3D}), \tag{3.7}$$

where, the central positions $u_0(k_{3D}, \Sigma) = \Sigma l_{so}^2 k_{3D}$; χ_Σ are eigenstates of 3D helicity $\hat{\Sigma}_{3D}$ with eigenvalues $\Sigma = \pm 1$. Inside each LL, the spectra are flat with respect to $\vec{k}_{3D}$ and Σ. This realizes the spatial separation of the 3D Weyl fermion modes as shown in Fig. 3.1 (B). After the LLL projection for H_{LL}^{4D}, the non-commutative relations among coordinates are $[r_i, u] = il_{so}^2\sigma_i$ and $[r_i, r_j] = 0$ for $i = x, y, z$. Similar to the discussions of the 3D case, the 4D LLs can be viewed as states of the 6D phase space of a 3D system: increasing the width along the u-direction corresponds to increasing the bulk momentum cut-off $k_{3D} < k_{3D}^B \equiv L_u/(2l_{so}^2)$. If the LLL is fully-filled, the total number of states is given by $\mathcal{N} = \frac{L_x L_y L_z L_u^3}{24\pi^2 l_{so}^6}$. Re-expressing $L_u = 2k_{3D}^B l_{so}^2$ we find $\mathcal{N} = \frac{1}{3\pi^2}L_x L_y L_z (k_{3D}^B)^3$, which is the conventional state counting of a 3D system expressed in terms of the 6D phase space volume. With an open boundary imposed along the u direction, 3D helical Weyl fermion modes appear on the boundary.

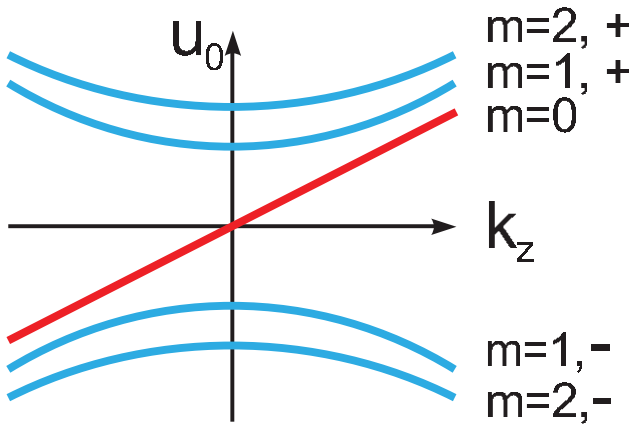

Figure 3.2: The central positions $u_0(m, k_z, \nu)$ of the 4D LLs in the presence of the magnetic field $\vec{B} = B\hat{z}$. The branch of $m = 0$ runs across the entire u-axis, which gives rise to quantized charge transport along u-axis in the presence of $\vec{E} \parallel \vec{B}$ as indicated in Eq. 3.10.

Now let us consider the generalized 4D QHE[57, 22] as the nonlinear electromagnetic response of $(4+1)$D LL system to the external electric and magnetic (EM) fields, with $\vec{E} \parallel \vec{B}$ in the xyz-space. Without loss of generality, we choose the EM fields as $\vec{E} = E\hat{z}$ and $\vec{B} = B\hat{z}$, which are minimally coupled to the spin-1/2 fermion,

$$H_{LL}^{4D}(E,B) = -\frac{\hbar^2}{2m}\nabla_u^2 + \frac{1}{2}m\omega^2\Big(u + il_{so}^2\vec{D}\cdot\vec{\sigma}\Big)^2, \tag{3.8}$$

where $\vec{D} = \vec{\nabla} - i\frac{e}{\hbar c}\vec{A}_{em}$. Here $\vec{A}_{em}$ is the $U(1)$ magnetic vector potential in the Landau gauge with $A_{em,x} = 0, A_{em,y} = Bx$ and $A_{em,z} = -cEt$. We define $l_B = \sqrt{\frac{\hbar c}{eB}}$, where $eB > 0$ is assumed.

The $\vec{B}$-field further reorganizes the chiral plane-wave states inside the n-th 4D LL into a series of 2D magnetic LLs in the xy-plane. For the moment, let us set $E_z = 0$. The eigenvalues $E_n = (n + \frac{1}{2})\hbar\omega_{so}$ remain the same as before without splitting, while the eigen-wavefunctions are changed. We introduce a magnetic LL index m in the xy-plane. For the case of $m = 0$, the eigen-wavefunctions are spin polarized as

$$\begin{aligned}\Psi_{n,m=0}(k_y,k_z) &= e^{ik_y y + ik_z z}\phi_n[u - u_0(k_z, m=0)] \\ &\otimes \chi_{m=0}[x - x_0(k_y)],\end{aligned} \tag{3.9}$$

where $x_0 = l_B^2 k_y$ and $\chi_0 = [\phi_0(x - x_0), 0]^T$ is the zero mode channel of the operator $-i\vec{D}\cdot\vec{\sigma}$ with the eigenvalue of $\lambda_0 = k_z$. The central positions of the u-direction harmonic oscillators are $u_0(k_z, m = 0) = l_{so}^2 k_z$. For $m \geq 1$, the eigen-modes of $-i\vec{D}\cdot\vec{\sigma}$ come in pairs as $\chi_{m,\pm}[x - x_0(k_y)] = [\alpha_{m,\pm}\phi_m(x - x_0), \beta_m\phi_{m-1}(x - x_0)]^T$, where, coefficients $\alpha_{m,\pm} = l_B k_z \pm \sqrt{l_B^2 k_z^2 + 2m}$, $\beta_m = -i\sqrt{2m}$, and the eigenvalues are $\lambda_{m,\pm} = \pm\sqrt{k_z^2 + 2ml_B^{-2}}$. The corresponding eigen-wavefunctions are $\Psi_{n,m,\pm}(k_y, k_z) = e^{ik_y y + ik_z z}\phi_n[u - u_0(k_z, m, \pm)]\chi_{m,\pm}[x - x_0(k_y)]$, where the central positions $u_0(k_z, m, \pm) = \pm l_{so}^2\sqrt{k_z^2 + 2ml_B^{-2}}$.

For the solutions of Eq. 3.9 with the same 4D LL index n, the 2D magnetic LLs with index $m = 0$ are singled out. The central positions of states in this branch are linear with k_z, and thus run across the entire u-axis, while those of other branches with $m \geq 1$ only lie in one half of the space as shown in Fig. 3.2. After turning on E_z, k_z is accelerated with time as $k_z(t) = k_z(0) + eE_z t/\hbar$, and thus the central positions $u_0(m = 0, k_z)$ moves along the u-axis. Only the $m = 0$ branch of the magnetic LL states contribute to the charge pumping which results in an electric current along the u-direction. Within the time interval Δt, the number of states with each filled 4D LL passing a cross section perpendicular to the u-axis is $N = \frac{L_x L_y}{2\pi l_B^2}\frac{eE\Delta t L_z}{2\pi}$, which results in the electric current density $\frac{e}{L_x L_y L_z}\frac{dN}{dt}$. If the number of fully filled 4D LLs is n_{occ}, the total current density along the u-axis is

$$j_u = n_{occ}\alpha\frac{e}{4\pi^2\hbar}\vec{E}\cdot\vec{B}, \tag{3.10}$$

where $\alpha = e^2/(\hbar c)$ is the fine-structure constant. This quantized non-linear electromagnetic response is in agreement with results from the effective theory [22] as the 4D generalization of the QH effect. If we impose open boundary conditions perpendicular to the u-direction, the above charge pump process corresponds to the chiral anomalies of Weyl fermions with opposite chiralities on the two 3D boundaries, respectively. Since they are spatially separated, the chiral current corresponds to the electric current along the u-direction.

Although the DOS of our 4D LL systems is different from the 4D TIs in the lattice system with translational symmetry [22], their electromagnetic responses obey the same Eq. 3.10. It is because that only the spin-polarized $m = 0$ branch of LLs, $\Psi_{n,m=0}(k_y, k_z)$, is responsible for the charge pumping. For this branch,

B_z-field quantizes the motion in the xy-plane so that the x and u coordinates play the role of k_y and k_z, respectively. Consequently, the system can be viewed as the 4D phase space of coordinates y and z, and scales uniformly as $L_xL_yL_zL_u$ with the conventional thermodynamic limit of a 4D system.

3.4 High dimensional LLs of Dirac electrons

The above procedure can be generalized to Dirac fermions as square root problems to Eq. (3.1) and Eq. (3.6). For the 3D case, we have

$$H^{3D}_{LL,Dirac} = \frac{l_{so}\omega_{so}}{\sqrt{2}} \begin{bmatrix} 0 & \vec{\sigma}\cdot\vec{p} + i\frac{z\hbar}{l^2_{so}}\sigma_z \\ \vec{\sigma}\cdot\vec{p} - i\frac{z\hbar}{l^2_{so}}\sigma_z & 0 \end{bmatrix}, \tag{3.11}$$

whose square exhibits a diagonal block form with a super-symmetric structure as $(H^{3D}_{Dirac})^2/(\hbar\omega_{so}) = \mathrm{diag}(H^{3D,+}_{LL} - \frac{\hbar\omega_{so}}{2}, H^{3D,-}_{LL} + \frac{\hbar\omega_{so}}{2})$. The eigenvalues of Eq. (3.11) are $E_{\pm n} = \pm\sqrt{n}\hbar\omega_{so}$. The eigen-wavefunctions are constructed based on the eigenstates of $H^{3D,\nu=\pm}_{LL}$ as $\Psi^{3D}_{\pm n,Dirac}(\vec{k}_{2D},\Sigma) = \frac{1}{\sqrt{2}}[\Psi^{+}_{n,\vec{k}_{2D},\Sigma}, \pm\Psi^{-}_{n-1,\vec{k}_{2D},-\Sigma}]^T$, where $\Psi^{-}_{n,\vec{k}_{2D},\Sigma} = e^{i\vec{k}_{2D}\cdot\vec{r}_{2D}}\phi_n[z + z_0(k_{2D},\Sigma)] \otimes \chi_\Sigma(\hat{k}_{2D})$ is the eigenstate of $H^{3D,-}_{LL}$. The 0th LL states are Jackiw-Rebbi half-fermion modes with only the upper two components nonzero [85, 86]. The 4D Hamiltonian can be constructed as

$$H^{4D}_{LL,Dirac} = \frac{l_{so}\omega_{so}}{\sqrt{2}} \begin{bmatrix} 0 & \vec{\sigma}\cdot\vec{p}_{3D} - i\frac{a_u}{l_{so}} \\ \vec{\sigma}\cdot\vec{p}_{3D} + i\frac{a^\dagger_u}{l_{so}} & 0 \end{bmatrix}, \tag{3.12}$$

where $a_u = \frac{1}{\sqrt{2}l_{so}}(u + i\frac{l^2_{so}}{\hbar}p_u)$ is the phonon annihilation operator in the u-direction. The eigen-values are still $E_{\pm n} = \pm\sqrt{n}\hbar\omega_{so}$, and the eigenstates are

$$\Psi^{4D}_{\pm n,Dirac}(\vec{k}_{3D},\Sigma) = \frac{1}{\sqrt{2}}[\Psi^{+}_{n,\vec{k}_{2D},\Sigma}, \pm\Psi^{+}_{n-1,\vec{k}_{2D},\Sigma}]^T. \tag{3.13}$$

3.5 Laughlin-type wavefunctions

The construction of the Laughlin-type wavefunctions for interacting fermions is difficult for these SO coupled high dimensional LL systems. Nevertheless, for the 4D case in the magnetic field, the LLL states with both $n = 0$ and $m = 0$ are

spin-polarized, and their total DOS is finite as $\rho^{4D}_{n=m=0} = \frac{1}{4\pi^2 l_{so}^2 l_B^2}$. Even though they are degenerate with other LLL states with $(n = 0, m \neq 0)$, they are favored by repulsive interactions if they are partially filled. The Laughlin wavefunction in the Landau gauge for the 2D LLs has been constructed in Ref. [87]. We generalize it to the 4D case, and define $w = e^{i\frac{x+iy}{L_x}}$ and $v = e^{i\frac{z+iu}{L_z}}$, then LL states are represented as $w^{h_x}v^{h_z}$ up to a Gaussian factor $e^{-\frac{u^2}{2l_{so}}-\frac{y^2}{2l_B^2}}$. The Laughlin-type wavefunction can be constructed as

$$\Psi(w_1, v_1; ...; w_{N_x N_y}, v_{N_x N_y}) \quad = \quad (\det[w_i^{h_x} v_i^{h_z}])^q, \tag{3.14}$$

where q is an odd number; $\det[w_i^{h_x} v_i^{h_z}]$ represents the Slater determinant for the fully filled single particle states $w^{h_x}v^{h_z}$ and $0 \leq h_x \leq N_x - 1$ and $0 \leq h_z \leq N_z - 1$. The study of the topological properties of Eq. 3.14 will be deferred to a later publication.

3.6 Summary

We have generalized LLs into 3D and 4D in the Landau-like gauge by coupling spatially dependent SO couplings with harmonic potentials. This method can be generalized to arbitrary dimensions by replacing the Pauli-matrices with the Γ-matrices in corresponding dimensions. These high dimensional LLs exhibit spatial separation of helical or chiral fermion modes with opposite helicities, which give rises to gapless helical or chiral boundary modes. The 4D LLs give rise to the quantized non-linear electromagnetic responses as a spatially separated (3+1)D chiral anomaly.

Acknowledgements: We thank helpful discussions and early collaborations with Jorge Hirsch. And I am indebt to Nai Phuan Ong and Zhong Wang for helpful advices and the Inamori Fellowship. This chapter is in part of a paper being submitted for publication at Physical Review series, "Topological insulators with SU(2) Landau levels", authored by Yi Li, Shou-Cheng Zhang, and Congjun Wu.

Chapter 4

2D and 3D topological insulators with isotropic and parity-breaking Landau levels

4.1 Introduction

The study of topological insulators has become an important research focus in condensed matter physics [25, 26]. Historically, the research of topological band insulators started from the two dimensional (2D) quantum Hall effect. Landau level (LL) quantization gives rise to nontrivial band topology characterized by integer-valued Chern numbers. [7, 11] In fact, LLs are not the only possibility for realizing topological band structures. Quantum anomalous Hall band insulators with the regular Bloch-wave structure are in the same topological class as 2D LL systems in magnetic fields [8]. Later developments generalize the anomalous Hall insulators to time-reversal (TR) invariant systems in both two and three dimensions. [21, 16, 17, 15, 18, 19, 20, 22, 24] This is a new class of topological band insulators with TR symmetry which are characterized by the Z_2 index. Experimentally, the most obvious signatures of band topology appear on open boundaries, in which they exhibit helical edge or surface states. Various 2D and 3D materials are identified as topological insulators, and their stable helical boundary modes have been detected [27, 31, 77, 32, 33, 88]. Furthermore, systematic classifications have been performed

in topological insulators and superconductors in all the spatial dimensions, which contain ten different universal classes [41, 79].

Although the current research is mostly interested in topological insulators with Bloch-wave band structures, the advantages of LLs make them appealing for further studies. We use the terminology of LLs here in the following general sense not just for the usual 2D LLs in magnetic fields: *topological* single-particle level structures labeled by *angular momentum* quantum numbers with flat or nearly flat spectra. On open boundaries, LL systems develop gapless surface or edge modes which are robust against disorders. For example, in the 2D quantum Hall LL systems, chiral edge states are responsible for quantized charge transport. For the 2D LL based quantum spin Hall systems, helical edge modes are robust against TR-invariant disorders [21]. Similar topological properties are expected for even high-dimensional LL systems, which exhibit stable gapless surface modes. For the usual 2D LLs, the symmetric gauge is used in which angular momentum is conserved. We do not use the Landau gauge because it does not maintain rotational symmetry explicitly. LL wavefunctions are simple and explicit, and their elegant analytical properties nicely provide a platform for further study of topological many-body states in high dimensions.

Generalizing LLs to high dimensions started by Zhang and Hu [57] on the compact S^4 sphere by coupling large spin fermions to the SU(2) magnetic monopole, where fermion spin scales with the radius as R^2. Later on various generalizations to other manifold were developed. [80, 59, 61, 62, 60] The LLs of non-relativistic fermions have been generalized to arbitrary dimensional flat space R^D in Chapter 2. The general strategy is very simple: the harmonic oscillator plus spin-orbit (SO) coupling $L_{ij}\Gamma_{ij}$, where L_{ij} and Γ_{ij} are the orbital and spin angular momenta in a general dimension. Reducing back to two dimensions, it becomes the quantum spin Hall Hamiltonian in which each spin component exhibits the usual 2D LLs in the symmetric gauge, but the chiralities are opposite for two spin components [15]. For a concrete example, say, in three dimensions, each LL contributes a branch of helical Dirac surface modes at the open boundary, thus its topology belong to the Z_2-class. Furthermore, LLs have also been constructed to arbitrary dimensional flat spaces for relativistic fermions [83], which is a square root prob-

lem of the above non-relativistic cases. It is a generalization of the quantum Hall effect in graphene [89, 90, 91] to high dimensional systems with the full rotational symmetry. This construction can also be viewed as a generalization of the Dirac equation from momentum space to phase space by replacing the momentum operator with the creation and annihilation operators of phonons. The zero-energy LL is a branch of half-fermion modes. When it is empty or fully occupied, fermions are pumped from the vacuum, a generalization of parity anomaly [92, 93, 94, 95] to high dimensions.

In this chapter, we study another class of isotropic LLs with TR symmetry but breaking parity in two and three dimensions, which can also be straightforwardly generalized to arbitrary dimensions. The Hamiltonians are again harmonic oscillator plus SO couplings, but here the SO coupling is the coupling between spin and linear momentum, not orbital momentum. In 2D, it is simply the standard Rashba SO coupling, and in 3D it is the $\vec{\sigma} \cdot \vec{p}$-type SO coupling. In both cases, parity is broken. The strong SO coupling provides the projection of the low energy Hilbert space composed of states with the proper helicity. The radial quantization from the harmonic potential further generates gaps between LLs. The SO coupling strongly suppresses the dispersion with respect to the angular momentum within each LL. In two and three dimensions, they exhibit gapless helical boundary modes which are stable against TR-invariant perturbations, thus they belong to the Z_2 topological class. In fact, parent Hamiltonians, whose first LL wavefunctions are obtained analytically and whose spectra are exactly flat, can be constructed by the dimensional reduction method from the high-dimensional LL Hamiltonians constructed in Chapter 2.

This chapter is organized as follows. The study of isotropic and TR-invariant LLs with parity breaking is presented in Sect. 4.2. The generalization to three dimensions is given in Sec. 4.3. The experimental realization of the 3D Rashba-like $\vec{\sigma} \cdot \vec{p}$ -type SO coupling is performed in Sec. 4.4. Conclusions and outlook are summarized in Sec. 4.5.

4.2 Two-dimensional spin-orbit coupled Landau levels with harmonic potential

In this section, we consider the Hamiltonian of Rashba SO coupling combined with a harmonic potential

$$H_{2D} = -\frac{\hbar^2\nabla^2}{2m} + \frac{1}{2}m\omega^2 r^2 - \lambda(-i\hbar\nabla_x\sigma_y + i\hbar\nabla_y\sigma_x), \tag{4.1}$$

where ω is the trapping frequency; λ is the SO coupling strength with the unit of velocity. Equation (4.1) is invariant under the $SO(2)$ rotation and the vertical-plane mirror reflection. In other words, the system enjoys $C_{v\infty}$ symmetry. Equation (4.1) also satisfies the TR symmetry of fermions, *i.e.*, $T = i\sigma_2 K$, with $T^2 = -1$ and K the complex conjugation. However, parity symmetry is broken explicitly by the Rashba term.

Equation 4.1 can be realized in solid-state quantum wells and ultra-cold atomic traps. Rashba SO coupling due to inversion symmetry breaking at 2D interfaces has been studied extensively in the condensed matter literature; [96] its energy scale can reach very large values. [97] Furthermore, Wigner crystallization in the presence of Rashba SO coupling has been studied. [98] In the context of ultra cold atoms, Bose-Einstein condensation with Rashba SO coupling plus harmonic potential was studied by Wu and Mondragon in Ref. [99], in which the spontaneous generation of a half-quantum vortex is found. Later, there was great experimental progress in generating a synthetic gauge field from light-atom interaction, [72] which inspired a great deal of theoretical interest. [100, 101, 102, 103, 104, 105]

4.2.1 Energy spectra

In a homogeneous system with Rashba SO coupling, *i.e.*, $\omega = 0$ in Eq. (4.1), the single-particle states $\psi_\pm(\vec{k})$ are eigenstates of the helicity operator $\vec{\sigma}\cdot(\vec{k}\times\hat{z})$ with eigenvalues ± 1, respectively. The spectra for these two branches are $\epsilon_\pm(\vec{k}) = \hbar^2(k \mp k_0)^2/(2m)$, and the lowest energy states are located around a ring with radius $k_0 = m\lambda/\hbar$ in momentum space. Such a system has two length scales: the characteristic length of the harmonic trap $l_T = \sqrt{\frac{\hbar}{m\omega}}$, and the SO length scale

$l_{so} = 1/k_0$. The dimensionless parameter $\alpha = l_T/l_{so}$ describes the SO coupling strength with respect to the harmonic potential.

As presented in Ref. [106] for the case of strong SO coupling, *i.e.*, $\alpha \gg 1$, the physics picture is mostly clear in momentum representation. The lowest energy states are reorganized from the plane-wave states $\psi_+(\vec{k})$ with $\vec{k}$ near the SO ring. Energetically, these states are separated from the opposite-helicity ones $\psi_-(\vec{k})$ at the order of $E_{so} = \hbar k_0 \lambda = \alpha^2 E_{tp}$, where $E_{tp} = \hbar\omega$ is the scale of the trapping energy. As shown below, the band gap in such a system is at the scale of E_{tp}. Since $\alpha \gg 1$, we can safely project out the negative helicity states $\psi_-(\vec{k})$. After the projection, the harmonic potential in momentum representation becomes Laplacian coupled to a Berry connection $\vec{A}_k$ as

$$V_{tp} = \frac{m}{2}\omega^2(i\vec{\nabla}_k - \vec{A}_k)^2, \tag{4.2}$$

which drives particle moving around the ring with a moment of inertial $I = M_k k_0^2$; $M_k = \hbar^2/(m\omega^2)$ is the effective mass in momentum representation. The Berry connection A_k is defined as

$$\vec{A}_k = i\langle\psi_{k+}|\vec{\nabla}_k|\psi_{k+}\rangle = \frac{1}{2k}\hat{e}_k, \tag{4.3}$$

where $|\psi_{k+}\rangle$ is the lower branch eigenstate with momentum $\vec{k}$. It is well known that for the Rashba Hamiltonian, the Berry connection A_k gives rise to a π flux at $\vec{k} = (0,0)$ but without Berry curvature at $\vec{k} \neq 0$. [107] This is because a two-component spinor after a 360° rotation does not come back to itself but acquires a minus sign.

The crucial effect of the π flux in momentum space is that the angular momentum eigenvalues become half-integers as $j_z = m + \frac{1}{2}$. The angular dispersion of the spectra becomes $E_{agl}(j_z) = \hbar^2 j_z^2/2I = (j_z^2/2\alpha^2)E_{tp}$. On the other hand, the radial potential in momentum representation is $V(k) = \frac{1}{2}M_k\omega^2(k-k_0)^2$ for positive-helicity states. For states with energies much lower than E_{so}, we approximate $V(k)$ as harmonic potential, thus the radial quantization is $E_{rad}(n_r) = (n_r + \frac{1}{2})E_{tp}$ up to a constant. The same dispersion structure was also noted in recent works [102, 104, 103], which show

$$E_{n_r,j_z} \approx \Big(n_r + \frac{1}{2} - \frac{\alpha^2}{2} + \frac{j_z^2}{2\alpha^2}\Big)E_{tp}, \tag{4.4}$$

where the zero point energy is restored here. Since $\alpha \gg 1$, we treat n_r as a band index and j_z as a good quantum number for labeling states inside each band.

4.2.2 Dimensional reduction from the 3D Landau level Hamiltonian

Equation (4.1) not only can be introduced from the solid-state and cold atom physics contexts, but also can be viewed as a result of dimensional reduction from a 3D LL Hamiltonian [Eq. (4.5)] proposed in Chapter 2. This method builds up the connection of two topological Hamiltonians in three dimensions with inversion symmetry and two dimensons with inversion symmetry breaking. The resultant 2D Hamiltonian Eq. (4.7) exhibits the same physics that Eq. (4.1) does for eigenstates with $j_z < \alpha$ in the case of $\alpha \gg 1$. The advantage of Eq. (4.7) is that its lowest LL wavefunctions are analytically solvable and their spectra are flat.

Just like the usual 2D LL Hamiltonian in the symmetric gauge, which is equivalent to a 2D harmonic oscillator plus the orbital Zeeman term, the 3D LL Hamiltonian is as simple as a 3D harmonic potential plus SO coupling as explained in Chapter 2,

$$H_{3D,LL} = \frac{p^2}{2m} + \frac{1}{2}m\omega^2 r^2 - \omega \vec{L} \cdot \vec{\sigma}, \tag{4.5}$$

which possesses 3D rotational symmetry and TR symmetry. Its eigen-solutions are classified into positive- and negative-helicity channels according to the eigenvalues of $\vec{\sigma} \cdot \vec{L} = l\hbar$ or $-(l+1)\hbar$, respectively. In the positive (negative)-helicity channel, the total angular momentum $j_\pm = (l \pm \frac{1}{2})\hbar$. The spectra in the positive-helicity channel, $E_{n_r,l} = (2n_r + \frac{3}{2})\hbar\omega$, are dispersionless with respect to the value of j_+, thus these states are LLs. In the presence of an open boundary, each filled LL contributes a branch of helical Dirac Fermi surface described as

$$H_{sf} = v_f(\vec{\sigma} \times \vec{p}) \cdot \hat{e}_r - \mu, \tag{4.6}$$

where $\hat{e}_r$ is the local normal direction of the surface, v_f the Fermi velocity, and μ the chemical potential. The stability of surface states under TR-invariant perturbations are characterized by the Z_2 topological index.

Now let us perform the dimension reduction on Eq. (4.5) by cutting a 2D off-centered plane perpendicular to the z-axis with the interception z_0. Within this 2D plane of $z = z_0$, Eq. (4.5) reduces to

$$H_{2D,re} \;=\; H_{2D} - \omega L_z \sigma_z. \tag{4.7}$$

The first term is just Eq. (4.1) with Rashba SO strength $\lambda = \omega z_0$, and the 2D harmonic trap frequency is the same as the coefficient of the $L_z\sigma_z$ term. The dimensionless parameter $\alpha = l_T/l_{so} = |z_0|/l_T$. If $z_0 = 0$, Rashba SO coupling vanishes. In this case, Eq. (4.7) becomes the 2D quantum spin Hall Hamiltonian proposed in Ref. [21], which is a double copy of the usual 2D LL with opposite chiralities for spin-up and -down components. At $z_0 \neq 0$, Rashba coupling appears which breaks the conservation of σ_z.

The lowest LL solutions have been found for Eq. (4.5), whose center is shifted from the origin to $\vec{r}_c = (0, 0, z_0)$ in Chapter 2. These states do not keep j conserved but do maintain j_z as a good quantum number as

$$\begin{aligned} \psi_{3D,j_z,z_0}(\rho,\phi,z) \;&=\; e^{-\frac{\rho^2+(z-z_0)^2}{2l_T^2}} e^{im\phi} \\ &\times \begin{pmatrix} J_m(k_0\rho) \\ -\mathrm{sgn}(z_0) e^{i\phi} J_{m+1}(k_0\rho) \end{pmatrix}, \end{aligned} \tag{4.8}$$

where $\rho = \sqrt{x^2+y^2}$; $j_z = m + \frac{1}{2}$; $k_0 = z_0/l_T^2$; and ϕ is the azimuthal angle around the z axis. The ψ_{3D,j_z,z_0}'s form a complete set of the lowest LL wave functions, but they are nonorthogonal if their j_z's are the same. By setting $z = z_0$ in the above wavefunctions, we define the 2D reduced wave functions as

$$\psi_{2D,j_z}(\rho,\phi) = e^{-\frac{\rho^2}{2l_T^2}} \begin{pmatrix} e^{im\phi} J_m(k_0\rho) \\ -\mathrm{sgn}(z_0) e^{i(m+1)\phi} J_{m+1}(k_0\rho) \end{pmatrix}. \tag{4.9}$$

Noticing that $\partial_z \psi_{3D,j_z,z_0}|_{z=z_0} = 0$, it is straightforward to check that ψ_{2D,j_z}'s are solutions for the lowest LLs for the 2D reduced Hamiltonian in Eq. (4.7) as

$$H_{2D,re}\ \psi_{2D,j_z} = \Big(1 - \frac{\alpha^2}{2}\Big)\hbar\omega\ \psi_{2D,j_z}. \tag{4.10}$$

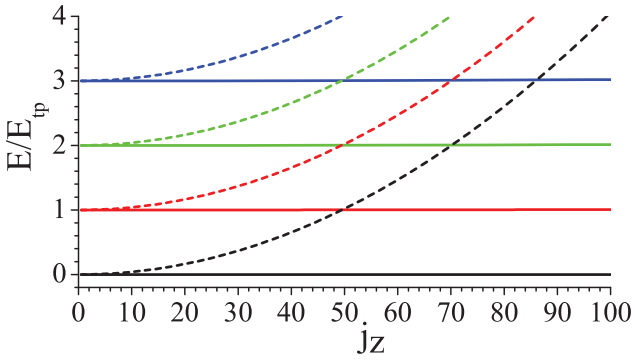

Figure 4.1: (Color online) Energy dispersions of the solutions for the first four LLs to the 2D reduced Hamiltonian Eq. (4.7) (solid lines), and those for (Eq. 4.1) (dashed lines). The value of $\alpha = l_T/l_{so} = 35$. The lowest LLs of Eq. (4.7) are dispersionless with respect to j_z. Please note that the overall shift of the zero-point energy difference $\frac{1}{2}\hbar\omega$ is performed for the spectra of Eq. (4.1) for a better illustration.

The TR partner of Eq. (4.9) can be written as

$$\begin{aligned}\psi_{2D,-j_z}(\rho,\phi) &= e^{-\frac{\rho^2}{2l_T^2}}\begin{pmatrix}\mathrm{sgn}(z_0)e^{-i(m+1)\phi}J_{m+1}(k_0\rho)\\ e^{-im\phi}J_m(k_0\rho)\end{pmatrix}\\ &= (-)^{m+1}\mathrm{sgn}(z_0)e^{-\frac{\rho^2}{2l_T^2}}\begin{pmatrix}e^{-i(m+1)\phi}J_{-(m+1)}(k_0\rho)\\ -\mathrm{sgn}(z_0)e^{-im\phi}J_{-m}(k_0\rho)\end{pmatrix}. \quad (4.11)\end{aligned}$$

4.2.3 Relation between Eq. (4.1) and Eq. (4.7)

The difference between the two Hamiltonians, Eq. (4.7) and (Eq. 4.1), is the $L_z\sigma_z$ term. Its effect depends on the distance ρ from the center. We are interested in the case of $|z_0| \gg l_T$, *i.e.*, $\alpha \gg 1$. Let us first consider the lowest LL. With small values of j_z, *i.e.*, $m < \alpha$, $J_m(k_0\rho)$ and $J_{m+1}(k_0\rho)$ already decay before reaching the characteristic length l_T of the Gaussian factor. We approximate their classic orbital radii as the locations of the maxima of Bessel functions, which are roughly $\rho_{c,j_z} \approx \frac{m}{\alpha}l_T < l_T$. In this regime, the effect of $L_z\sigma_z$ compared to the Rashba part is a small perturbation, of the order of $\omega\rho_{c,j_z}/\lambda = \rho_{c,j_z}/z_0 \ll 1$. Thus, these two Hamiltonians share the same physics. On the other hand, let us consider the case of very large values of j_z, say, $m \gg \alpha^2$. The Bessel function behaves like ρ^m or ρ^{m+1} at $0 < \rho < \frac{m}{\alpha}l_T$. The classic orbit radii are just $\rho_{c,j_z} \approx \sqrt{m}l_T$. The physics

of Eq. (4.7) in this regime is dominated by the $L_z\sigma_z$ term and, thus, is the same as that of 2D quantum spin Hall LL wave functions. However, for Eq. (4.1), the projection to the sub-Hilbert space spanned by $\psi_+(\vec{k})$ is not valid. Its eigenstates in this regime cannot be viewed as LLs anymore. For intermediate values of j_z, i.e., $\alpha < m < \alpha^2$, the physics is a crossover between the above two limits.

For higher LLs of Eqs. (4.7) and (4.1), we expect that their wave functions can be approximated by a form of Eq. (4.9) by multiplying a polynomial of ρ at the n_r-th power. As a result, the physics is similar to what is analyzed in the previous paragraph. At small values of $j_z < \alpha$, the energy gap is quantized in terms of the unit of $E_{tp} = \hbar\omega$ as in Eq. (4.4) for both Hamiltonians. At very large values of $j_z \gg \alpha^2$, the LLs of Eq. (4.7) become flat again and the quantization gap is at $2E_{tp} = 2\hbar\omega$.

We perform the numerical calculation of the energy levels of the reduced 2D Hamiltonian Eq. (4.7), as plotted in Fig. 4.1. The numerically calculated spectra of Eq. 4.1, which were plotted in Refs. [102] and [104], are also presented for comparison. Only the spectra of $j_z > 0$ are plotted, and those of $j_z < 0$ are degenerate with their partners by the TR transformation which flips the sign of j_z. The lowest LL of Eq. (4.7) is flat as expected, while higher LLs are weakly dispersive which is hardly observable for the range of j_z presented. The LLs of Eq. (4.1) are dispersive with the dependence on j_z shown in Eq. (4.4). Inside the gaps between adjacent LLs of Eq. (4.1), the number of states is of the order of α.

4.2.4 The Z_2 nature of the topological properties

Due to their connection to the 2D reduced version of the LL Hamiltonian, we still denote the low-energy bands of Eq. (4.1) as 2D parity breaking LLs. As shown in Eq. (4.4), although these LLs are not exactly flat, their dispersion over j_z is strongly suppressed by the large value of α. If the chemical potential μ lies in the middle of the band gap, the Fermi angular momentum $j_{kf,z}$ is at the order of α. The classic radius of such a state is roughly l_T. As analyzed in Sec. 4.2.2, for states with $|j_z| < \alpha$, two Hamiltonians Eqs. (4.1) and (4.7) share the same physics.

Compared to the usual 2D LL states, the SO coupled LLs of Eq. (4.1) in the form of Eq. (4.9) are markedly different. The smallest length scale is not l_T, but the SO coupling length scale $l_{so} = l_T/\alpha \ll l_T$. Instead, we can use l_T as the cut-off of the sample size by imposing an open boundary condition at the radius of l_T. States with $|j_z| < \alpha$ are considered as bulk states which localize within the region of $\rho < l_T$. States with $|j_z| \sim \alpha$ are edge states.

We take the thermodynamic limit as follows. First, ω is fixed, which determines the LL gaps. Then we set $m \to 0$ and $\lambda \to \infty$ while keeping $l_{so} = \hbar/(m\lambda)$ unchanged, such that $l_T = \sqrt{\frac{\hbar}{m\omega}} \to \infty$. The number of bulk states scales linearly with α, and the level spacing scales as $1/\alpha \to 0$ at the Fermi angular momentum $j_{k_f,z} \sim \alpha$.

The next important question is the stability of the gapless edge modes. This situation is different from the usual 2D LL problem, in which inside each LL for each value of angular momentum m, there is only one state. Those edge modes are chiral and, thus, robust against external perturbations. Since Eq. (4.1) is TR symmetric, for each filled LL there is always a pair of degenerate edge modes $\psi_{n_r,\pm j_z}$ on the Fermi energy, where n_r is the LL index. Nevertheless, these two states are Kramer pairs under the TR transformation satisfying $T^2 = -1$. In other words, the edge modes are helical rather than chiral.

We generalize the reasoning in Ref. [16] and [17] for topological insulators with good quantum numbers of lattice momenta to our case with angular momentum good quantum numbers. Any TR-invariant perturbation cannot mix these two states to open a gap. In other words, the mixing term,

$$H_{mx} = g(\psi^\dagger_{2D,n_r,j_z}\psi_{2D,n_r,-j_z} + h.c.), \tag{4.12}$$

is forbidden by TR symmetry. On the other hand, if two LLs with indices n_r and n_r' cut the Fermi energy, the mixing term,

$$\begin{aligned} H_{mx} &= g'(\psi^\dagger_{2D,n_r,j_z}\psi_{2D,n_r',-j_z} - \psi^\dagger_{2D,n_r',j_z}\psi_{2D,n_r,-j_z} \\ &+ h.c.), \end{aligned} \tag{4.13}$$

is allowed by TR symmetry and opens the gap. Consequently, the topological nature of such a system is characterized by the Z_2 index, even though it is not

clear how to define the Pfaffian-like formula for it due to the lack of translational symmetry. [17] Similarly to the 2D topological insulators based on lattice Bloch-wave states, in our case, if odd numbers of LLs are filled such that there are odd numbers of helical edge modes, the gapless edge modes are robust.

Imagining an open boundary at $\rho \approx l_T$, we derive an effective edge Hamiltonian for these helical edge modes. As $|j_z| \sim \alpha$ and taking the limit of $\alpha \to +\infty$, these edge modes are pushed to the boundary. We expand the spectra around $j_{z,fm}$. The edge Hamiltonian in the basis of j_z can be written as

$$H_{edge} = \sum_{j_z} (\frac{\hbar v_f}{l_T}|j_z| - \mu)\psi^{\dagger}_{n_r,j_z}\psi_{n_r,j_z} \tag{4.14}$$

where $\mu = \frac{\hbar v_f}{l_T} j_{z,fm}$. The edge modes $\psi_{n_r,\pm j_z}$ around $j_{z,fm}$ can also be expanded as

$$\psi_{n_r,j_z} = \begin{pmatrix} f_{n_r} e^{im\phi} \\ g_{n_r} e^{i(m+1)\phi} \end{pmatrix}, \quad \psi_{n_r,-j_z} = T\psi_{n_r,j_z}. \tag{4.15}$$

f_{n_r} and g_{n_r} are real numbers parameterized as

$$f_{n_r} = \cos\frac{\theta_{n_r}}{2}, \quad g_{n_r} = \sin\frac{\theta_{n_r}}{2}, \tag{4.16}$$

which are determined by the details of the edge. We neglect their dependence on $|j_z|$ for states close enough to the Fermi energy. The effective edge Hamiltonian can also be expressed in the plane-wave basis if we locally treat the edge as flat

$$\begin{aligned} H_{n_r,edge} &= v_f \Big(\sin\theta_{n_r}[(\vec{p}\times\hat{e}_r)\cdot\hat{z})](\vec{\sigma}\cdot\hat{e}_r) \\ &+ \cos\theta_{n_r}(\vec{p}\times\hat{e}_r)\cdot\sigma_z \Big) - \mu, \end{aligned} \tag{4.17}$$

where $\hat{e}_r$ is the local normal direction on the circular edge; both terms are allowed by rotational symmetry, TR symmetry, and the vertical mirror symmetry in such a system. Each edge channel is a branch of helical one-dimensional Dirac fermion modes.

Equation (4.1) can be defined on the compact S^2 sphere, which takes the simple form

$$H = \frac{L^2}{2I} - \omega\vec{L}\cdot\vec{\sigma}. \tag{4.18}$$

The eigenvalues of $\vec{L}\cdot\vec{\sigma}$ take $l\hbar$ and $-(l+1)\hbar$ for the positive and negative helicities of $j_\pm = l \pm \frac{1}{2}$, respectively. For convenience, we choose the parameter value of $I\omega/\hbar$ as a large half-integer, then for the lower energy branch, the energy minimum takes place at $j_{0,+} = l_0 + \frac{1}{2} = I\omega/\hbar$. The lowest LLs become SO-coupled harmonics with $j_+ = j_{0,+}$ and $(2l_0+2)$-fold degeneracy. The gap between the lowest LLs and higher LLs is $\Delta = \hbar^2/(2I)$, which is independent of ω. To take the thermodynamic limit, we keep I constant while increasing the sphere radius R, and maintain ω scaling with R^2, such that the density of states on the sphere is a constant.

4.3 Three-dimensional spin-orbit $\vec{\sigma}\cdot\vec{p}$ coupling in the harmonic trap

In this section, we generalize the results in Sec. 4.2 to three dimensions. We consider the $\vec{\sigma}\cdot\vec{p}$-type SO coupling combined with a 3D harmonic potential

$$H_{3D} = -\frac{\hbar^2\nabla^2}{2m} + \frac{1}{2}m\omega^2 r^2 - \lambda(-i\hbar\vec{\nabla}\cdot\vec{\sigma}). \tag{4.19}$$

Equation (4.19) possesses the 3D rotational symmetry, and TR symmetry of fermions with $T^2 = -1$. The parity symmetry is broken by the $\vec{\sigma}\cdot\vec{k}$ term, and there is no mirror plane symmetry either. The quantities l_{so}, l_T, α, and k_0 are defined in the same way as in Sec. 4.2.

Although it is difficult to realize strong SO coupling in the form of $\sigma\cdot\vec{p}$ in solid-state systems, it can be designed through light-atom interactions in ultra cold atom systems. We present an experimental scheme to realize Eq. (4.19) in Sec. 4.4.

4.3.1 Energy spectra

Again, we consider the limit of strong SO coupling, *i.e.*, $\alpha \gg 1$. It is straightforward to generalize the momentum space picture in Sec. 4.2 to the 3D case as presented in Ref. [103] and summarized below. The helicity operator $\vec{\sigma}\cdot\hat{k}$ is employed to define the helicity eigenstates of plane waves $(\vec{\sigma}\cdot\hat{k})\psi_{\vec{k},\pm} = \pm\psi_{\vec{k},\pm}$. Only positive-helicity states $\psi_{\vec{k}+}$ are kept in the low energy Hilbert space. The

harmonic potential becomes the Laplacian operator in momentum space, and thus is equivalent to a quantum rotor subject to the Berry phase in momentum space as $V_{tp} = \frac{1}{2}m(i\vec{\nabla}_k - \vec{A}_k)^2$. The moment of inertial is again $I = M_k k_0^2$ and $M_k = \hbar^2/(m\omega^2)$. The Berry connection $\vec{A}_k = i\langle\psi_{\vec{k},\pm}|\vec{\nabla}_k|\psi_{\vec{k},\pm}\rangle$ is the vector potential of the U(1) magnetic monopole. As a result, the angular momentum quantization changes to that j takes half-integer values starting from $\frac{1}{2}$. The energy dispersion becomes $E_{agl}(j) = \hbar^2 j(j+1)/2I = (j(j+1)/2\alpha^2)E_{tp}$, and each level is $(2j+1)$-fold degenerate. The radial quantization is the same as before. Thus the dispersion can be summarized as

$$E_{n_r,j,j_z} \approx \Big(n_r + \frac{1}{2} - \frac{\alpha^2}{2} + \frac{j(j+1)}{2\alpha^2}\Big)E_{tp}, \tag{4.20}$$

where n_r is the band index, or, the LL index, and j is the angular momentum quantum number.

4.3.2 Dimensional reduction from the 4D Landau level Hamiltonian

Following the same logic as in Sec. 4.2.2, we present the dimensional reduction from the 4D LL Hamiltonian [Eq. (4.22)] to arrive at a 3D SO coupled Hamiltonian closely related to Eq. (4.19). The 3D LL Hamiltonian, Eq. (4.5), can be easily generalized to arbitrary dimensions by combining the n-D harmonic potential and the n-D SO coupling between orbital angular momenta and fermion spins in the fundamental spinor representations. In four dimensons, there are two non-equivalent fundamental spinors, both of which have two components. Without loss of generality, we choose one of them as

$$\sigma_{ij} = \epsilon_{ijk}\sigma_k, \quad \sigma_{i4} = \sigma_i, \tag{4.21}$$

where $i, j = 1, 2,$ and 3. The orbital angular momentum operators are defined as $L_{ij} = -i\hbar x_i\nabla_j + i\hbar x_j\nabla_i$ where $i, j = 1, 2, 3,$ and 4. The 4D LL Hamiltonian in the

flat space is defined as

$$\begin{aligned} H_{4D,LL} &= \sum_{i=1}^{4} -\frac{\hbar^2\nabla_i^2}{2m} + \frac{m\omega^2}{2}\sum_{i=1}^{4} r_i^2 \\ &- \omega \sum_{1\le i<j\le 4} L_{ij}\sigma_{ij}, \end{aligned} \tag{4.22}$$

which possesses TR and parity symmetry.

The lth-order 4D orbital spherical harmonics coupled to the fundamental spinor can be decomposed into the 4D SO-coupled spherical harmonics in the positive- and negative-helicity sectors, where $L_{ij}\sigma_{ij}$ take eigenvalues of $l\hbar$ and $-(l+2)\hbar$, respectively. The eigen wave functions of Eq. (4.22) in the positive-helicity channel are dispersionless with respect to l as $E_{n_r,+} = (2n_r+2)\hbar\omega$. Their radial wave functions are $R_{n_r,l}(r) = r^l e^{-r^2/2l_T^2} F(-n_r, l+2, r^2/l_T^2)$, where F is the standard confluent hypergeometric function. With an open boundary of an S^3 sphere, each filled LL contributes to a gapless surface mode of 3D Weyl fermions as

$$H_{3D,surface} = v_f \hat{e}_{r,i}\sigma_{ij}p_j - \mu, \tag{4.23}$$

where $\hat{e}_r$ is the unit vector normal to the S^3 sphere. The topological index for such a 4D LL systems with TR symmetry is Z rather than Z_2.

We perform the dimensional reduction on Eq. (4.22) from four to three dimensions. We cut a 3D off-center hyper-plane perpendicular to the fourth axis with the interception $x_4 = w_0$ Within this 3D hyper-plane of $(x_1, x_2, x_3, x_4 = w_0)$, Eq. (4.22) reduces to

$$H_{3D,redc} = H_{3D,SO} - \omega\vec{L}\cdot\vec{\sigma}, \tag{4.24}$$

where the first term is just Eq. (4.22) with the SO-coupling strength $\lambda = \omega w_0$. It contains another SO-coupling term, $\vec{L}\cdot\vec{\sigma}$, and its coefficient is the same as the harmonic trapping frequency. Similarly to the previous reduction from three to two dimensions, here we have $\alpha = l_T/l_{so} = |w_0|/l_T$. At $w_0 = 0$, Eq. (4.24) becomes the 3D LL Hamiltonian of Eq. (4.5) with parity symmetry. If $w_0 \neq 0$, the $\vec{\sigma}\cdot\vec{p}$ term breaks parity symmetry. Following the same reasoning as in Sec. 4.2.2, Eqs.

(4.19) and (4.24) share the same physics for eigenstates with $j < \alpha$ in the case of $\alpha \gg 1$.

Similarly as before, we construct an off-center solution to the 4D LL problem. We use $\vec{r}$ to denote a point in the subspace of $x_{1,2,3}$, and $\hat{\Omega}$ as an arbitrary unit vector in the x_1-x_2-x_3 space. We consider the plane of $\hat{\Omega}$-$\hat{x}_4$ spanned by the orthogonal vectors $\hat{\Omega}$ and $\hat{x}_4$. It is easy to check that the following wave functions, which depends only on coordinates in the $\hat{\Omega}$-$\hat{x}_4$ plane are the lowest LL solutions to the 4D LL Hamiltonian, Eq. (4.22)

$$(\vec{r}\cdot\hat{\Omega}+ix_4)^l e^{-\frac{r^2+x_4^2}{2l_T^2}}\otimes\alpha_{\hat{\Omega}}, \tag{4.25}$$

where $\alpha_{\hat{\Omega}}=(\cos\frac{\theta}{2},\sin\frac{\theta}{2}e^{i\phi})^T$ satisfies

$$(\sigma_{i4}\Omega_i)\alpha_{\hat{\Omega}}=(\vec{\sigma}\cdot\hat{\Omega})\alpha_{\hat{\Omega}}=\alpha_{\hat{\Omega}}. \tag{4.26}$$

In this set of wavefunctions, both the orbital angular momentum and spin are conserved and added up; they are called the highest weight states in group theory. In fact, these states can be rotated into any plane accompanied by a simultaneous rotation in the spin channel. Based on the structure of the highest weight states, we can still define the magnetic translation operator in the $\hat{\Omega}$-x_4 plane along the x_4 axis as

$$T_{\hat{\Omega}x_4}(w_0\hat{x}_4)=\exp\Big(-w_0\partial_{x_4}-\frac{i}{l_T^2}(\vec{r}\cdot\Omega)w_0\Big). \tag{4.27}$$

Applying this operator to the Gaussian pocket of the solution with $l=0$ in Eq. (4.25), we arrive at the off-center solution

$$\psi_{\Omega,w_0}(\vec{r},x_4)=e^{-\frac{r^2+x_4^2}{2l_T^2}}e^{-i\frac{rw_0}{l_T^2}}\otimes\alpha_{\hat{\Omega}}. \tag{4.28}$$

This solution, however, breaks the rotational symmetry. In order to restore the 3D rotational symmetry around the new center $(0,0,0,w_0)$, we perform a Fourier transformation over the direction of Ω as

$$\psi_{4D;j,j_z}(\vec{r},x_4) \;=\; \int d\Omega\; \mathcal{Y}_{-\frac{1}{2},l+\frac{1}{2},m+\frac{1}{2}}(\hat{\Omega})\psi_{\Omega,w_0}(\vec{r},x_4). \tag{4.29}$$

where $j = l + \frac{1}{2}$ and $j_z = m + \frac{1}{2}$. Please note that due to the singularity of α_Ω over the direction of $\hat{\Omega}$, monopole spherical harmonics, $\mathcal{Y}_{-\frac{1}{2},l+\frac{1}{2},m+\frac{1}{2}}(\Omega)$, are used instead of regular spherical harmonics.

Again, noting that $\partial_{x_4}\psi_{4D;j,j_z}(\vec{r},x_4)|_{x_4,w_0} = 0$, we simply set $x_4 = w_0$; then it is simple to check that the reduced 3D wave functions

$$\psi_{3D,j,j_z}(\vec{r}) = \psi_{4D;j,j_z}(\vec{r},w_0) \tag{4.30}$$

are the solutions to Eq. (4.24) for the lowest LLs as

$$H_{3D,redc}\psi_{3D,j,j_z}(\vec{r}) = \Big(\frac{3}{2} - \frac{\alpha^2}{2}\Big)\hbar\omega\psi_{3D,j,j_z}(\vec{r}). \tag{4.31}$$

$\psi_{3D,j,j_z}(\vec{r})$ can be simplified as

$$\begin{aligned}\psi_{3D,jj_z}(\vec{r}) &= e^{-\frac{r^2}{2l_T^2}}\Big\{j_l(k_0r)Y_{+,j,l,j_z}(\Omega_r) + ij_{l+1}(k_0r) \\ &\times \; Y_{-,j,l+1,j_z}(\Omega_r)\Big\},\end{aligned} \tag{4.32}$$

where $k_0 = w_0/l_T^2 = m\lambda/\hbar$ and $\lambda = w_0\omega$; j_l is the lth-order spherical Bessel function. $Y_{\pm,j,l,j_z}$'s are the SO-coupled spherical harmonics defined as

$$Y_{+,j,l,j_z}(\Omega) = \Big(\sqrt{\frac{l+m+1}{2l+1}}Y_{lm}, \sqrt{\frac{l-m}{2l+1}}Y_{l,m+1}\Big)^T$$

with a positive eigenvalue of $l\hbar$ for $\vec{\sigma}\cdot\vec{L}$, and

$$Y_{-,j,l,j_z}(\Omega) = \Big(-\sqrt{\frac{l-m}{2l+1}}Y_{lm}, \sqrt{\frac{l+m+1}{2l+1}}Y_{l,m+1}\Big)^T$$

with a negative eigenvalue of $-(l+1)\hbar$ for $\vec{\sigma}\cdot\vec{L}$.

The difference between Eq. (4.24) and Eq. (4.19) is the term $\vec{\sigma}\cdot\vec{L}$, whose effect is weakened as the distance from center r gets small. The radial distributions of $j_l(k_0r)$ in Eq. (4.32) and $J_m(k_0\rho)$ in Eq. (4.9) are similar. Following the same reasoning presented in Sec. 4.2.2, in the limit of $\alpha \gg 1$, we can divide the lowest LL states of Eq. (4.32) into three regimes: $j < \alpha$, $j \gg \alpha^2$, and $\alpha < j < \alpha^2$. At $j < \alpha$, the classic orbit radius scales as $r_{c,j} \approx \frac{j}{\alpha}l_T < l_T$. Again in this regime, the effect of $\vec{\sigma}\cdot\vec{L}$ is a perturbation of the order of $r_{c,j_z}/z_0 \ll 1$; thus the two Hamiltonians, Eq. (4.24) and Eq. (4.19), share the same physics. Similarly, in the regime of $j \gg \alpha^2$, $\vec{\sigma}\cdot\vec{L}$ dominates, and the physics of Eq. (4.24) comes back to the 3D LL Hamiltonian, Eq. (4.5), while that of Eq. (4.19) is no longer LL-like.

4.3.3 The Z_2 helical surface states

Following the same reasoning as in Sec. 4.2.4, we denote the low-energy bands of Eq. (4.19) as 3D parity breaking LLs. For the lowest LL, below the energy of the bottom of the second LL, the angular momentum j takes values from $\frac{1}{2}$ to the order of α at which the radius of the LL approaches l_T. For this regime $j < \alpha$, Eqs. (4.19) and (4.24) share the same physics. Again, the smallest length scale is the SO coupling length scale $l_{so} = l_T/\alpha \ll l_T$. States with $|j| \ll \alpha$ are considered bulk states which localize within the region $\rho \ll l_T$. States with $|j_z| \sim \alpha$ are edge states. The number of bulk states scales linearly with α^2.

Now we impose an open boundary condition of an S^2 sphere with radius $r \approx l_T$, and consider the stability of the edge modes against TR invariant perturbations. Let us consider one filled LL. The Fermi energy lies between the gap, and thus cuts the dispersion at surface states. In the limit of $\alpha \to \infty$, the energy level spacing between adjacent angular momenta j and $j+1$ scales as $\hbar\omega/\alpha \to 0$ for surface modes with $j \sim \alpha$. Thus we can always choose the Fermi angular momentum j_f satisfying $j_f = 2l + \frac{1}{2}$. For this value of j_f, there is an odd number of $2l+1$ Kramer pairs between $\psi_{j_f,\pm j_z}$ for $j_z = \frac{1}{2}$ to j_f. Again according to the reasoning of the Z_2-classification in Refs. [16] and [17], these states cannot be fully gapped out by applying TR invariant perturbations. Certainly, for those states with $j = 2l + \frac{3}{2}$ close to the Fermi energy, they can be fully gapped, but they are only part of the spectra, and do not change the topological properties. Again, if two LLs with different indices n_r and n_r' cut the Fermi energy, the zero energy states at the Fermi level can be fully gapped out. Thus, the topological nature of Eq. (4.19) is Z_2.

We further present the effective surface Hamiltonian for surface modes in the limit of $j_f \sim \alpha \to +\infty$. The effective surface Hamiltonian of the 3D topological insulators with the spherical boundary condition has also been discussed in Refs. [108] and [109]. The surface Hamiltonian in the eigen-basis of j and j_z can be written as

$$H_{sf} = \sum_{j,j_z} (\frac{\hbar v_f}{l_T}|j| - \mu)\psi^\dagger_{n_r,j,j_z}\psi_{n_r,j,j_z}, \tag{4.33}$$

where $\mu = \frac{\hbar v_f}{l_T} j_f$. The construction of the accurate surface Hamiltonian in the

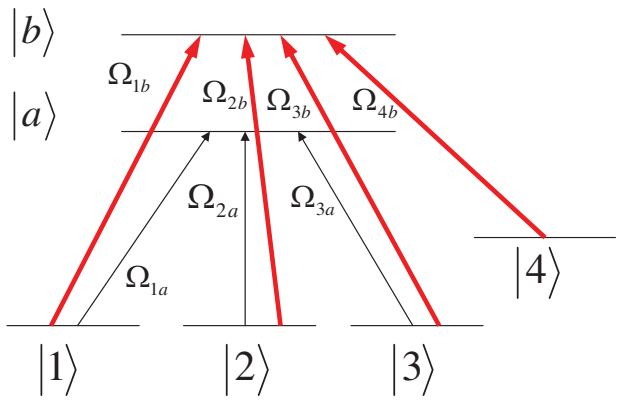

Figure 4.2: (Color online) Level diagram for atom-laser coupling. Four lower energy levels are coupled to two excited levels to compose a hybrid tripod and tetrapod configuration.

plane-wave basis depends on the detailed information of surface modes $\psi_{j,j_z}(r,\Omega_r)$ for $j \approx j_f$ and, thus, is cumbersome. Nevertheless based on the symmetry analysis, we can write the general form as

$$\begin{aligned} H_{n_r,edge} &= v_f \Big\{ \sin\theta_{n_r} (\vec{p}\times\vec{\sigma})\cdot\hat{e}_r \\ &+ \cos\theta_{n_r} \left[\vec{p}\cdot\vec{\sigma} - (\vec{p}\cdot\hat{e}_r)(\vec{\sigma}\cdot\hat{e}_r)\right] \Big\} - \mu. \end{aligned} \tag{4.34}$$

where $\hat{e}_r$ is the local norm direction on the S^2-sphere. Both terms obey the local $SO(2)$ rotational symmetry around the $\hat{e}_r$ and TR symmetry. The first Rashba term also obeys the vertical mirror symmetry, while the second term does not. The second term favors the spin aligning with the momentum, while the second favors a relative angle of 90°. For a general value of θ_{n_r}, which is determined by the non-universal surface properties and θ_{n_r}, Eq. (4.34) determines a relative rotation between spin and momentum orientation at the angle of θ_{n_r}. It is still a helical Dirac Fermi surface.

4.4 Experimental realization for 3D SO coupling

In the ultra cold atom context, there has been great progress in the synthetic gauge field, or, artificial SO coupling from light-atom interactions [73]. Experimentally, artificial SO coupling has been generate in ultra cold atom systems. [72] Two

dimensional Rashba and Dresselhaus SO coupling in the harmonic potential has been proposed using a double-tripod configuration [110]. Since the pseudo-spin degrees of freedom are represented by the two lowest energy levels, this scheme is immune to decay due to collision and spontaneous emission process. [111]

In this section, we propose the experimental realization for the 3D SO coupling of the $\vec{\sigma}\cdot\vec{p}$ type in Eq. (4.19). Here we generalize the scheme in Ref. [110] to a combined tripod and tetrapod level configuration as depicted in Fig. 4.2. Three internal levels $|1\rangle$, $|2\rangle$, and $|3\rangle$ couple the excited state $|a\rangle$ to form a tripod configuration. A tetrapod-like coupling is formed by coupling the four levels $|1\rangle - |4\rangle$ to the common excited state $|b\rangle$. The single-particle Hamiltonian reads

$$H = \frac{p^2}{2m} + \frac{1}{2}m\omega^2 r^2 + H_{al}, \tag{4.35}$$

where m is the mass of the atom; H_{al} represents the atom-laser coupling. In the interaction picture, H_{al} can be written under the rotating wave approximation as

$$\begin{aligned} H_{al} &= -\hbar \sum_{m=a,b} \big\{\Omega_{1m}|m\rangle\langle 1| + \Omega_{2m}|m\rangle\langle 2| + \Omega_{3m}|m\rangle\langle 3| \\ &+ h.c.\big\} - \hbar\left[\Omega_{4b}|b\rangle\langle 4| + h.c.\right], \end{aligned} \tag{4.36}$$

where Ω_{im} are the corresponding Rabi frequencies between the internal states $|i\rangle$ and $|m\rangle$ with $m = a, b$.

We introduce the following two bright states

$$|B_m\rangle = (\Omega_{1m}^*|1\rangle + \Omega_{2m}^*|2\rangle + \Omega_{3m}^*|3\rangle)/\Omega_m, \tag{4.37}$$

where $m = a, b$ and $\Omega_m = \sqrt{|\Omega_{1m}|^2 + |\Omega_{2m}|^2 + |\Omega_{3m}|^2}$. The atom-laser coupling can be rewritten as

$$\begin{aligned} H_{al} &= -\hbar\Big\{\Omega_a|a\rangle\langle B_a| + h.c.\Big\} \\ &- \hbar\Big\{\Omega_b|b\rangle\langle B_b| + \Omega_{4b}|b\rangle\langle 4| + h.c.\Big\}. \end{aligned} \tag{4.38}$$

To further simplify the model, here we assume $\langle B_a|B_b\rangle = 0$, which can be achieved by choosing

$$\Omega_{jm} = \frac{\Omega_m}{\sqrt{3}} e^{i(\vec{k}_j\cdot\vec{r}+\theta_{jm})}, \quad (j = 1, 2, 3; m = a, b) \tag{4.39}$$

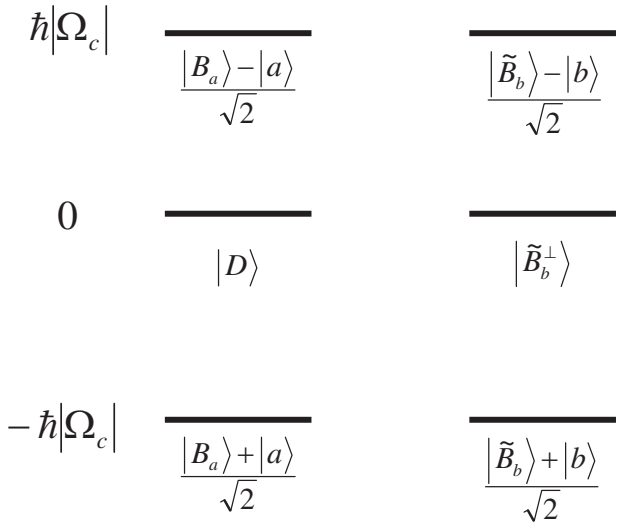

Figure 4.3: Energy levels of the atom-laser coupling Hamiltonian Eq. 4.40.

with $\theta_{ja} = (j-2)2\pi/3$ and $\theta_{jb} = -(j-2)2\pi/3$. We also choose $\Omega_{4b} = \Omega_4 e^{i(\vec{k}_4\cdot\vec{r}+\theta_4)}$, and set $\Omega_c = \Omega_a$, $\Omega_b = \Omega_c \cos\phi$, and $\Omega_4 = \Omega_c \sin\phi$. Using these notations, H_{al} is simplified as

$$H_{al} = -\hbar\left[\Omega_c(|a\rangle\langle B_a| + |b\rangle\langle\tilde{B}_b|) + h.c.\right], \tag{4.40}$$

where $|\tilde{B}_b\rangle = \cos\phi|B_b\rangle + \sin\phi|\tilde{4}\rangle$ and $|\tilde{4}\rangle = e^{-i(\vec{k}_4\cdot\vec{r}+\theta_4)}|4\rangle$. The above Hamiltonian supports three pairs of degenerated eigenstates with energy difference $\hbar|\Omega_c|$, as depicted in Fig. 4.3. Explicitly, the eigen-vectors are written as

$$\begin{aligned}
|G_1\rangle &= \frac{|B_a\rangle + |a\rangle}{\sqrt{2}}, \quad |G_2\rangle = \frac{|\tilde{B}_b\rangle + |b\rangle}{\sqrt{2}}, \\
|G_3\rangle &= |D\rangle, \qquad\qquad |G_4\rangle = |\tilde{B}_b^{\perp}\rangle, \\
|G_5\rangle &= \frac{|B_a\rangle - |a\rangle}{\sqrt{2}}, \quad |G_6\rangle = \frac{|\tilde{B}_b\rangle + |b\rangle}{\sqrt{2}},
\end{aligned} \tag{4.41}$$

where $|D\rangle = \sum_j e^{-i\vec{k}_j\cdot\vec{r}}|j\rangle/\sqrt{3}$ and $|\tilde{B}_b^{\perp}\rangle = \sin\phi|B_b\rangle - \cos\phi|\tilde{4}\rangle$. Therefore, the two degenerate ground states can be used as pseudo-spin 1/2 degrees of freedom.

If the trapping frequency satisfies $\omega \ll |\Omega_c|$, according to the adiabatic approximation, we neglect the coupling between the ground-state manifold and other states. Therefore, atoms in the subspace spanned by $|G_1\rangle$ and $|G_2\rangle$ evolve

according to the effective Hamiltonian

$$H_e = \frac{(\vec{p} - \vec{A})^2}{2m} + \frac{1}{2}m\omega^2 r^2 + \Phi, \tag{4.42}$$

where the non-Abelian gauge potential $\vec{A}$ is a 2×2 matrix with the elements

$$\vec{A}_{ij} = i\hbar\langle G_i|\vec{\nabla}|G_j\rangle, \tag{4.43}$$

where $i, j = 1, 2$; Φ is a scalar potential induced by the coupling laser beams.

An isotropic 3D $\vec{\sigma} \cdot \vec{p}$-like SO coupling can be obtained by a 3D set-up of laser configurations as

$$\begin{aligned} \vec{k}_1 &= \kappa(-\frac{1}{2}, -\frac{\sqrt{3}}{2}, 0), \quad \vec{k}_2 = \kappa(0, 1, 0), \\ \vec{k}_3 &= \kappa(-\frac{1}{2}, \frac{\sqrt{3}}{2}, 0), \quad \vec{k}_4 = \kappa(0, 0, -\sqrt{\frac{7+\sqrt{17}}{8}}). \end{aligned} \tag{4.44}$$

In this case, the corresponding vector and scale potential are calculated as

$$\begin{aligned} \frac{\vec{A}}{\hbar} &= 0.166\kappa\left[\sigma_x\vec{e}_x + \sigma_y\vec{e}_y + (\sigma_z - I)\vec{e}_z\right], \\ \Phi &= 0.445\frac{\hbar^2\kappa^2}{2m}\hat{I}. \end{aligned} \tag{4.45}$$

The Φ term is a constant and, thus, can be dropped off. The Abelian part in the gauge potential A_z is a constant, which can be absorbed by a gauge transformation. Consequently, the remaining constant non-Abelian gauge potential behaves as a $\vec{\sigma} \cdot \vec{p}$ type SO coupling.

The above-considered level structure can be found for example, in alkali atoms with large spins. Figure 4.4 shows the hyperfine ground state manifolds of $^2S_{1/2}$ for ^{40}K atoms under an external magnetic field. The energy levels $|1\rangle \sim |4\rangle$, $|a\rangle$, and $|b\rangle$ can be selected as different Zeeman sublevels of $F = \frac{9}{2}$ and $F = \frac{7}{2}$. Using the notation of $|FM_F\rangle$ to denote each state, we choose $|1\rangle = |\frac{9}{2}, -\frac{1}{2}\rangle$, $|2\rangle = |\frac{9}{2}, \frac{3}{2}\rangle$, $|3\rangle = |\frac{7}{2}, \frac{3}{2}\rangle$, $|4\rangle = |\frac{7}{2}, -\frac{1}{2}\rangle$, $|a\rangle = |\frac{9}{2}, \frac{1}{2}\rangle$ and $|b\rangle = |\frac{7}{2}, \frac{1}{2}\rangle$. The coupling between different levels is achieved for example, by using two laser beams under second-order resonant Raman process. The two lasers can be chosen to be circularly polarized and π polarized, respectively, in order to satisfy the selection rule. Finally, wave vectors of individual laser beams can also be adjusted so that Eq. (4.45) is fulfilled.

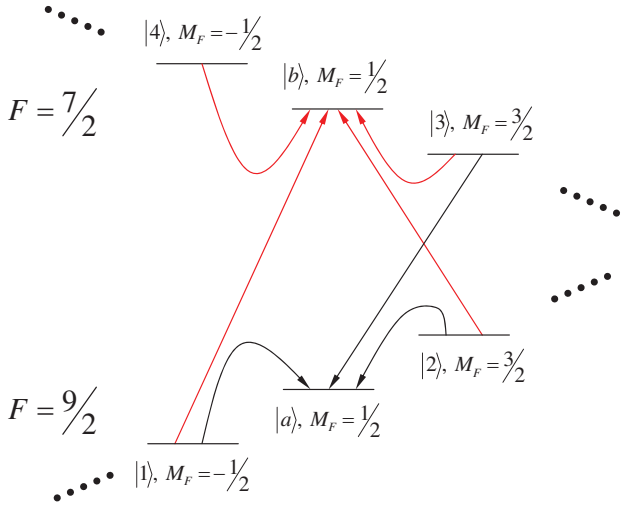

Figure 4.4: (Color online) Energy level scheme for alkali atoms ^{40}K. The Zeeman sublevels of two hyperfine states $F = \frac{9}{2}$ and $F = \frac{7}{2}$ can be used to fulfill our requirements. Lines or curves with an arrow indicate effective transitions between different magnetic levels which can be implemented using resonant Raman processes. Other levels, which are not involved in the scheme, are not shown.

4.5 Summary and Discussions

We have studied rotationally and TR symmetric LL systems in both 2D and 3D systems with breaking parity symmetry, whose topological properties are characterized by the Z_2 class. These Hamiltonians are simply 2D harmonic potentials plus Rashba SO coupling, or 3D harmonic potentials plus $\vec{\sigma} \cdot \vec{p}$-type SO coupling with a strong SO coupling strength. For low-energy bands, the dispersions over angular momenta are strongly suppressed by SO coupling, to be nearly flat. Up to a small difference which can be treated perturbatively, these Hamiltonians can be systematically investigated through dimensional reduction on the high-dimensional LL problems by cutting an off-center plane in the 3D LL Hamiltonian or an off-center hyper plane in the 4D LL Hamiltonian. The parity breaking LL wavefunctions in two and three dimensions are presented explicitly. With open boundary conditions, helical edge states are found in two dimensions, and surface states are found in three dimensions. These states can be realized in ultra cold atom systems in a harmonic trap combined with synthetic gauge fields, *i.e.*, artifi-

cial SO coupling. In particular, we propose an experimental scheme to realize the 3D Hamiltonian.

The above dimensional procedure can be straightforwardly generalized to arbitrary dimensions based on our previous construction of high dimensional LL Hamiltonians in Chapter 2, and so can the general parity breaking LL wavefunctions in N dimensions. The nice analytic properties of the 2D and 3D LL wave functions breaking parity symmetry also provide a good opportunity to further construct many-body wave functions of the factional topological states. These properties will be investigated in a future publication.

Acknowledgements: This chapter is in part a reprint of the paper "2D and 3D topological insulators with isotropic and parity-breaking Landau levels", authored by Yi Li, Xiangfa Zhou, and Congjun Wu, *Phys. Rev. B*, 85, 125122 (2012).

Chapter 5

Isotropic Landau levels of Dirac fermions in high dimensions

5.1 Introduction

The integer quantum Hall effect in two-dimensional (2D) electron gas arises from the quantized 2D Landau levels (LL). The non-trivial band structure topology is characterized by non-zero Chern numbers [7, 11]. Later on, quantum anomalous Hall insulators based on Bloch-wave band structures were proposed in the absence of Landau levels [8]. In recent years, the study of topological insulators (TI) in both 2D and three dimensions (3D) has become a major focus of condensed matter physics [26, 25, 21, 16, 17, 15, 27]. TIs maintain time-reversal (TR) symmetry, and their band structures are characterized by the nontrivial Z_2-index. As for the 3D TIs, various materials with Bloch-wave band structures have been realized and the stable helical surface modes have been detected [18, 19, 20, 22, 24, 31, 77, 32, 33]. Since LL wavefunctions have explicit forms with elegant analytical properties, TIs based on high dimensional LL structures would provide a nice platform for further theoretical studies. In particular, interaction effects in the flat LLs are non-perturbative, which could lead to non-trivial many-body states in high dimensions.

The seminal work by Zhang and Hu [57] generalizes LLs to the compact S^4 sphere with particles coupled to the $SU(2)$ gauge potential. The isospin of particles

I scales as R^2 where R is the radius of the sphere. Such a system realizes the four dimensional integer and fractional TIs. The 3D and 2D TIs can be constructed from the 4D TIs by dimensional reduction [22]. Further generalizations to other manifold have also been developed [59, 61, 62, 80, 112, 60]. The LLs of non-relativistic fermions have been generalized to arbitrary dimensional flat space R^D [82] in Chapter 2. For the simplest case of 3D, the $SU(2)$ Aharanov-Casher gauge potential replaces the role of the usual $U(1)$ vector potential. Depending on the sign of the coupling constant, the flat LLs are characterized by either positive or negative helicity. In the positive and negative helicity channels, the eigenvalues of spin-orbit coupling term $\vec{\sigma} \cdot \vec{L}$ take values of l and $-(l+1)$, respectively. Each LL contributes a branch of helical surface modes at the open boundary. When odd numbers of LLs are fully filled, there are odd numbers of helical Fermi surfaces. Thus the system is a 3D strong topological insulator. This construction can be easily generalized to arbitrary D-dimensions by coupling the fundamental spinors to the $SO(D)$ gauge potential.

Quantized LLs of 2D Dirac fermions have also been extensively investigated in the field theory context known as the parity anomaly [92, 93, 95, 94, 113, 114, 8]. This can be viewed as the square root problem of the usual 2D non-relativistic LLs. External magnetic fields induce vacuum charges with the density proportional to the field strength. The sign of the charge density is related to the sign of the fermion mass. There is an ambiguity if the Dirac fermions are massless. In this case, there appear a branch of zero energy Landau levels. Each of them contributes $\pm\frac{1}{2}$ fermion charge. It is similar to the soliton charge in the Jackiw-Rebbi model [85, 86], which is realized in condensed matter systems of one dimensional conducting polymer [115]. Depending on whether the zero energy Landau levels are fully occupied or empty, the vacuum charge density is $\pm\frac{1}{2\pi l'^2}$ where l' is the magnetic length. In condensed matter physics, the best known example of Dirac fermions is in graphene, which realizes a pair of Dirac cones. The quantized LLs in graphene have been observed which distribute symmetrically with respect to zero energy. Their energies scale as the square root of the Landau level index. The observed Hall conductance per spin component are quantized at odd integer values, which reflects the nature of two Dirac cones in graphene for each spin component [89, 90, 91, 116].

In this chapter, we generalize the LLs with full rotational symmetry of Dirac fermions to the three dimensional flat space and above. It is a square root problem of the high dimensional LLs investigated in Chapter 2. Our Hamiltonian is very simple: replacing the momentum operator in the Dirac equation by the creation or annihilation phonon operators, which are complex combinations of momenta and coordinates. The LLs exhibit the same spectra as those in the 2D case but with the full rotational symmetry in D-dimensional space. Again the zero energy Landau levels are half-fermion modes. Each LL contributes to a branch of helical surface mode at open boundaries.

This chapter is organized as follows. In Sect. 5.2, after a brief review of the 2D LL Hamiltonian of Dirac fermions in graphene, we construct the 3D LL Hamiltonian of Dirac fermions. Reducing this 3D system to 2D, it gives rise to 2D quantum spin Hall Hamiltonian of Dirac fermions with LLs. In Sect. 5.3, we further solve this 3D LL Hamiltonian of Dirac fermions, and its edge properties are discussed. For the later discussion of generalizing the 3D LL Hamiltonian to arbitrary higher dimensions, in Sect. 5.4, we briefly review some properties of D dimensional spherical harmonics and spinors. In Sect. 5.5 and Sect. 5.6, we extend the solutions of LL Hamiltonians to arbitrary odd and even dimensions, respectively. Conclusions are given in Sect. 5.7.

5.2 The Landau level Hamiltonian of 3D Dirac fermions

5.2.1 A Brief Review of the 2D LL Hamiltonian

Before discussing the LL problem of Dirac fermions in 3D, we briefly review the familiar 2D case [91, 116] to gain the insight on how to generalize it to high dimensions. The celebrated condensed matter system to realize 2D Dirac fermion is the monolayer of graphene [91, 116], which possesses a pair of Dirac cones with spin degeneracy. Here for simplicity, we only consider a single 2D Dirac cone under

a uniform magnetic field $B\hat{z}$. The Landau level Hamiltonian in the xy-plane reads

$$H_{2D,LL} = v_F\Big\{(p_x - \frac{e}{c}A_x)\sigma_x + (p_y - \frac{e}{c}A_y)\sigma_y\Big\}, \tag{5.1}$$

where the Dirac fermion with momentum $\vec{p}$ is minimally coupled to the $U(1)$ magnetic field with symmetric gauge potentials

$$A_x = -\frac{B}{2}y, \quad A_y = \frac{B}{2}x, \tag{5.2}$$

satisfying $\nabla \times \vec{A} = B\hat{z}$; the Fermi velocity v_F is related to the cyclotron frequency ω via the magnetic length l' as

$$l' = \sqrt{\frac{\hbar c}{eB}}, \quad v_F = \frac{l'\omega}{\sqrt{2}}. \tag{5.3}$$

For later convenience, we define $l_0 = \sqrt{2}l'$ which will be termed as cyclotron length below. The spectra of Eq. (5.1) consist of a branch of zero energy LL, and other LLs with positive and negative energies distribute symmetrically around zero energy. The energy of each LL scales as the square root of the Landau level index. It is well-known that Eq. (5.1) can be recast in term of creation and annihilation operators

$$H_{2D,LL} = \frac{\hbar\omega}{\sqrt{2}}\begin{bmatrix} 0 & \hat{a}_y^\dagger + i\hat{a}_x^\dagger \\ \hat{a}_y - i\hat{a}_x & 0 \end{bmatrix}, \tag{5.4}$$

where $\hat{a}_i (i = x, y)$ are the phonon annihilation operators along the x and y-directions, with the form as

$$\hat{a}_i = \frac{1}{\sqrt{2}}\Big\{\frac{1}{l_0}r_i + i\frac{l_0}{\hbar}p_i\Big\}. \tag{5.5}$$

In Eq. (5.4), two sets of creation and annihilation operators combine with 1 and the imaginary unit i. In order to generalize to 3D, in which there exist three sets of creation and annihilation operators, we employ Pauli matrices to match them as explained below.

5.2.2 The construction of the 3D LL Hamiltonian

We define the rotationally invariant operator $\hat{B}$ as

$$\hat{B}_{3D} = -i\sigma_i\hat{a}_i = \sigma_i\frac{1}{\sqrt{2}}\Big\{\frac{p_i l_0}{\hbar} - i\frac{r_i}{l_0}\Big\}, \tag{5.6}$$

where the repeated index i runs over x, y and z; $\hat{a}_i$ is the phonon annihilation operator along the i-direction; l_0 is the cyclotron length. We design the 3D Landau level Hamiltonian of Dirac fermions as

$$H_{3D} = \frac{\hbar\omega}{2}\begin{bmatrix} 0 & B_{3D}^{\dagger} \\ B_{3D} & 0 \end{bmatrix}. \tag{5.7}$$

Eq. (5.7) contains the complex combination of momenta and coordinates, thus it can be viewed as the generalized Dirac equation defined in the phase space. Using the convention of α, β and γ-matrices defined as

$$\begin{aligned} \alpha_i &= \begin{bmatrix} 0 & \sigma_i \\ \sigma_i & 0 \end{bmatrix}, \ \beta = \begin{bmatrix} I_{2\times 2} & 0 \\ 0 & -I_{2\times 2} \end{bmatrix}, \\ \gamma_i &= \beta\alpha_i = \begin{bmatrix} 0 & \sigma_i \\ -\sigma_i & 0 \end{bmatrix}, \\ \gamma_5 &= i\gamma_0\gamma_1\gamma_2\gamma_3 = \begin{bmatrix} 0 & I_{2\times 2} \\ I_{2\times 2} & 0 \end{bmatrix}, \end{aligned}$$

Eq. (5.7) is represented as

$$H_{3D} = v_F \sum_{i=x,y,z} \Big\{\alpha_i p_i + \gamma_i i\hbar \frac{r_i}{l_0^2}\Big\}, \tag{5.8}$$

where $v_F = \frac{1}{2} l_0 \omega$. A mass term can be added into Eq. (5.8) as

$$H_{3D,ms} = \Delta\beta = \begin{pmatrix} \Delta I_{2\times 2} & 0 \\ 0 & -\Delta I_{2\times 2} \end{pmatrix}. \tag{5.9}$$

A similar Hamiltonian was studied before under the name of Dirac oscillator [117, 118], which corresponds to Eq. (5.7) plus the mass term of Eq. (5.9) with the special relation $l_0 = \sqrt{\hbar c^2/\Delta\omega}$. However, the relation between the solution of such a Hamiltonian to the LLs and its topological properties were not noticed before.

The corresponding Lagrangian of Eq. (5.8) reads

$$\mathcal{L} = \bar{\psi}\Big\{\gamma_0 i\hbar\partial_t - iv\gamma_i\hbar\partial_i\Big\}\psi - v_F\hbar\bar{\psi}i\gamma_0\gamma_i\psi F^{0i}(r), \tag{5.10}$$

where $F^{0i} = x_i/l_0^2$. Compared with the usual way that Dirac fermions minimally couple to the $U(1)$ gauge field, here they couple to the background field in Eq.

(5.10) through $i\gamma_0\gamma_i$. It can be viewed as a type of non-minimal coupling, the Pauli coupling. Apparently, Eq. (5.7) is rotationally invariant. It is also time-reversal invariant, and the time-reversal operation T is defined as

$$T = \gamma_1\gamma_3 K = \begin{pmatrix} i\sigma_2 & 0 \\ 0 & i\sigma_2 \end{pmatrix} K, \tag{5.11}$$

where K represents the complex conjugation operation, and $T^2 = -1$.

5.2.3 Reduction to the 2D quantum spin Hall Hamiltonian of Dirac fermions with LLs

If we suppress the z-component part in the definition of Eq. (5.6), we will arrive at double copies of the usual LL problem of 2D Dirac fermions with Kramer degeneracy, which can be considered as the Z_2-topological insulator Hamiltonian arising from LLs of 2D Dirac fermions. We define the operator $\hat{B}_{2D}$ as $\hat{B}_{2D} = -i\sigma_x\hat{a}_x - i\sigma_y\hat{a}_y$, and the Eq. (5.7) reduces to

$$\begin{aligned} & \frac{\sqrt{2}}{2}\hbar\omega \begin{pmatrix} 0 & 0 & 0 & \hat{a}_y^\dagger + i\hat{a}_x^\dagger \\ 0 & 0 & -\hat{a}_y^\dagger + i\hat{a}_x^\dagger & 0 \\ 0 & -\hat{a}_y - i\hat{a}_x & 0 & 0 \\ \hat{a}_y - i\hat{a}_x & 0 & 0 & 0 \end{pmatrix}, \\ = \; & v_F \begin{pmatrix} 0 & 0 & 0 & p_- - A_- \\ 0 & 0 & p_+ + A_+ & \\ 0 & p_- + A_- & 0 & 0 \\ p_+ - A_+ & 0 & 0 & 0 \end{pmatrix}, \end{aligned}$$

where $p_\pm = p_x \pm ip_y$ and $A_\pm = A_x \pm iA_y$. It is reducible into a pair of 2×2 matrices as

$$H_{2D,\pm} = v_F \begin{pmatrix} 0 & p_- \pm A_- \\ p_+ \pm A_+ & 0 \end{pmatrix}, \tag{5.12}$$

which are time-reversal partner to each other. Thus Eq. (5.12) can be viewed as the quantum spin Hall Hamiltonian of 2D Dirac fermions.

A similar situation occurs in the strained graphene systems in which lattice distortions behave like a gauge field coupling. Signatures of LLs due to strains have been observed in Ref. [119]. Due to the TR symmetry, the Dirac cones at two non-equivalent vertices of the Brillouin zone see gauge fields with a opposite sign to each other. Such a coupling is also spin-independent. However, the TR transformation connecting two Dirac cones satisfies $T^2 = 1$, thus LLs due to strain are not topologically protected. They are unstable under inter-valley scattering.

Equation (5.12) exhibits the standard minimal coupling to the background $U(1)$ gauge field. Its solutions are well-known thus will not be repeated here. After all, there is no non-minimal coupling in 2D. Each state of the zero energy LL is actually a half-fermion zero mode. Whether it is filled or empty contributes the fermion charge $\pm\frac{1}{2}$. As the chemical potential $\mu = 0^{\pm}$, magnetic field pumps vacuum charge density $\rho(r) = \pm\frac{1}{2}\frac{e}{hc}B$. In the field theory context, this is an example of the parity anomaly [92, 93, 95, 94, 113, 114, 8]. Our 3D version and generalizations to arbitrary dimensions exhibit similar effects as will be discussed below.

5.3 The bulk spectra of the 3D Dirac fermion LLs

In this section, we will present the solution of the spectra and wavefunctions of the 3D LL Hamiltonian for Dirac fermions, which can be obtained based on solutions of the 3D LL problem of the non-relativistic case in Chapter 2. We start with a brief review of the non-relativistic case of the 3D LL problem.

5.3.1 The 3D isotropic non-relativistic LL wavefunctions

As shown in Chapter 2, the 3D isotropic LL Hamiltonians for non-relativistic particles are just spin-$\frac{1}{2}$ fermions in the 3D harmonic oscillator plus spin-orbit coupling as

$$H_{3D,\mp} = \frac{p^2}{2M} + \frac{1}{2}M\omega^2 \mp \omega \vec{L}\cdot\vec{\sigma}. \tag{5.13}$$

Their eigenfunctions are essentially the same as those of the 3D harmonic oscillator of spin-$\frac{1}{2}$ fermions organized in the total angular momentum eigen-basis of j, j_z as

$$\psi_{n_r,j_\pm,l,j_z}(\vec{r}) = R_{n_r,l}(r)\mathcal{Y}_{j_\pm,l,j_z}(\hat{\Omega}), \tag{5.14}$$

where n_r is the radial quantum number; $j_\pm = l \pm \frac{1}{2}$ represent positive and negative helicity channels, respectively; and l is the orbital angular momentum. Please note that l is not an independent variable from $j_\pm$. We write it explicitly in order to keep track of the orbital angular momentum. The radial wavefunction can be represented through the confluent hypergeometric functions as

$$R_{n_r,l}(r) = N_{n_r,l}\Big(\frac{r}{l_0}\Big)^l F(-n_r, l+\frac{3}{2}, \frac{r^2}{l_0^2})e^{-\frac{r^2}{2l_0^2}}, \tag{5.15}$$

where F is the standard first kind confluent hypergeometric function,

$$\begin{aligned} F(-n_r, l+\frac{3}{2}, \frac{r^2}{l_0^2}) &= \sum_{n=0}^{\infty} \frac{\Gamma(-n_r+n)}{\Gamma(-n_r)} \frac{\Gamma(l+\frac{3}{2})}{\Gamma(l+\frac{3}{2}+n)} \\ &\times \frac{1}{\Gamma(n+1)} \left(\frac{r^2}{l_0^2}\right)^n. \end{aligned} \tag{5.16}$$

When n_r is a positive integer, the sum over n is cut off at n_r. The normalization factor reads as

$$N_{n_r,l} = \frac{l_0^{-\frac{3}{2}}}{\Gamma(l+\frac{3}{2})} \sqrt{\frac{2\Gamma(l+n_r+\frac{3}{2})}{\Gamma(n_r+1)}}. \tag{5.17}$$

The angular part of the wavefunction is the standard spin-orbit coupled spinor spherical harmonic function, which reads as

$$\mathcal{Y}_{j_\pm,l,j_z=m+\frac{1}{2}}(\hat{\Omega}) = \begin{pmatrix} \pm\sqrt{\frac{l\pm j_z+\frac{1}{2}}{2l+1}} Y_{l,m}(\hat{\Omega}) \\ \sqrt{\frac{l\mp j_z+\frac{1}{2}}{2l+1}} Y_{l,m+1}(\hat{\Omega}) \end{pmatrix}. \tag{5.18}$$

Depending on the sign of the spin-orbit coupling in Eq. (5.13), one of the two branches of positive or negative helicity states are dispersionless with respect to j, and thus are dispersionless LLs. For $H_{3D,-}$, the positive helicity states become dispersionless LLs as

$$H_{3D,-}\psi_{n_r,j_+,l,j_z} = (2n_r + \frac{3}{2})\hbar\omega\psi_{n_r,j_+,l,j_z} \tag{5.19}$$

where n_r serves as Landau level index. However, the negative helicity states are dispersive whose eigen-equation reads

$$H_{3D,-}\psi_{n_r,j_-,l,j_z} = (2n_r + 2l + \frac{5}{2})\hbar\omega\psi_{n_r,j_-,l,j_z}. \tag{5.20}$$

Similarly, we have the following eigen-equations for the $H_{3D,+}$ as

$$\begin{aligned} H_{3D,+}\psi_{n_r,j_-,l,j_z} &= (2n_r + \frac{1}{2})\hbar\omega\psi_{n_r,j_-,l,j_z} \\ H_{3D,+}\psi_{n_r,j_+,l,j_z} &= (2n_r + 2l + \frac{3}{2})\hbar\omega\psi_{n_r,j_+,l,j_z}. \end{aligned} \tag{5.21}$$

In this case, the negative helicity states become dispersionless LLs with respect to j, while the positive ones are dispersive.

5.3.2 3D LL wavefunctions of Dirac fermions

Now we are ready to present the spectra and the four-component eigenfunctions of Eq. (5.8) for the massless case. Its square is block-diagonal, and two blocks become the non-relativistic 3D Landau level Hamiltonians with opposite signs of spin-orbit coupling presented in Chapter 2,

$$\begin{aligned} \frac{H_{3D}^2}{\frac{1}{2}\hbar\omega} &= \begin{bmatrix} H_- & 0 \\ 0 & H_+ \end{bmatrix} \\ &= \frac{p^2}{2M} + \frac{1}{2}M\omega^2 r^2 - \omega\Big\{\vec{L}\cdot\vec{\sigma} + \frac{3}{2}\hbar\Big\}\begin{bmatrix} I & 0 \\ 0 & -I \end{bmatrix}, \end{aligned} \tag{5.22}$$

where M is defined through the relation $l_0 = \sqrt{\hbar/(M\omega)}$.

Its eigenfunctions can be represented in terms of non-relativistic Landau levels of Eq. (5.14) as presented in Sect. 5.3.1. Eq. (5.7) has a conserved quantity as

$$K = \begin{bmatrix} \vec{\sigma}\cdot\vec{l} + \hbar & 0 \\ 0 & -(\vec{\sigma}\cdot\vec{l} + \hbar) \end{bmatrix}. \tag{5.23}$$

According to its eigenvalues, the eigenfunctions of Eq. (5.7) are classified as

$$\begin{aligned} K\Psi^I_{\pm n_r,j,j_z} &= (l+1)\hbar\Psi^I_{\pm n_r,j,j_z}, \\ K\Psi^{II}_{\pm n_r,j,j_z} &= -l\hbar\Psi^{II}_{\pm n_r,j,j_z}, \end{aligned} \tag{5.24}$$

respectively. $\Psi^{I}_{\pm n_r,j,j_z}$ is dispersionless with respect to j, while $\Psi^{II}_{\pm n_r,j,j_z}$ is dispersive, respectively. The dispersionless branch is solved as

$$\Psi^{I}_{\pm n_r,j,j_z}(\vec{r}) = \frac{1}{\sqrt{2}} \begin{bmatrix} \psi_{n_r,j_+,l,j_z}(\vec{r}) \\ \pm i\psi_{n_r-1,j_-,l+1,j_z}(\vec{r}) \end{bmatrix} \tag{5.25}$$

with the energy

$$E_{\pm n_r,j,j_z} = \pm\hbar\omega\sqrt{n}_r. \tag{5.26}$$

Please note that the upper and lower two components of Eq. (5.25) possess different values of orbital angular momenta. They exhibit opposite helicities of $j_\pm$, respectively. The zeroth Landau level ($n_r = 0$) is special: only the first two components are non-zero.

On the other hand, the wavefunctions of the dispersive branch read

$$\Psi^{II}_{\pm n_r,j,j_z}(\vec{r}) = \frac{1}{\sqrt{2}} \begin{bmatrix} \mp i\psi_{n_r,j_-,l+1,j_z}(\vec{r}) \\ \psi_{n_r,j_+,l,j_z}(\vec{r}) \end{bmatrix}, \tag{5.27}$$

with the spectra solved as

$$E_{\pm n_r,j,j_z} = \pm\hbar\omega\sqrt{n_r + j + 1}. \tag{5.28}$$

These states are just discrete energy levels lying between two adjacent LLs. For simplicity, let us only consider the positive energy states. The degeneracy of these mid-gap states lying between the n-th and $(n+1)$-th Landau levels with $n = n_r + j + \frac{1}{2}$ is finite, $n(n+1)$, due to finite combinations of n_r and j. In particular, between the zeroth LL and the LLs with $n_r = \pm 1$, these discrete states do not exist at all.

Because Eq. (5.8) satisfies $\beta H_{3D}\beta = -H_{3D}$, its spectra are symmetric with respect to zero energy. If the zeroth branch of Landau levels ($n_r = 0$) are occupied, each of them contribute a half-fermion charge. The vacuum charge is $\rho^{3D}(\vec{r}) = \frac{1}{2}\sum_{j,j_z} \Psi^{\dagger}_{0;j,j_z}(\vec{r})\Psi_{0;j,j_z}(\vec{r})$, which are calculated as

$$\begin{aligned} \rho^{3D}(\vec{r}) &= \frac{1}{2l_0^3}\Big\{\sum_{l=0}^{\infty}\frac{l+1}{2\pi}\frac{1}{\Gamma(l+\frac{3}{2})}\Big(\frac{r^2}{l_0^2}\Big)^l\Big\}e^{-\frac{r^2}{l_0^2}} \\ &= \frac{1}{2\pi l_0^3}\Big\{\frac{1}{\sqrt{\pi}}e^{-\frac{r^2}{l_0^2}} + \big(\frac{r}{l_0} + \frac{l_0}{2r}\big)\mathrm{erf}\big(\frac{r}{l_0}\big)\Big\}, \\ &\longrightarrow \frac{r}{2\pi l_0^4}, \quad \text{as} \quad r \to +\infty. \end{aligned} \tag{5.29}$$

In 2D, the induced vacuum charge density in the gapless Dirac LL problem is a constant, $\rho^{2D}(r) = \frac{1}{2\pi l_0^2} = \frac{1}{4\pi}\frac{e}{\hbar c}B$, which is known as "parity anomaly". However, in the 3D case, the vacuum charge density $\rho^{3D}(r)$ diverges linearly, which is dramatically different from that in 2D. This can be easily understood in the semi-classic picture. Each Landau level with orbital angular momentum l has a classic radius $r_l = \sqrt{2l}l_0$. In 2D, between $r_l < r < r_{l+1}$, there is only one state. However, in 3D there is the $2j_+ + 1 = 2l + 2$ fold degeneracy, which is the origin of the divergence of the vacuum charge density as r approaches infinity. Generally speaking, in the case of D dimensions, the degeneracy density scales as r^{D-2} as shown in Sect. 5.5 and Sect.5.6. The intrinsic difference between high-D and 2D is that the high dimensional LL problems exhibit the form of non-minimal coupling. In 2D, due to the specialty of Pauli matrices, this kind of coupling reduces back to the usual minimal coupling. In Eq. (5.10), the background field is actually a linear divergent electric field, not the magnetic vector potential. Eq. (5.29) can be viewed as a generalization of "parity anomaly" to 3D for non-minimal couplings.

Now we consider the full Hamiltonian with the mass term Eq. (5.9). The mass term mixes the LLs in Eq. (5.25 with opposite level indices $\pm n_r$ but the same values of j and j_z. The new eigenfunctions become

$$\begin{bmatrix} \Psi^{I,\prime}_{n_r,j,j_z} \\ \Psi^{I,\prime}_{-n_r,j,j_z} \end{bmatrix} = \begin{bmatrix} \cos\theta & -\sin\theta \\ \sin\theta & \cos\theta \end{bmatrix} \begin{bmatrix} \Psi_{n_r,j,j_z} \\ \Psi_{-n_r,j,j_z} \end{bmatrix}, \tag{5.30}$$

where $\cos^2\theta = \frac{1}{2}\left[1 + \sqrt{n}_r/\sqrt{n_r + [\Delta/(\hbar\omega)]^2}\right]$. The spectra are

$$E^{I,ms}_{\pm n_r,j,j_z} = \pm\sqrt{n_r(\hbar\omega)^2 + \Delta^2}. \tag{5.31}$$

The zeroth LL $\Psi^I_{n_r=0,j,j_z}(\vec{r})$ singles out, which is not affected by the mass term. Only its energy is shifted to Δ.

5.3.3 Gapless surface modes

As shown in Eq. (5.29), the 3D LL system of Dirac fermions has a center, and does not have translational symmetry. Thus how to calculate its topological index remains a challenging problem. Nevertheless, we can still demonstrate its non-trivial topological properties through the solution of its gapless surface modes.

We consider the surface spectra at a spherical boundary with a large radius $R \gg l_0$. The Hamiltonian $H_{r<R}$ inside the sphere takes the massless form of Eq. (5.8), while $H_{r>R}$ outside takes the mass term of Eq. (5.9) in the limit of $|\Delta| \to \infty$. Again the square of this Hamiltonian $(H_{r<R} + H_{r>R})^2$ is just Eq. (5.22) subject to the open boundary condition at the radius of R. The spectra of the open surface problem of the non-relativistic 3D LL Hamiltonian have been calculated and presented in Fig. 2.4, in which the spectra of each Landau level remain flat for bulk states and develop upturn dispersions as increasing j near the surface. The solution to the Dirac spectra is just to take the square root. Except the zeroth LL, each of the non-relativistic LL and its surface branch split into a pair of bulk and surface branches in the relativistic case. The relativistic spectra take the positive and negative square roots of the non-relativistic spectra, respectively. The zeroth LL branch singles out. We can only take either the positive or negative square root, but not both. It surface spectra are upturn or downturn with respect to j depending on the sign of the vacuum mass. For the current Hamiltonian, only the first two components of the zeroth LL wavefunction are non-zero, thus it only senses the upper 2×2 diagonal block of vacuum mass in Eq. (5.9), thus its surface spectra are pushed upturn.

5.4 Review of D-dimensional spherical harmonics and spinors

We will study the LL of Dirac fermions for general dimensions in the rest part of this chapter. For later convenience, we present here some background knowledge of the $SO(D)$ group which can found in standard group theory textbooks [120].

The D-dimensional spherical harmonic functions $Y_{l,\{m\}}(\hat{\Omega})$ form the representation of the $SO(D)$ group with the one-row Young pattern, where l is the number of boxes and $\{m\}$ represents a set of $D-2$ quantum numbers of the

subgroup chain from $SO(D-1)$ down to $SO(2)$. The degeneracy of $Y_{l;\{m\}}$ is

$$d_{[l]}(SO(D)) = (D+2l-2)\frac{(D+l-3)!}{l!(D-2)!}. \tag{5.32}$$

Its Casimir is $\sum_{i<j} L_{ij}^2 = l(l+D-2)\hbar^2$, where the orbital angular momenta are defined as $L_{ij} = r_i p_j - r_j p_i$.

We also need to employ the Γ-matrices. The 2×2 Pauli matrices are just the rank-1 Γ-matrices. They can be generalized to rank-k Γ-matrices which contains $2k+1$ matrices anti-commuting with each other. Their dimensions are $2^k \times 2^k$. A convenient recursive definition is constructed based on the rank-$(k-1)$ Γ-matrices as

$$\begin{aligned} \Gamma_i^{(k)} &= \begin{bmatrix} 0 & \Gamma_a^{(k-1)} \\ \Gamma_a^{(k-1)} & 0 \end{bmatrix}, \quad \Gamma_{2k}^{(k)} = \begin{bmatrix} 0 & -iI \\ iI & 0 \end{bmatrix}, \\ \Gamma_{2k+1}^{(k)} &= \begin{bmatrix} I & 0 \\ 0 & -I \end{bmatrix}, \end{aligned} \tag{5.33}$$

where $i = 1, ..., 2k-1$. For $D = 2k+1$-dimensional space, its fundamental spinor is 2^k-dimensional. The generators are constructed $S_{ij} = \frac{1}{2}\Gamma_{ij}^{(k)}$ where

$$\Gamma_{ij}^{(k)} = -\frac{i}{2}[\Gamma_i^{(k)}, \Gamma_j^{(k)}]. \tag{5.34}$$

For the $D = 2k$-dimensional space, there are two irreducible fundamental representations with 2^{k-1} components. Their generators are denoted as S_{ij} and S'_{ij}, respectively, which can be constructed based on both rank-$(k-1)$ $\Gamma_i^{(k-1)}$ and $\Gamma_{ij}^{(k-1)}$-matrices. For the first $2k-1$ dimensions, the generators share the same form as

$$S_{ij} = S'_{ij} = \frac{1}{2}\Gamma_{ij}^{(k-1)}, \quad 1 \le i < j \le 2k-1, \tag{5.35}$$

while other generators $S_{i,2k}$ and $S'_{i,2k}$ differ by a sign as

$$S_{i,2k} = S'_{i,2k} = \pm\frac{1}{2}\Gamma_i^{(k-1)}, \quad 1 \le i \le 2k-1. \tag{5.36}$$

We couple $Y_{l,\{m\}}$ to the $SO(D)$ fundamental irreducible spinors. For simplicity, we use the same symbol s in this paragraph to denote the fundamental

spinor representation (Rep.) for $SO(D)$ with $D = 2k + 1$ and the two irreducible spinor Reps. for $SO(D)$ with $D = 2k$. The states split into the positive (j_+) and negative (j_-) helicity sectors. The bases are expressed as $\mathcal{Y}_{j_\pm;s,l,\{j_m\}}(\hat{\Omega})$, where $\{j_m\}$ is a set of $D-2$ quantum numbers for the subgroup chain. The degeneracy number of $\mathcal{Y}_{j_+;s,l,\{j_m\}}(\hat{\Omega})$ is

$$d_{j_+} = d_s \frac{(D+l-2)!}{l!(D-2)!}, \tag{5.37}$$

where d_s is the dimension of the fundamental spinor representation. Similarly, the degeneracy number of $\mathcal{Y}_{j_-,;s,l,\{j_m\}}(\hat{\Omega})$ is

$$d_{j_-} = d_s \frac{(D+l-3)!}{(l-1)!(D-2)!}. \tag{5.38}$$

The eigenvalues of the spin-orbit coupling term $\sum_{i<j} \Gamma_{ij} L_{ij}$ for the sectors of $\mathcal{Y}_{j_+;s,l,\{j_m\}}(\hat{\Omega})$ and $\mathcal{Y}_{j_-;s,l,\{j_m\}}(\hat{\Omega})$ are $l\hbar$ and $-(l+D-2)\hbar$, respectively. We present the eigenstates of the D-dimensional harmonic oscillator with fundamental spinors in the total angular momentum basis as

$$\psi^D_{n_r,j_\pm,s,l,\{j_m\}}(\vec{r}) = R_{n_r,l}(r)\mathcal{Y}_{j_\pm,s,l,\{j_m\}}(\hat{\Omega}), \tag{5.39}$$

where the radial wavefunction reads

$$R_{n_r,l}(r) = N^D_{n_r,l} \left(\frac{r}{l_0}\right)^l e^{-\frac{r^2}{2l_g^2}} F(-n_r, l+\frac{D}{2}, \frac{r^2}{l_0^2}) \tag{5.40}$$

and the normalization constant reads

$$N^D_{n_r,l} = \frac{l_0^{-\frac{D}{2}}}{\Gamma(l+\frac{1}{2}D)} \sqrt{\frac{2\Gamma(n_r+l+\frac{D}{2})}{\Gamma(n_r+1)}}. \tag{5.41}$$

5.5 The LLs of odd dimensional Dirac fermions

In this section, we generalize the 3D LL Hamiltonian for Dirac fermions to an arbitrary odd spatial dimensions $D = 2k + 1$. We need to use the rank-k Γ-matrices, which contains $2k + 1$ anti-commutable matrices at the dimensions of $2^k \times 2^k$ denoted as $\Gamma_i^{(k)} (1 \le i \le 2k+1)$. The definition of $\Gamma_i^{(k)}$ and the background information of the representation of the $SO(D)$ group is given in Sect. 5.4.

We define $\hat{B}_{2k+1} = -i\Gamma_i^{(k)}\hat{a}_i$ and the $2k+1$-dimensional LL Hamiltonian of Dirac fermions H_{2k+1} in the same way as in Eq. (5.7). Again the square of H_{2k+1} reduces to a block-diagonal form as

$$\begin{aligned}\frac{(H_{2k+1})^2}{\frac{1}{2}\hbar\omega} &= \frac{p^2}{2M} + \frac{1}{2}M\omega^2 r^2 - \omega\Big\{\sum_{i<j} L_{ij}\Gamma_{ij}^{(k)} \\ &+ \frac{2k+1}{2}\hbar\Big\}\begin{bmatrix} I & 0 \\ 0 & -I \end{bmatrix}, \end{aligned} \tag{5.42}$$

where $\Gamma_{ij}^{(k)} = -\frac{i}{2}[\Gamma_i^{(k)}, \Gamma_j^{(k)}]$. Each diagonal block of Eq. (5.42) is just the form the $2k+1$ D LL problem of non-relativistic fermions in Chapter 2.

Again we can define the following conserved quantity

$$K = \begin{bmatrix} \Gamma_{ij}^{(k)} L_{ij} + (D-2)\hbar & 0 \\ 0 & -(\Gamma_{ij}L_{ij} + \hbar) \end{bmatrix}, \tag{5.43}$$

K divides the eigenstates into two sectors $\Psi^I_{\pm n_r,j,\{j_m\}}$ and $\Psi^{II}_{\pm n_r,j,\{j_m\}}$,

$$\begin{aligned} K\Psi^I_{\pm n_r,j,\{j_m\}} &= \hbar(l+D-2)\Psi^I_{\pm n_r,j,\{j_m\}}, \\ K\Psi^{II}_{\pm n_r,j,\{j_m\}} &= -\hbar l\Psi^{II}_{\pm n_r,j,\{j_m\}}, \end{aligned} \tag{5.44}$$

respectively. As explained in Sect. 5.4, j represents the spin-orbit coupled representation for the $SO(D=2k+1)$ group, and $\{j_m\}$ represents a set of good quantum number of the subgroup chain from $SO(D-1)$ down to $SO(2)$.

Similarly as before, the sectors of $\Psi^{I,II}_{\pm n_r,j,\{j_m\}}$ are dispersionless and dispersive with respect to j, respectively. The concrete wavefunctions are the same as those in Eq. (5.25) and Eq. (5.27) by replacing the 3D wavefunction to the D-dimensional version of Eq. (5.39). The wavefunctions of $\Psi^{I,II}_{\pm n_r,j,\{j_m\}}$ are given explicitly as

$$\begin{aligned} \Psi^I_{\pm n_r,j,j_z}(\vec{r}) &= \frac{1}{\sqrt{2}}\begin{bmatrix} \psi^D_{n_r,s,j_+,l,\{j_m\}}(\vec{r}) \\ \pm i\psi^D_{n_r-1,s,j_-,l+1,\{j_m\}}(\vec{r}) \end{bmatrix}, \\ \Psi^{II}_{\pm n_r,j,j_z}(\vec{r}) &= \frac{1}{\sqrt{2}}\begin{bmatrix} \mp i\psi^D_{n_r,s,j_-,l+1,\{j_m\}}(\vec{r}) \\ \psi^D_{n_r,s,j_+,l,\{j_m\}}(\vec{r}) \end{bmatrix}. \end{aligned} \tag{5.45}$$

The dispersion relation for the LL branch of $\Psi^I_{\pm n_r,j,\{j_m\}}$ still behaves as

$$E_{\pm n_r;j,\{j_z\}} = \pm\hbar\omega\sqrt{n_r}, \tag{5.46}$$

while that for the branch of $\Psi^{II}_{\pm n_r,j,\{j_m\}}$ reads as

$$E_{\pm n_r;j,\{j_z\}} = \pm\hbar\omega\sqrt{n_r + l + \frac{D}{2}}. \tag{5.47}$$

Again each occupied zero energy LL contributes to $\frac{1}{2}$-fermion vacuum charge. If the zeroth LLs are fully filled, the vacuum charge is expressed as

$$\rho^D(r) = \frac{1}{2}\sum_{j,\{j_m\}} |\Psi^I_{0,j,\{j_m\}}(\vec{r})|^2 = \frac{1}{l_0^D}\Big\{\sum_{l=0}^{\infty}\frac{1}{\Gamma(l+\frac{D}{2})}\Big(\frac{r}{l_0}\Big)^{2l}\frac{g_l(D)}{\Omega_D}\Big\}e^{-\frac{r^2}{l_0^2}}, \tag{5.48}$$

where $D = 2k+1$; $g_l(D)$ is the degeneracy of the positive helicity sector of the fundamental spinor coupling to the l-th D-dimensional spherical harmonics, and its expression is the same as d_{j_+} given in Eq. (5.37); $\Omega_D = D\pi^{D/2}/\Gamma(D/2+1)$ is the area of D-dimensional unit sphere. Eq. (5.48) can be summed analytically as

$$\begin{aligned}\rho(r) &= \frac{\sqrt{2}}{4}\Big(\frac{2}{\pi l_0^2}\Big)^{\frac{D}{2}}F(D-1,\frac{D}{2},\frac{r^2}{l_0^2})e^{-\frac{r}{l_0^2}} \\ &\longrightarrow \frac{1}{(2\pi)^{\frac{D-1}{2}}l_0^D}\frac{1}{\Gamma(\frac{D-1}{2})}\Big(\frac{r}{l_0}\Big)^{D-2}, \text{ as } r\to\infty.\end{aligned} \tag{5.49}$$

Similarly, if the D-dimensional version of the mass term inside Eq. (5.9) is added, every wavefunction with the radial quantum number n_r hybridizes with its partner with $-n_r$ while keeping all other quantum numbers the same. The pair of new eigenvalues becomes $\pm\sqrt{(\hbar\omega)^2 n_r + \Delta^2}$. Again, the zero-th LL wavefunctions single out and remain the same, but their energies are shifted to Δ. For a similar open surface problem to that in Sect. 5.3.3, each LL with $n_r \neq 0$ develops a branch of gapless surface mode with the upturn (downturn) dispersion with respect to j for $n_r > 0$ ($n_r < 0$), respectively. The surface mode from the zeroth LL develops either upturn or downturn dispersions depending on the relative sign of the background field coupling and the vacuum mass.

5.6 The LLs of even dimensional Dirac fermions

The LL problem in the even dimensions with $D = 2k$ is more complicated. The $SO(2k)$ group has two irreducible fundamental spinor representations s and

s'. Each of them is with the dimension of 2^{k-1}. The construction of the $SO(2k)$ generators for the irreducible representations are introduced in Sect. 5.4.

Now we define $\hat{B}_{2k} = -i\Gamma_i^{(k)}\hat{a}_i$ where i runs over 1 to $2k$. Similarly to the 2D case, the counterpart of Eq. (5.7) in the $D = 2k$ dimensions $H_{D=2k}$ is reducible into two $2^k \times 2^k$ blocks as

$$H_\pm = \frac{\hbar\omega}{2}\begin{bmatrix} 0 & \pm\hat{a}_{2k}^\dagger + i\Gamma_i^{(k-1)}\hat{a}_i^\dagger \\ \pm\hat{a}_{2k} - i\Gamma_i^{(k-1)}\hat{a}_i & 0 \end{bmatrix}, \tag{5.50}$$

where the repeated index i runs over from 1 to $2k-1$. For each one of the reduced Hamiltonians $H_\pm$, each off-diagonal block has only the $SO(2k-1)$ symmetry. Nevertheless, each of $H_\pm$ is still $SO(2k)$ invariant. If we combine the two irreducible fundamental spinor representations s and s' together, the spin generators are defined as

$$S_{ij;s\oplus s'} = -\frac{i}{4}[\Gamma_i^{(k)}, \Gamma_j^{(k)}]. \tag{5.51}$$

Both of $H_\pm$ commute with the total angular momentum operators in the combined representation of $s \oplus s'$ defined as

$$J_{ij;s\oplus s'} = L_{ij} + S_{ij;s\oplus s'}. \tag{5.52}$$

We choose H_+ as an example to present the solutions of the LL wavefunctions in even dimensions. The K-operator is similarly defined as in Eq. (5.43) as

$$K_+ = \begin{bmatrix} 2S_{ij}L_{ij} + (D-2)\hbar & 0 \\ 0 & -(2S'_{ij}L_{ij} + \hbar) \end{bmatrix}, \tag{5.53}$$

where i, j run from 1 to $2k$, and S_{ij} and S'_{ij} are generators in the two fundamental spinor representations given in Eqs. (5.35) and (5.36), respectively. They again can be divided into two sectors of $\Psi^{+,I}$ and $\Psi^{+,II}$ whose eigenvalues of K_+ are $\hbar(l + D - 2)$ and $-\hbar l$, respectively. The dispersionless branch of $\Psi^{+,I}$ can be viewed as LLs, whose wavefunctions read

$$\Psi^{+,I}_{\pm n_r,j,\{j_m\}}(\vec{r}) = \frac{1}{\sqrt{2}}\begin{bmatrix} \psi_{n_r,j_+,s,l,\{j_m\}}(\vec{r}) \\ \mp i\psi_{n_r-1,j_-,s',l+1,\{j_m\}}(\vec{r}) \end{bmatrix}. \tag{5.54}$$

Their spectra are same as before $E_{\pm n_r,j,\{j_m\}} = \pm\hbar\omega\sqrt{n_r}$. Please note that the upper and lower components involve the s and s' representations, respectively. Similarly, the dispersive solutions of Ψ^{II} become

$$\Psi^{+,II}_{\pm n_r,j,\{j_m\}}(\vec{r}) = \frac{1}{\sqrt{2}}\begin{bmatrix} \mp i\psi_{n_r,j_-,s,l+1,\{j_m\}}(\vec{r}) \\ \psi_{n_r,j_+,s',l,\{j_m\}}(\vec{r}) \end{bmatrix}, \tag{5.55}$$

whose dispersions read $E_{\pm n_r,j,\{j_m\}} = \pm\hbar\omega\sqrt{n_r + l + \frac{D}{2}}$. The solutions to H_- are very similar to Eq. (5.54) and Eq. (5.55) by exchanging the irreducible fundamental spinor representation indices s and s'.

Again if the zeroth branch LLs are filled, the vacuum charge $\rho^D(\vec{r}) = \frac{1}{2}\sum_{j,\{j_m\}} |\Psi^I_{0,j,\{j_m\}}(\vec{r})|^2$ is calculated as

$$\rho^D(r) = \frac{1}{l_0^D}\Big\{\sum_{l=0}^{\infty}\frac{1}{\Gamma(l+\frac{D}{2})}\Big(\frac{r}{l_0}\Big)^{2l}\frac{g_l(D)}{\Omega_D}\Big\}e^{-\frac{r^2}{l_0^2}}, \tag{5.56}$$

where $D = 2k$, Ω_D and $g_l(D)$ are defined similarly as in Eq. (5.48). It can be summed over analytically as

$$\rho^D(r) = \frac{1}{4}\Big(\frac{2}{\pi l_0}\Big)^{\frac{D}{2}}F(D-1,\frac{D}{2},\frac{r^2}{l_0^2})e^{-\frac{r^2}{l_0^2}}, \tag{5.57}$$

which $\rho^D(r) \longrightarrow \frac{\sqrt{\pi}}{(2\pi l_0^2)^{\frac{D}{2}}}\frac{1}{\Gamma(\frac{D-1}{2})}\Big(\frac{r}{l_0}\Big)^{D-2}$, as $r \to +\infty$.

5.7 Summary

We have generalized the LL problem of 2D Dirac fermions to arbitrary higher dimensional flat spaces with spherical symmetry. This problem is essentially the square root problem of its non-relativistic LL problem with spherical symmetry in high dimensions in Chapter 2. The zero energy LLs is a branch of $\frac{1}{2}$-fermion modes. On the open boundary, each LL contributes one branch of helical surface modes. This series of LL problems can be viewed as the generalization of parity anomaly in 2D to arbitrary dimensions in a spherical way. An open question is that how to experimentally realize the case of the 3D systems.

Acknowledgements: This chapter is in part a reprint of the paper "Isotropic Landau levels of Dirac fermions in high dimensions" authored by Yi Li, Kenneth Intriligator, Yue Yu, and Congjun Wu, *Phys. Rev. B*, 85, 085132 (2012).

Chapter 6

The J-triplet Cooper pairing with magnetic dipolar interactions

6.1 Introduction

Ultracold atomic and molecular systems with electric and magnetic dipolar interactions have become the research focus in cold atom physics [121, 122, 123, 124, 125, 126, 127]. When dipole moments are aligned by external fields, dipolar interactions exhibit the $d_{r^2-3z^2}$-type anisotropy. The anisotropic Bose-Einstein condensations of dipolar bosons (e.g. ^{52}Cr) have been observed [128, 129, 130, 131]. For the fermionic electric dipolar systems, ^{40}K-^{87}Rb has been cooled down to nearly quantum-degeneracy [121]. Effects of the anisotropic electric dipolar interaction on the fermion many-body physics have been extensively investigated. In the Fermi liquid theory, both the single particle properties and collective excitations exhibit the $d_{r^2-3z^2}$ anisotropy [132, 133, 134, 135, 136, 137]. In the single-component Fermi systems, the leading order Cooper pairing instability lies in the p-wave channel, which is the simplest one allowed by Pauli's exclusion principle. The anisotropy of the electric dipolar interaction selects the instability in the p_z-channel, which is slightly hybridized with other odd partial wave channels [138, 139, 140, 141, 142, 143, 144, 145]. For two-component cases, the dipolar interaction leads to anisotropic spin-triplet pairing, and its orbital partial wave is again in the p_z-channel [146, 147, 148, 149]. The triplet pairing competes with the singlet pairing

in the hybridized $s + d_{r^2-3z^2}$-channel. The mixing between the singlet and triplet pairings has a relative phase $\pm\frac{\pi}{2}$, which leads to a novel time-reversal symmetry breaking Cooper pairing state [147].

An important recent experimental progress is the laser cooling and trapping of magnetic dipolar fermions of ^{161}Dy and ^{163}Dy with large atomic magnetic moments ($10\mu_B$) [125, 126]. There are important differences between magnetic and electric dipolar interactions. Electric dipole moments are essentially non-quantized classic vectors from the mixing between different rotational eigenstates, which are induced by external electric fields [121, 122], thus electric dipoles are frozen. In the absence of external fields, even though at each instant of time there is a dipole moment of the heteronuclear molecule, it is averaged to zero at a long time scale. In contrast, magnetic dipole moments of atoms are intrinsic, proportional to their hyper-fine spins with a Lande factor. Unpolarized magnetic dipolar Fermi systems are available, in which dipoles are defrozen as non-commutative quantum mechanical operators, thus lead to richer quantum spin physics of dipolar interactions. Furthermore, the magnetic dipolar interaction is actually isotropic in the unpolarized systems. It is invariant under simultaneous spin-orbit rotations but not separate spin or orbit rotations. This spin-orbit coupling is different from usual single particle one, but an interaction effect. It plays an important role in the Fermi liquid properties such as the unconventional magnetic states and ferro-nematic states predicted by Fregoso *et al* [150, 151].

It is natural to expect that magnetic dipolar interaction brings novel pairing symmetries not studied in condensed matter systems before. The systems of ^{161}Dy and ^{163}Dy are with a very large hyperfine spin of $F = \frac{21}{2}$, thus their Cooper pairing problem is expected to be very challenging. As a first step, we study the simplest case of spin-$\frac{1}{2}$, and find that the magnetic dipolar interaction provides a novel and robust mechanism to the p-wave ($L = 1$) spin triplet ($S = 1$) Cooper pairing to the first order of interaction strength, which comes from the attractive part of the magnetic dipolar interaction. In comparison, the p-wave triplet pairing in usual condensed matter systems, such as ^{3}He [152, 153, 154], is due to the spin-fluctuation mechanism, which is at the second order of interaction strength (see Refs. [155, 2] for reviews). This mechanism is based on strong ferromagnetic tendency from

the repulsive part of the ^{3}He-^{3}He interactions. Furthermore, the p-wave triplet Cooper pairing symmetry patterns in magnetic dipolar systems are novel, which do not appear in ^{3}He. The orbital and spin angular momenta of the Cooper pair are entangled into the total angular momentum $J = 1$, which is denoted as the J-triplet channel below. In contrast, in the ^{3}He-B phase [153], L and S are combined into $J = 0$; and in the ^{3}He-A phase, L and S are decoupled and J is not well-defined [154, 152]. There are two competing pairing possibilities in this J-triplet channel with different values of J_z: the helical polar state ($J_z = 0$) preserving time reversal (TR) symmetry, and the axial state ($J_z = \pm 1$) breaking TR symmetry. The helical polar state has point nodes and gapless Dirac spectra, which is a time-reversal invariant generalization of the ^{3}He-A phase with entangled spin and orbital degrees of freedom. In addition to usual phonon modes, its Goldstone modes contain the total angular momentum wave as entangled spin-orbital modes.

6.2 The magnetic dipolar interaction and spin-orbit couplings

We begin with the magnetic dipolar interaction between spin-$\frac{1}{2}$ fermions

$$V_{\alpha\beta,\beta'\alpha'}(\vec{r}) = \frac{\mu^2}{r^3}\big\{\vec{S}_{\alpha\alpha'}\cdot\vec{S}_{\beta\beta'} - 3(\vec{S}_{\alpha\alpha'}\cdot\hat{r})(\vec{S}_{\beta\beta'}\cdot\hat{r})\big\}, \tag{6.1}$$

where $\vec{r}$ is the relative displacement vector between two fermions; μ is the magnitude of the magnetic moment. Such an interaction is invariant under the combined $SU(2)$ spin rotation and $SO(3)$ space rotation. In other words, orbital angular momentum $\vec{L}$ and spin $\vec{S}$ are not separately conserved, but the total angular momentum $\vec{J} = \vec{L} + \vec{S}$ remains conserved. Its Fourier transformation reads [151]

$$V_{\alpha\beta;\beta'\alpha'}(\vec{q}) = \frac{4\pi}{3}\mu^2\big\{3(\vec{S}_{\alpha\alpha'}\cdot\hat{q})(\vec{S}_{\beta\beta'}\cdot\hat{q}) - \vec{S}_{\alpha\alpha'}\cdot\vec{S}_{\beta\beta'}\big\}. \tag{6.2}$$

The Hamiltonian in the second quantization form is written as

$$\begin{aligned} H &= \sum_{\vec{k},\alpha}\big[\epsilon(\vec{k}) - \mu_c\big]c^\dagger_\alpha(\vec{k})c_\alpha(\vec{k}) + \frac{1}{2V}\times \\ &\quad \sum_{\vec{k},\vec{k}',\vec{q}} V_{\alpha\beta;\beta'\alpha'}(\vec{k}-\vec{k}')P^\dagger_{\alpha\beta}(\vec{k};\vec{q})P_{\beta'\alpha'}(\vec{k}';\vec{q}), \end{aligned} \tag{6.3}$$

where $\epsilon(\vec{k}) = \hbar k^2/(2m)$; μ_c is the chemical potential; $P_{\beta'\alpha'}(\vec{k};\vec{q}) = c_{\beta'}(-\vec{k}+\vec{q})c_{\alpha'}(\vec{k}+\vec{q})$ is the pairing operator; the Greek indices α, β, α' and β' refer to $\uparrow$ and $\downarrow$; V is the volume of the system. We define a dimensionless parameter characterizing the interaction strength as the ratio between the characteristic interaction energy and the Fermi energy: $\lambda \equiv E_{int}/E_F = \frac{2}{3}\frac{\mu^2 m k_f}{\pi^2\hbar^2}$.

6.3 Unconventional Cooper pairing in magnetic dipolar interactions

We next study the symmetry of the Cooper pairing in the presence of Fermi surface, i.e., in the weak coupling theory. An important feature of the magnetic dipolar interaction in Eq. (6.1) is that it vanishes in the total spin singlet channel. Thus, we only need to study the triplet pairing in odd orbital partial wave channels. Considering uniform pairing states at the mean-field level, we set $\vec{q} = 0$ in Eq. (6.3), and define triplet pairing operators $P_s(\vec{k})$, which are eigen-operators of $\vec{S}_{1z} + \vec{S}_{2z}$ with eigenvalues $s_z = 0, \pm 1$, respectively. More explicitly, they are $P_0(\vec{k}) = \frac{1}{\sqrt{2}}[P_{\uparrow\downarrow}(\vec{k}) + P_{\downarrow\uparrow}(\vec{k})]$, $P_1(\vec{k}) = P_{\uparrow\uparrow}(\vec{k})$, $P_{-1}(\vec{k}) = P_{\downarrow\downarrow}(\vec{k})$. The pairing interaction of Eq. (6.3) reduces to

$$H_{pair} = \frac{1}{2V}\sum_{\vec{k},\vec{k}',s_z s_z'} \Big\{ V^T_{s_z s_z'}(\vec{k};\vec{k}') P^\dagger_{s_z}(\vec{k}) P_{s_z'}(\vec{k}') \Big\}, \tag{6.4}$$

where

$$\begin{aligned} V^T_{s_z s_z'}(\vec{k};\vec{k}') &= \frac{1}{2}\sum_{\alpha\beta\beta'\alpha'} \langle 1 s_z | \frac{1}{2}\alpha\frac{1}{2}\beta\rangle \langle 1 s_z' | \frac{1}{2}\alpha'\frac{1}{2}\beta'\rangle^* \\ &\quad \Big\{ V_{\alpha\beta,\beta'\alpha'}(\vec{k}-\vec{k}') - V_{\alpha\beta,\beta'\alpha'}(\vec{k}+\vec{k}') \Big\}. \end{aligned} \tag{6.5}$$

$\langle 1 s_z | \frac{1}{2}\alpha\frac{1}{2}\beta\rangle$ is the Clebsch-Gordan coefficient for two spin-$\frac{1}{2}$ states to form the spin triplet; and $V_{s_z s_z'}(\vec{k};\vec{k}')$ is an odd function of both $\vec{k}$ and $\vec{k}'$.

The decoupled mean-field Hamiltonian reads

$$H_{mf} = \frac{1}{2V}{\sum_{\vec{k}}}' \Psi^\dagger(\vec{k}) \begin{pmatrix} \xi(\vec{k})I & \Delta_{\alpha\beta}(\vec{k}) \\ \Delta^*_{\beta\alpha}(\vec{k}) & -\xi(\vec{k})I \end{pmatrix} \Psi(\vec{k}), \tag{6.6}$$

where we only sum over half of the momentum space; $\xi(\vec{k}) = \epsilon(\vec{k}) - \mu_{ch}$ and μ_{ch} is the chemical potential; $\Psi(\vec{k}) = (c_\uparrow(\vec{k}), c_\downarrow(\vec{k}), c_\uparrow^\dagger(-\vec{k}), c_\downarrow^\dagger(-\vec{k}))^T$; $\Delta_{\alpha\beta}$ is defined as $\Delta_{\alpha\beta} = \sum_{s_z} \langle 1 s_z | \frac{1}{2}\alpha \frac{1}{2}\beta \rangle^* \Delta_{s_z}$. Δ_{s_z} satisfies the mean-field gap function as

$$\begin{aligned} \Delta_{s_z}(\vec{k}) &= \frac{1}{V} \sum_{\vec{k}', s_z'} V^T_{s_z s_z'}(\vec{k}; \vec{k}') \langle |P_{s_z'}(\vec{k}')| \rangle \\ &= -\int \frac{d^3k'}{(2\pi)^3} V^T_{s_z s_z'}(\vec{k}; \vec{k}') [K(\vec{k}') - \frac{1}{2\epsilon_k}] \Delta_{s_z'}(\vec{k}'), \end{aligned} \tag{6.7}$$

where $K(\vec{k}') = \tanh[\frac{\beta}{2} E_i(\vec{k}')]/[2E_i(\vec{k}')]$. The integral in Eq. (6.7) is already normalized following the standard procedure [138]. For simplicity, we use the Born approximation in Eq. (6.7) by employing the bare interaction potential rather than the fully renormalized T-matrix, which applies in the dilute limit of weak interactions. The pairing symmetry, on which we are interested below, does not depend on the details that how the integral of Eq. (6.7) is regularized in momentum space. The Bogoliubov quasiparticle spectra become $E_{1,2}(\vec{k}) = \sqrt{\xi_k^2 + \lambda_{1,2}^2(\vec{k})}$, where $\lambda_{1,2}^2(\vec{k})$ are the eigenvalues of the positive-definite Hermitian matrix $\Delta^\dagger(\vec{k})\Delta(\vec{k})$. The free energy can be calculated as

$$\begin{aligned} F &= -\frac{2}{\beta} \sum_{\vec{k}, i=1,2} \ln \left[2 \cosh \frac{\beta E_{\vec{k},i}}{2} \right] \\ &\quad -\frac{1}{2V} \sum_{\vec{k}, \vec{k}', s_z, s_z'} \left\{ \Delta^*_{s_z}(\vec{k}) V^{T,-1}_{s_z s_z'}(\vec{k}; \vec{k}') \Delta_{s_z'}(\vec{k}) \right\}, \end{aligned} \tag{6.8}$$

where $V^{T,-1}_{s_z s_z'}(\vec{k}; \vec{k}')$ is the inverse of the interaction matrix defined as

$$\frac{1}{V} \sum_{\vec{k}', s_z'} V^T_{s_z, s_z'}(\vec{k}; \vec{k}') V^{T,-1}_{s_z', s_z''}(\vec{k}'; \vec{k}'') = \delta_{\vec{k}, \vec{k}''} \delta_{s_z, s_z''}. \tag{6.9}$$

We next linearize Eq. (6.7) around T_c and perform the partial wave analysis to determine the dominant pairing channel. Since the total angular momentum is conserved, we can use J to classify the eigen-gap functions denoted as $\phi^{a,JJ_z}_{s_z}(\vec{k})$. The index a is used to distinguish different channels sharing the same value of J. $\phi^{a,JJ_z}_{s_z}(\vec{k})$ satisfies

$$N_0 \int \frac{d\Omega_{k'}}{4\pi} V^T_{s_z s_z'}(\vec{k}; \vec{k}') \phi^{a;JJ_z}_{s_z'}(\vec{k}') = w^a_J \phi^{a;JJ_z}_{s_z}(\vec{k}), \tag{6.10}$$

where $N_0 = \frac{mk_f}{\pi^2\hbar^2}$ is the density of state at the Fermi surface; w_j^a are dimensionless eigenvalues; $\vec{k}, \vec{k}'$ are at the Fermi surface. Then Eq. (6.7) is linearized into a set of decoupled equations

$$\phi^{a;JJ_z}\{1 + w_J^a[\ln(2e^\gamma\bar{\omega})/(\pi k_B T)]\} = 0, \tag{6.11}$$

where $\bar{\omega}$ is an energy scale at the order of the Fermi energy playing the role of energy cut-off from the Fermi surface.

The decomposition of $V^T_{s_z s'_z}(\vec{k};\vec{k}')$ into spherical harmonics can be formulated as

$$\begin{aligned} &\frac{N_0}{4\pi}V^T_{s_z s'_z}(\vec{k};\vec{k}') \\ = &\sum_{Lm,L'm'} V_{Lms_z;L'm's'_z}Y^*_{Lm}(\Omega_k)Y_{L'm'}(\Omega_{\vec{k}'}), \end{aligned} \tag{6.12}$$

where $L = L'$ or $L = L' \pm 2$, and L, L' are odd numbers. The expressions of the dimensionless matrix elements $V_{Lms_z;L'm's'_z}$ are lengthy and will be presented elsewhere. By diagonalizing this matrix, we find that the most negative eigenvalue is $w^{J=1} = -3\pi\lambda/4$ lying in the channel with $J = L = 1$. All other negative eigenvalues are significantly smaller. Therefore, dominate pairing symmetry is identified as the J-triplet channel with $L = S = 1$ in the weak coupling theory. Following the standard method in Ref. [138], the transition temperature T_c is expressed as $T_c \approx \frac{2e^\gamma\bar{\omega}}{\pi}e^{-\frac{1}{|w^{J=1}|}}$. For a rough estimation of the order of magnitude of T_c, we set the prefactor in the expression of T_c as E_f.

In order to understand why the J-triplet channel is selected by the magnetic dipolar interaction, we present a heuristic picture based on a two-body pairing problem in real space. Dipolar interaction has a characteristic length scale $a_{dp} = m\mu^2/\hbar^2$ at which the kinetic energy scale equals the interaction energy scale. We are not interested in solving the radial equation but focus on the symmetry properties of the angular solution, thus, the distance between two spins is taken fixed at a_{dp}. We consider the lowest partial-wave, p-wave, channel with $L = 1$. The $3 \times 3 = 9$ states ($L = S = 1$) are classified into three sectors of $J = 0, 1$ and 2. In each channel of J, the interaction energies are diagonalized as

$$E_0 = E_{dp}, \quad E_1 = -\frac{1}{2}E_{dp}, \quad E_2 = \frac{1}{10}E_{dp}, \tag{6.13}$$

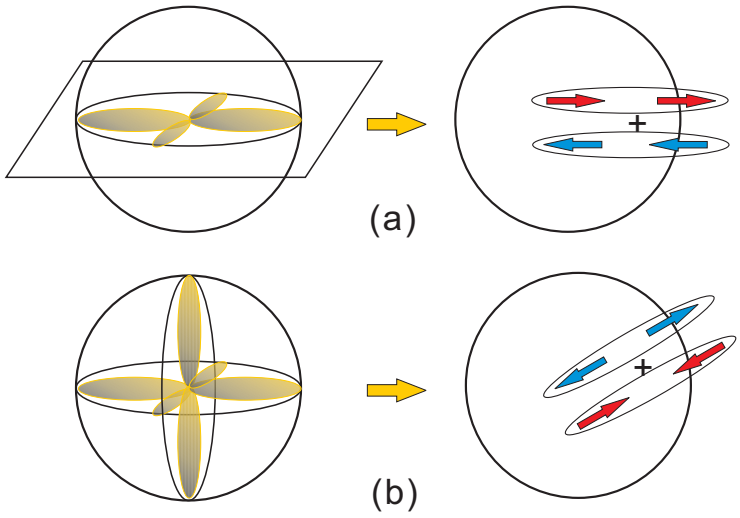

Figure 6.1: The spin configurations of the two-body states with a) $J = 1$ and $j_z = 0$ and b) $J = j_z = 0$. The interactions are attractive in a) but repulsive in b).

respectively, where $E_{dp} = \mu^2/a_{dp}^3$. Only the total angular momentum triplet sector with $J = 1$ supports bound states, thus is the dominant pairing channel and is consistent with the pairing symmetry in the weak-coupling theory.

This two-body picture applies in the strong coupling limit. Although a complete study of the strong coupling problem is beyond the scope of this thesis, this result provides an intuitive picture to understand pairing symmetry in the J-triplet sector from spin configurations. We define that χ_μ and $p_\mu(\hat{\Omega})$ are eigenstates with eigenvalues zero for operators $\hat{e}_\mu \cdot (\vec{S}_1 + \vec{S}_2)$ and $\hat{e}_\mu \cdot \vec{L}$ ($\mu = x, y, z$), which are the total spin and orbital angular momenta projected along the e_μ-direction. The J-triplet sector states are $\phi_\mu(\Omega) = \frac{1}{\sqrt{2}}\epsilon_{\mu\nu\lambda}\chi_\nu p_\lambda(\Omega)$ with ϕ_μ satisfying $(\hat{e}_\mu \cdot \vec{J})\phi_\mu = 0$. For example,

$$\begin{aligned} \phi_z(\hat{\Omega}) &= \frac{1}{\sqrt{2}}[\chi_x p_y(\hat{\Omega}) - \chi_y p_x(\hat{\Omega})] \\ &= \sqrt{\frac{3}{2}}\sin\theta\big\{|\alpha_{\hat{e}_\rho}\rangle_1|\alpha_{\hat{e}_\rho}\rangle_2 + |\beta_{\hat{e}_\rho}\rangle_1|\beta_{\hat{e}_\rho}\rangle_2\big\}, \end{aligned} \tag{6.14}$$

where $\hat{e}_\rho = \hat{x}\cos\phi + \hat{y}\sin\phi$ and $|\alpha_{e_\rho}\rangle$ and $|\beta_{e_\rho}\rangle$ are eigenstates of $\hat{e}_\rho \cdot \vec{\sigma}$ with eigenvalues of ± 1. As depicted in Fig. 6.1 (a), along the equator where ϕ_z has the largest weight, two spins are parallel and along $\hat{r}$, thus the interaction is dominated

by attraction. On the other hand, the eigenstate of $J = 0$ reads

$$\phi_0(\Omega) = \chi_\mu p_\mu(\Omega) = \frac{1}{\sqrt{2}}\big\{|\alpha_\Omega\rangle_1|\beta_\Omega\rangle_2 + |\beta_\Omega\rangle_1|\alpha_\Omega\rangle_2\big\}, \tag{6.15}$$

where $|\alpha_\Omega\rangle$ and $|\beta_\Omega\rangle$ are eigenstates of $\hat{\Omega}\cdot\vec{\sigma}$ with eigenvalues ± 1. As shown in Fig. 6.1 (b), along any direction of $\hat{\Omega}$, two spins are anti-parallel and longitudinal, thus the interaction is repulsive.

6.4 Ginzburg-Landau analysis of the competition in Cooper pairings

Let us come back to momentum space and study the competition between three paring branches in the J-triplet channel under the Ginzburg-Landau (GL) framework. We define

$$\begin{aligned}
\Delta_x(\vec{k}) &= \frac{1}{\sqrt{2}}[-\Delta_1(\vec{k}) + \Delta_{-1}(\vec{k})], \\
\Delta_y(\vec{k}) &= \frac{i}{\sqrt{2}}[\Delta_1(\vec{k}) + \Delta_{-1}(\vec{k})], \\
\Delta_z(\vec{k}) &= \Delta_0(\vec{k}).
\end{aligned} \tag{6.16}$$

The bulk pairing order parameters are defined as $\Delta_\mu = \frac{1}{V}\sum_k \hat{k}_\mu \Delta_\mu(\vec{k})$, where no summation over μ is assumed. We define pairing parameters and their real and imaginary parts as the following 3-vectors $\vec{\Delta} = (\Delta_x, \Delta_y, \Delta_z)$. The GL free energy is constructed to maintain the $U(1)$ and $SO(3)$ rotational symmetry as

$$F = \alpha\vec{\Delta}^*\cdot\vec{\Delta} + \gamma_1|\vec{\Delta}^*\cdot\vec{\Delta}|^2 + \gamma_2|\vec{\Delta}^*\times\vec{\Delta}|^2, \tag{6.17}$$

where

$$\alpha = N_0 \ln(\frac{T}{T_c}). \tag{6.18}$$

The sign of γ_2 determines two different pairing structures: $\mathrm{Re}\vec{\Delta} \parallel \mathrm{Im}\vec{\Delta}$ at $\gamma_2 > 0$, and $\mathrm{Re}\vec{\Delta} \perp \mathrm{Im}\vec{\Delta}$ at $\gamma_2 < 0$, respectively. Using the analogy of the spinor condensation of spin-1 bosons, the former is the polar pairing state and the latter is the axial pairing state [156, 157, 158, 159].

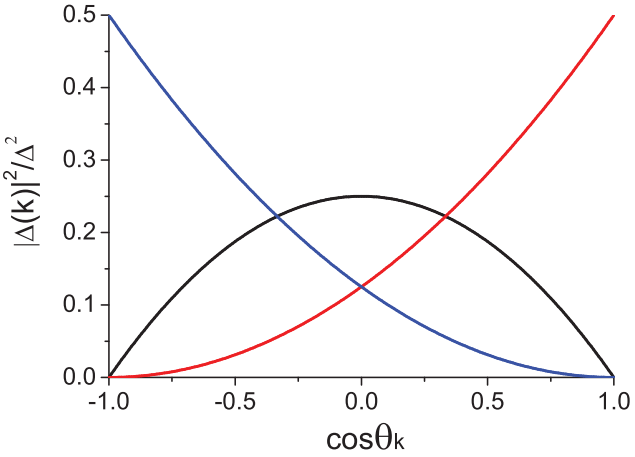

Figure 6.2: The angular distribution of the gap function $|\Delta(\vec{k})|^2$ v.s. $\cos\theta_k$ in the helical polar pairing state (the red line) and the axial pairing state (the black line).

For the polar pairing state, the order parameter configuration can be conveniently denoted as $\vec{\Delta} = e^{i\phi}|\Delta|\hat{z}$ up to a $U(1)$ phase and $SO(3)$-rotation. This pairing carries the quantum number $J_z = 0$. The pairing matrix $\Delta^{pl}_{\alpha\beta} = \frac{1}{2}|\Delta|[k_y\sigma_1 - k_x\sigma_2)i\sigma_2]_{\alpha\beta}$ reads

$$\Delta^{pl}_{\alpha\beta} = \frac{1}{2}|\Delta| \begin{bmatrix} -(\hat{k}_y + i\hat{k}_x) & 0 \\ 0 & \hat{k}_y - i\hat{k}_x \end{bmatrix}. \tag{6.19}$$

It equivalents to a superposition of $p_x \mp ip_y$ orbital configurations for spin-$\uparrow\uparrow$ ($\downarrow\downarrow$) pairs, respectively. Thus, this pairing state is helical. It is a unitary pairing state because $\hat{\Delta}^\dagger\hat{\Delta}$ is proportional to a 2×2 identity matrix. The Bogoliubov quasiparticle spectra are degenerate for two different spin configurations as $E^{pl}_{k,\alpha} = \sqrt{\xi_k^2 + |\Delta^{pl}(\vec{k})|^2}$ with the anisotropic gap function $|\Delta^{pl}(\vec{k})|^2 = \frac{1}{4}|\Delta|^2\sin^2\theta_k$ depicted in Fig. 6.2. They exhibit Dirac cones at north and south poles with opposite chiralities for two spin configurations.

Similarly, the order parameter configuration in the axial pairing state can be chosen as $\vec{\Delta} = \frac{1}{\sqrt{2}}e^{i\phi}|\Delta|(\hat{e}_x + i\hat{e}_y)$ up to the symmetry transformation. This state carries the quantum number of $J_z = 1$. The pairing matrix $\Delta^{ax}_{\alpha\beta} = \frac{1}{2\sqrt{2}}|\Delta|\{[\hat{k}_z(\sigma_1 +$

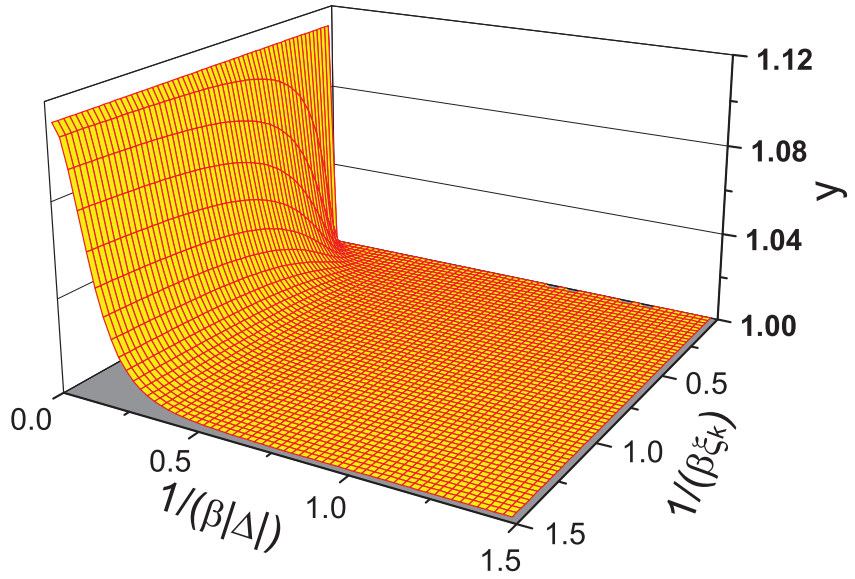

Figure 6.3: The ratio of the angular integrals of the free energy kernels $y(\frac{1}{\beta|\Delta|}, \frac{1}{\beta|\xi|})$, which is always larger than 1. This means that the polar pairing is favored at the mean-field level.

$i\sigma_2) + \sigma_z(\hat{k}_x + i\hat{k}_y]i\sigma_2\}_{\alpha\beta}$ takes the form

$$\Delta^{ax}_{\alpha\beta} = \frac{\sqrt{2}}{2}|\Delta| \begin{bmatrix} \hat{k}_z & \frac{1}{2}(\hat{k}_x + i\hat{k}_y) \\ \frac{1}{2}(\hat{k}_x - i\hat{k}_y) & 0 \end{bmatrix}. \tag{6.20}$$

This is a non-unitary pairing state since $\Delta^\dagger\Delta = |\Delta|^2[\frac{1}{2}(1+\hat{k}_z^2) + \hat{k}_z(\hat{k}\cdot\vec{\sigma})]$. The Bogoliubov quasiparticle spectra have two non-degenerate branches with anisotropic dispersion relations as $E^{ax}_{1,2}(\vec{k}) = \sqrt{\xi_k^2 + |\Delta^{ax}_{\pm}(\vec{k})|^2}$. The angular gap distribution $|\Delta^{ax}_{\pm}(\vec{k})|^2 = \frac{1}{8}|\Delta|^2(1 \pm \cos\theta_k)^2$ is depicted in Fig. 6.2. Each of branch 1 and 2 exhibits one node at north pole and south pole, respectively. Around the nodal region, the dispersion simplifies into $E_{1,2}(\vec{k}) = \sqrt{v_f^2(k_z \mp k_f)^2 + \frac{1}{32}|\Delta|^2(k_\parallel/k_f)^4}$, which is quadratic in the transverse momentum $k_\parallel = \sqrt{k_x^2 + k_y^2}$.

At the mean-field level, the helical polar pairing state is more stable than the axial state. Actually, this conclusion is not so obvious as in the case of ^{3}He-B phase, where the isotropic gap function is the most stable among all the possible gap functions [153]. Here, the gap functions are anisotropic in both the polar and helical pairing phases. We need to compare them by calculating their free energies in Eq. (6.8). The second term contributes the same to both pairing phases. Thus,

the first term determines the difference in free energies. Let us define the ratio between angular integrals of the free energy kernels in Eq. (6.8) of the two phases as

$$y(\lambda_1,\lambda_2)=\frac{\int d\Omega_k\ 2\ln\left[2\cosh\frac{\beta}{2}\sqrt{\xi_k^2+|\Delta^{pl}(\vec{k})|^2}\right]}{\int d\Omega_k\sum_{\pm}\ln\left[2\cosh\frac{\beta}{2}\sqrt{\xi_k^2+|\Delta_{\pm}^{ax}(\vec{k})|^2}\right]}, \tag{6.21}$$

where $\lambda_1=\frac{1}{\beta|\Delta|},\lambda_2=\frac{1}{\beta|\xi_k|}$. $y(\lambda_1,\lambda_2)$ is numerically plotted in Fig. 6.3. For arbitrary values of β, ξ_k, and $|\Delta|$, y is always larger than 1. Therefore, the polar state is favored more than the axial state. This can be understood from the convexity of the nonlinear term in Eq. (6.8), which favors isotropic angular distributions of $|\Delta(\vec{k})|^2$ [160]. Although neither gap function of these two states is absolutely isotropic as in the ^{3}He-B phase, the polar gap function is more isotropic from Fig. 6.2 and thus is favored. However, we need to bear in mind that we cannot rule out the possibility that certain strong coupling effects can stabilize the axial state. In fact, the ^{3}He-A phase can be stabilized under the spin feedback mechanism [155], which is a higher order effect in terms of interaction strength.

Next we discuss the classification of Goldstone modes and vortices in these two states. In the helical polar state, the remaining symmetries are $SO_J(2)\times Z_2$ as well as parity and time-reversal (TR), where Z_2 means the combined operation of rotation π around any axis in the xy-plane and a flip of the pairing phase by π. The Goldstone manifold is

$$[SO_J(3)\times U_c(1)]/[SO_J(2)\otimes Z_2]=[S_J^2\times U_c(1)]/Z_2. \tag{6.22}$$

The Goldstone modes include the phase phonon mode and two branches of spin-orbital modes. Vortices in this phase can be classified into the usual integer vortices in the phase sector and half-quantum vortices combined with π-disclination of the orientation of $\vec{\Delta}$. In the axial state, the rotation around z-axis generates a shift of the pairing phase, which can be canceled by a $U_c(1)$ transformation, thus, the remaining symmetry is $SO_{J_z-\phi}(2)$. The Goldstone manifold is $S^2\times U_c(1)$. Only integer vortices exist.

6.5 Summary and Discussions

In summary, we have found that the magnetic dipolar interaction provides a robust mechanism at first order in the interaction strength for a novel p-wave ($L = 1$) spin triplet ($S = 1$) Cooper pairing state, in which the total angular momentum of the Cooper pair is $J = 1$. This is a novel pairing pattern which does not appear in ^{3}He, and, to our knowledge, neither in any other condensed matter systems. These pairing states include the TR invariant helical polar pairing state and the TR breaking axial pairing state, both of which are distinct from the familiar ^{3}He-A and B phases.

Many interesting questions are open for further exploration, including the topological properties of these pairing states, vortices, spin textures, and spectra of collective excitations. The above theory only applies for spin-$\frac{1}{2}$ systems, in which the magnetic dipolar interaction is too small. For the pairing symmetry in a magnetic dipolar system with a large spin S, our preliminary results show that the basic features of the J-triplet pairing remains. The spins of two fermions are parallel forming $S_{tot} = 2S$ with orbital partial-wave $L = 1$, and the total $J = 2S$. In the current experiments in Ref. [161], the highest attainable density reaches $4 \times 10^{13}\text{cm}^{-1}$ for ^{161}Dy atoms with $S = \frac{21}{2}$. The corresponding dipolar energy is $E_{int} \approx 2\text{nK}$ and the Fermi energy for unpolarized gases $E_f \approx 13.6\text{nK}$, and thus $\lambda = E_{int}/E_f \approx 0.15$. If we use the same formula of $w^{J=1}$ above for an estimation of the most negative eigenvalue, we arrive at $T_c/T_f \approx 0.06$, which means that $T_c \approx 0.8\text{nK}$. Although it is still slightly below the lower limit of the accessible temperature in current experiments, we expect that further increase of fermions density, say, in optical lattices will greatly increase T_c.

Acknowledgements: This chapter is in part a reprint of the paper "The J-triplet Cooper pairing with magnetic dipolar interactions" authored by Yi Li and Congjun Wu, *Scientific Report*, 2, 392 (2012).

Chapter 7

Spin-orbit coupled Fermi liquid theory of ultra-cold magnetic dipolar fermions

7.1 Introduction

Recent experimental progress of ultracold electric dipolar heteronuclear molecules has become a major focus of ultracold atom physics [121, 122, 162]. Electric dipole moments are essentially classic polarization vectors induced by the external electric field. When they are aligned along the z axis, the electric dipolar interaction becomes anisotropic exhibiting the $d_{r^2-3z^2}$-type anisotropy. In Fermi systems, this anisotropy has important effects on many-body physics including both single-particle and collective properties [132, 133, 134, 135, 136, 163, 164, 165, 166, 167, 168]. Fermi surfaces of polarized electric dipolar fermions exhibit quadrupolar distortion elongated along the z axis [132, 133, 167, 136]. Various Fermi surface instabilities have been investigated including the Pomeranchuk type nematic distortions [134, 136] and stripelike orderings [163, 164]. The collective excitations of the zero sound mode exhibit anisotropic dispersions: The sound velocity is largest if the propagation wavevector $\vec{q}$ is along the z axis, and the sound is damped if $\vec{q}$ lies in the xy plane [136, 135]. Under the dipolar anisotropy, the phenomenological Landau interaction parameters become tridiagonal matrices, which

are calculated at the Hartree-Fock level [136, 134], and the anisotropic Fermi liquid theory for such systems has been systematically studied [136].

The magnetic dipolar gases are another type of dipolar system. Compared to the extensive research on electric dipolar Fermi systems, the study on magnetic dipolar ones is a new direction of research. On the experimental side, laser cooling and trapping Fermi atoms with large magnetic dipole moments (e.g., ^{161}Dy and ^{163}Dy with $\mu = 10\mu_B$)[125, 126, 169] have been achieved, which provides a new opportunity to study exotic many-body physics with magnetic dipolar interactions. There has also been a great amount of progress for realizing Bose-Einstein condensations of magnetic dipolar atoms [128, 129, 130, 131, 169].

Although the energy scale of the magnetic dipolar interaction is much weaker than that of the electric one, it is conceptually more interesting if magnetic dipoles are not aligned by external fields. Magnetic dipole moments are proportional to the hyperfine spin up to a Lande factor, thus, they are quantum-mechanical operators rather than the nonquantized classic vectors as electric dipole moments are. Furthermore, there is no need to use external fields to induce magnetic dipole moments. In fact, the unpolarized magnetic dipolar systems are isotropic. The dipolar interaction does not conserve spin nor orbit angular momentum, but is invariant under simultaneous spin-orbit (SO) rotation. This is essentially a spin-orbit coupled interaction. Different from the usual spin-orbit coupling of electrons in solids, this coupling appears at the interaction level but not at the kinetic-energy level.

The study of many-body physics of magnetic dipolar Fermi gases is just at the beginning. For the Fermi liquid properties, although magnetic dipolar Fermi gases were studied early in Refs. [170] and [134], the magnetic dipoles are frozen, thus, their behavior is not much different from the electric ones. It is the spin-orbit coupled nature that distinguishes non-polarized magnetic dipolar Fermi gases from polarized electric ones. The study along this line was was pioneered by Fregoso and Fradkin [150, 151]. They studied the coupling between ferromagnetic and ferronematic orders, thus, spin polarization distorts the spherical Fermi surfaces and leads to a spin-orbit coupling in the single-particle spectrum.

Since Cooper pairing superfluidity is another important aspect of the many-

body phase, we also briefly summarize the current progress in electric and magnetic dipolar systems. For the single-component electric dipolar gases, the simplest possible pairing lies in the p-wave channel because s-wave pairing is not allowed by the Pauli exclusion principle. The dipolar anisotropy selects the p_z-channel pairing [138, 139, 140, 141, 142, 143, 144, 145]. Interestingly, for the two-component case, the dipolar interaction still favors the triplet pairing in the p_z channel even though the s wave is also allowed. It provides a robust mechanism for the triplet pairing to the first order in the interaction strength [146, 147, 148, 149]. The mixing between the singlet and the triplet pairings is with a relative phase $\pm\frac{\pi}{2}$, which leads to a novel time-reversal symmetry-breaking pairing state [147]. The unconventional Cooper pairing symmetry in magnetic dipolar systems [165] was studied in Chapter 7. We have found that it provides a robust mechanism for a novel p-wave ($L = 1$) spin triplet ($S = 1$) Cooper pairing to the first order in interaction strength. It comes directly from the attractive part of the magnetic dipolar interaction. In comparison, the triplet Cooper pairings in ^{3}He and solid-state systems come from spin fluctuations, which is a second-order effect in interaction strength [155, 2]. Furthermore, that pairing symmetry was not studied in ^{3}He systems before in which orbital and spin angular momenta of the Cooper pair are entangled into the total angular momentum $J = 1$. In contrast, in the ^{3}He-B phase [153], L and S are combined as $J = 0$, and in the ^{3}He-A phase, L and S are decoupled and J is not well-defined [154, 152].

Fermi liquid theory is one of the most important paradigms in condensed matter physics on interacting fermions [171, 155]. Despite the pioneering papers [170, 134, 150, 151], a systematic study of the Fermi liquid properties of magnetic dipolar fermions is still lacking in the literature. In particular, Landau interaction matrices have not been calculated, and a systematic analysis of the renormalizations from magnetic dipolar interactions to thermodynamic quantities has not been performed. Moreover, collective excitations in magnetic dipolar ultracold fermions have not been studied before. All these are essential parts of Fermi liquid theory. The experimental systems of ^{161}Dy and ^{163}Dy are with a very large hyperfine spin of $F = \frac{21}{2}$, thus the Fermi liquid theory taking into account of all the complicated spin structure should be very challenging. We take the first step by considering

the simplest case of spin-$\frac{1}{2}$ magnetic dipolar fermions which preserve the essential features of spin-orbit physics and address the above questions.

In this chapter, we systematically investigate the Fermi liquid theory of the magnetic dipolar systems including both the thermodynamic properties and the collective excitations, focusing on the spin-orbit coupled effect. The Landau interaction functions are calculated and are diagonalized in the spin-orbit coupled basis. Renormalizations for thermodynamic quantities and the Pomeranchuk-type Fermi surface instabilities are studied. Furthermore, the collective modes are also spin-orbit coupled with a topologically non-trivial configuration of the spin distribution in momentum space. Their dispersion relation and configurations are analyzed.

Upon the completion of this work, we became aware of the nice work by Sogo *et al.* [172]. Reference [172] constructed the Landau interaction matrix for dipolar fermions with a general value of spin. The Pomeranchuk instabilities were analyzed for the special case of spin $\frac{1}{2}$, and collective excitations were discussed. This chapter has some overlaps on the above topics with Ref. [172] but with a significant difference, including the physical interpretation of the Pomeranchuk instability in the $J = 1^-$ channel and our discovery of an exotic propagating spin-orbit sound mode.

The remaining part of this chapter is organized as follows. The magnetic dipolar interaction is introduced in Sec. 7.2. The Landau interaction matrix is constructed at the Hartree-Fock level and is diagonalized in Sec. 7.3. In Sec. 7.4, we present the study of the Fermi liquid renormalization to thermodynamic properties from the magnetic dipolar interaction. The leading Pomeranchuk instabilities are analyzed. In Sec. 7.5, the spin-orbit coupled Boltzmann equation is constructed. We further perform the calculation of propagating spin-orbit coupled collective modes. We summarize this chapter in Sec. 7.6.

7.2 Magnetic Dipolar Hamiltonian

We introduce the magnetic dipolar interaction and the subtlety of its Fourier transform in this section.

The magnetic dipolar interaction between two spin-$\frac{1}{2}$ particles located at $\vec{r}_{1,2}$ reads

$$V_{\alpha\beta;\beta'\alpha'}(\vec{r}) = \frac{\mu^2}{r^3}\left[\vec{S}_{\alpha\alpha'}\cdot\vec{S}_{\beta\beta'} - 3(\vec{S}_{\alpha\alpha'}\cdot\hat{r})(\vec{S}_{\beta\beta'}\cdot\hat{r})\right], \tag{7.1}$$

where $\vec{S} = \frac{1}{2}\vec{\sigma}$; $\alpha, \alpha', \beta, \beta'$ take values of $\uparrow$ and $\downarrow$; $\vec{r} = \vec{r}_1 - \vec{r}_2$ and $\hat{r} = \vec{r}/r$ is the unit vector along $\vec{r}$.

The Fourier transform of Eq. (7.1) is

$$V_{\alpha\beta;\beta'\alpha'}(\vec{q}) = \frac{4\pi\mu^2}{3}\left[3(\vec{S}_{\alpha\alpha'}\cdot\hat{q})(\vec{S}_{\beta\beta'}\cdot\hat{q}) - \vec{S}_{\alpha\alpha'}\cdot\vec{S}_{\beta\beta'}\right], \tag{7.2}$$

which depends on the direction along the momentum transfer but not its magnitude. It is singular as $\vec{q} \to 0$. More rigorously, $V_{\alpha\beta,\beta'\alpha'}(\vec{q})$ should be further multiplied by a numeric factor [136] as

$$g(q) = 3\Big(\frac{j_1(q\epsilon)}{q\epsilon} - \frac{j_1(qL)}{qL}\Big), \tag{7.3}$$

where ϵ is a short range scale cut off, and L is the long distance cut off at the scale of sample size. The spherical Bessel function $j_1(x)$ shows the asymptotic behavior $j_1(x) \to \frac{x}{3}$ at $x \to 0$, and $j_1(x) \to \frac{1}{x}\sin(x - \frac{\pi}{2})$ as $x \to \infty$. In the long wavelength limit satisfying $q\epsilon \to 0$ and $qL \to \infty$, $g(q) \to 1$ and we recover Eq. (7.2). If $\vec{q}$ is exactly zero, $V_{\alpha\beta;\beta'\alpha'} = 0$, because the dipolar interaction is neither purely repulsive nor attractive, and its spatial average is zero.

The second quantization form for the magnetic dipolar interaction is expressed as

$$\begin{aligned} H_{int} &= \frac{1}{2V}\sum_{\vec{k},\vec{k}',\vec{q}} \psi^\dagger_\alpha(\vec{k}+\vec{q})\psi^\dagger_\beta(\vec{k}')V_{\alpha\beta;\beta'\alpha'}(\vec{q}) \\ &\times \psi_{\beta'}(\vec{k}'+\vec{q})\psi_{\alpha'}(\vec{k}), \end{aligned} \tag{7.4}$$

where V is the volume of the system. The density of states of two-component Fermi gases at the Fermi energy is $N_0 = \frac{mk_f}{\pi^2\hbar^2}$, and we define a dimensionless parameter $\lambda = N_0\mu^2$. λ describes the interaction strength, which equals the ratio between the average interaction energy and the Fermi energy up to a factor on the order of 1.

7.3 Spin-orbit coupled Landau interaction

In this section, we present the Landau interaction functions of the magnetic dipolar Fermi liquid, and perform the spin-orbit coupled partial wave decomposition.

7.3.1 The Landau interaction function

Interaction effects in the Fermi liquid theory are captured by the Landau interaction function. It describes the particle-hole channel forward-scattering amplitudes among quasiparticles on the Fermi surface. At the Hartree-Fock level, the Landau function is expressed as

$$f_{\alpha\alpha',\beta\beta'}(\hat{k},\hat{k}') = f^H_{\alpha\alpha',\beta\beta'}(\hat{q}) + f^F_{\alpha\alpha',\beta\beta'}(\hat{k},\hat{k}'), \tag{7.5}$$

where $\vec{k}$ and $\vec{k}'$ are at the Fermi surface with the magnitude of k_f and $\vec{q}$ is the small momentum transfer in the forward scattering process in the particle-hole channel. $f^H_{\alpha\alpha',\beta\beta'}(\vec{q}) = V_{\alpha\beta,\beta'\alpha'}(\hat{q})$ is the direct Hartree interaction, and $f^F_{\alpha\alpha',\beta\beta'}(\vec{k};\vec{k}') = -V_{\alpha\beta,\alpha'\beta'}(\vec{k}-\vec{k}')$ is the exchange Fock interaction. As $\vec{q}\to 0$, f^H is singular, thus we need to keep its dependence on the direction of $\hat{q}$. More explicitly,

$$f^H_{\alpha\alpha',\beta\beta'}(\hat{q}) = \frac{\pi\mu^2}{3} M_{\alpha\alpha',\beta\beta'}(\hat{q}), \tag{7.6}$$

$$f^F_{\alpha\alpha',\beta\beta'}(\hat{k};\hat{k}') = -\frac{\pi\mu^2}{3} M_{\alpha\alpha',\beta\beta'}(\hat{m}), \tag{7.7}$$

where the tensor is defined as $M_{\alpha\alpha',\beta\beta'}(\hat{q}) = 3(\vec{\sigma}_{\alpha\alpha'}\cdot\hat{q})(\vec{\sigma}_{\beta\beta'}\cdot\hat{q}) - \vec{\sigma}_{\alpha\alpha'}\cdot\vec{\sigma}_{\beta\beta'}$ and $\hat{m}$ is the unit vector along the direction of the momentum transfer $\hat{m} = \frac{\vec{k}-\vec{k}'}{|\vec{k}-\vec{k}'|}$. We have used the following identity:

$$\begin{aligned} & 3(\vec{\sigma}_{\alpha\beta'}\cdot\hat{m})(\vec{\sigma}_{\beta\alpha'}\cdot\hat{m}) - \vec{\sigma}_{\alpha\beta'}\cdot\vec{\sigma}_{\beta\alpha'} \\ = \; & 3(\vec{\sigma}_{\alpha\alpha'}\cdot\hat{m})(\vec{\sigma}_{\beta\beta'}\cdot\hat{m}) - \vec{\sigma}_{\alpha\alpha'}\cdot\vec{\sigma}_{\beta\beta'} \end{aligned} \tag{7.8}$$

to obtain Eq. (7.7).

7.3.2 The spin-orbit coupled basis

Due to the spin-orbit nature of the magnetic dipolar interaction, we introduce the spin-orbit coupled partial-wave basis for the quasiparticle distribution

over the Fermi surface following the steps below.

The $\delta n_{\alpha\alpha'}(\vec{k})$ is defined as

$$\delta n_{\alpha\alpha'}(\vec{k}) = n_{\alpha\alpha'}(\vec{k}) - \delta_{\alpha\alpha'} n_0(\vec{k}), \tag{7.9}$$

where $n_{\alpha\alpha'}(\vec{k}) = \langle \psi^\dagger_\alpha(\vec{k})\psi_{\alpha'}(\vec{k})\rangle$ is the Hermitian single-particle density matrix with momentum $\vec{k}$ and satisfies $n_{\alpha\alpha'} = n^*_{\alpha'\alpha}$ and $n_0(\vec{k})$ is the zero-temperature equilibrium Fermi distribution function $n_0(\vec{k}) = 1-\theta(k-k_f)$. $\delta n_{\alpha\alpha'}(\vec{k})$ is expanded in terms of the particle-hole angular momentum basis as

$$\begin{aligned} \delta n_{\alpha\alpha'}(\vec{k}) &= \sum_{Ss_z} \delta n_{Ss_z}(\vec{k}) \chi_{Ss_z,\alpha\alpha'} \\ &= \sum_{Ss_z} \delta n^*_{Ss_z}(\vec{k}) \chi^\dagger_{Ss_z,\alpha\alpha'}, \end{aligned} \tag{7.10}$$

where $\chi_{Ss_z,\alpha\alpha'}$ are the bases for the particle-hole singlet (density) channel with $S = 0$ and triplet (spin) channel with $S = 1$, respectively. They are defined as

$$\begin{aligned} \chi_{00,\alpha\alpha'} &= \delta_{\alpha\alpha'}, \\ \chi_{10,\alpha\alpha'} &= \sigma_{z,\alpha\alpha'}, \quad \chi_{1\pm1,\alpha\alpha'} = \frac{\mp1}{\sqrt{2}}(\sigma_{x,\alpha\alpha'} \pm i\sigma_{y,\alpha\alpha'}), \end{aligned} \tag{7.11}$$

which satisfy the orthonormal condition $\mathrm{tr}(\chi^\dagger_{Ss_z}\chi_{S's'_z}) = 2\delta_{SS'}\delta_{s_z s'_z}$.

Since quasiparticles are only well defined around the Fermi surface, we integrate out the radial direction and arrive at the angular distribution,

$$\delta n_{\alpha\alpha'}(\hat{k}) = \int \frac{k^2 dk}{(2\pi)^3} \delta n_{\alpha\alpha'}(\vec{k}). \tag{7.12}$$

Please note that angular integration is not performed in Eq. (7.12). We expand $\delta n_{\alpha\alpha'}(\hat{k})$ in the spin-orbit decoupled bases as

$$\begin{aligned} \delta n_{\alpha\alpha'}(\hat{k}) &= \sum_{LmSs_z} \delta n_{LmSs_z} Y_{Lm}(\hat{k}) \chi_{Ss_z,\alpha\alpha'}, \\ &= \sum_{LmSs_z} \delta n^*_{LmSs_z} Y^*_{Lm}(\hat{k}) \chi^\dagger_{Ss_z,\alpha\alpha'}, \end{aligned} \tag{7.13}$$

where $Y_{Lm}(\hat{k})$ is the spherical harmonics satisfying the normalization condition $\int d\hat{k} Y^*_{Lm}(\hat{k}) Y_{Lm}(\hat{k}) = 1$.

We can also define the spin-orbit coupled basis as

$$\begin{aligned}\mathcal{Y}_{JJz;LS}(\hat{k},\alpha\alpha') &= \sum_{ms_z}\langle LmSs_z|JJ_z\rangle Y_{Lm}(\hat{k})\chi_{Ss_z,\alpha\alpha'},\\ \mathcal{Y}^{\dagger}_{JJz;LS}(\hat{k},\alpha\alpha') &= \sum_{ms_z}\langle LmSs_z|JJ_z\rangle Y^{*}_{Lm}(\hat{k})\chi^{\dagger}_{Ss_z,\alpha\alpha'},\end{aligned} \tag{7.14}$$

where $\langle LmSs_z|JJ_z\rangle$ is the Clebsch-Gordon coefficient and $\mathcal{Y}_{JJz;LS}$ satisfies the orthonormal condition of

$$\int d\hat{k}\ \mathrm{tr}[\mathcal{Y}^{\dagger}_{JJ_z;LS}(\hat{k})\mathcal{Y}_{J'J'_z;L'S'}(\hat{k})] = 2\delta_{JJ'}\delta_{J_zJ'_z}\delta_{LL'}\delta_{SS'}. \tag{7.15}$$

Using the spin-orbit coupled basis, $\delta n_{\alpha\alpha'}(\hat{k})$ is expanded as

$$\begin{aligned}\delta n_{\alpha\alpha'}(\hat{k}) &= \sum_{JJ_z;LS}\delta n_{JJ_z;LS}\ \mathcal{Y}_{JJ_z;LS}(\hat{k},\alpha\alpha')\\ &= \sum_{JJ_z;LS}\delta n^{*}_{JJ_z;LS}\mathcal{Y}^{\dagger}_{JJ_z;LS}(\hat{k},\alpha\alpha'),\end{aligned} \tag{7.16}$$

where $\delta n_{JJz;LS} = \sum_{ms_z}\langle LmSs_z|JJ_z\rangle\delta n_{LmSs_z}$.

7.3.3 Partial-wave decomposition of the Landau function

We are ready to perform the partial-wave decomposition for Landau interaction functions. The tensor structures in Eqs. (7.6) and (7.7) only depend on $\vec{\sigma}_{\alpha\alpha'}$ and $\vec{\sigma}_{\beta\beta'}$, thus the magnetic dipolar interaction only contributes to the spin-channel Landau parameters, i.e., $S = 1$. In the spin-orbit decoupled basis, the Landau functions of the Hartree and Fock channels are expanded, respectively, as

$$\begin{aligned}\frac{N_0}{4\pi}f^{H,F}_{\alpha\alpha';\beta\beta'}(\hat{k},\hat{k}') &= \sum_{Lms_z;L'm's'_z} Y_{Lm}(\hat{k})\chi_{1s_z}(\alpha\alpha')\\ &\times\ T^{H,F}_{Lm1s_z;L'm'1s'_z}Y^{*}_{L'm'}(\hat{k}')\chi^{\dagger}_{1s'_z}(\beta\beta').\end{aligned} \tag{7.17}$$

For later convenience, we have multiplied the density of states N_0 and the factor of $1/4\pi$ such that $T^{H,F}$ are dimensionless matrices. Without loss of generality, in the Hartree channel, we choose $\hat{q} = \hat{z}$.

The matrix elements in Eq. (7.17) are presented below. In the Hartree channel,

$$T^{H}_{Lm1s_z;L'm'1s'_z} = \frac{\pi\lambda}{3}(2\delta_{s_z,0}-\delta_{s_z,\pm1})\delta_{L,0}\delta_{L',0}\delta_{m,0}\delta_{m',0}\delta_{s_z s'_z}; \tag{7.18}$$

and in the Fock channel,

$$T^{F}_{Lm1s_z;L'm'1s'_z} = -\frac{\pi\lambda}{2}\Big(\frac{\delta_{LL'}}{L(L+1)}-\frac{\delta_{L+2,L'}}{3(L+1)(L+2)}-\frac{\delta_{L-2,L'}}{3(L-1)L}\Big)$$
$$\times\int d\Omega_r[\delta_{s_z s'_z}-4\pi Y_{1s_z}(\Omega_r)Y^*_{1s'_z}(\Omega_r)]Y_{Lm}(\Omega_r)Y^*_{L'm'}(\Omega_r). \tag{7.19}$$

The magnetic dipolar interaction is isotropic, thus the spin-orbit coupled basis are the most convenient. In these basis, the Landau matrix is diagonal with respect to the total angular momentum J and its z-component J_z as

$$\frac{N_0}{4\pi}f_{\alpha\alpha';\beta\beta'}(\hat{k},\hat{k}') = \sum_{JJ_zLL'}\mathcal{Y}_{JJz;L1}(\hat{k},\alpha\alpha')F_{JJ_zL1;JJ_zL'1}\,\mathcal{Y}^{\dagger}_{JJz;L'1}(\hat{k},\beta\beta'). \tag{7.20}$$

The matrix kernel $F_{JJ_zL1;JJ_zL'1}$ reads as

$$F_{JJ_zL1;JJ_zL'1} = \frac{\pi\lambda}{3}\delta_{J,1}\delta_{L,0}\delta_{L',0}(2\delta_{J_z,0}-\delta_{J_z,\pm1})$$
$$+\sum_{ms_z;m's'_z}\langle Lm1s_z|JJ_z\rangle\langle L'm'1s'_z|JJ_z\rangle T^{F}_{Lm1s_z;L'm'1s'_z}. \tag{7.21}$$

We found that up to a positive numeric factor, the second term in Eq. (7.21) is the same as the partial-wave matrices in the particle-particle pairing channel, which was derived for the analysis of the Cooper pairing instability in magnetic dipolar systems presented in Chapter 7.

However, the above matrix kernel $F_{JJ_zL1;JJ_zL'1}$ is not diagonal for channels with the same values of JJ_z but different orbital angular momentum indices L and L'. Moreover, the conservation of parity requires that even and odd values of L do not mix. Consequently, $F_{JJ_zL1;JJ_zL'1}$ is either diagonalized or reduced into a small size of just 2×2. For later convenience of studying collective modes and thermodynamic instabilities, we present below the prominent Landau parameters in some low partial-wave channels. Below, we use $(J^{\pm}J_zLS)$ to represent these channels in which $\pm$ represents even and odd parities, respectively.

The parity odd channel of $J = 0^-$ only has one possibility of (0^-011) in which

$$F_{0^-011;0^-011} = \frac{\pi}{2}\lambda. \tag{7.22}$$

There is another even parity density channel with $J = 0^+$, i.e., (0^+000), which receives contribution from short range s-wave interaction but no contribution from the magnetic dipolar interaction at the Hartree-Fock level. The parity odd channel of $J = 1^-$ only comes from (1^-J_z11) in which

$$F_{1^-J_z11;1^-J_z11} = -\frac{\pi}{4}\lambda. \tag{7.23}$$

Another channel of $J = 1^-$, i.e., (1^-J_z10), channel from the p-wave channel density interactions, which again receives no contribution from magnetic dipolar interaction at the Hartree-Fock level. These two $J = 1^-$ modes are spin- and charge-current modes, respectively, and thus, do not mix due to their opposite symmetry properties under time-reversal transformation.

We next consider the even parity channels. The $J = 1^+$ channels include two possibilities of $(JJ_zLS) = (1^+J_z01), (1^+J_z21)$. The former is the ferromagnetism channel, and the latter is denoted as the ferronematic channel in Refs. [[134]] and [[150]]. Due to the spin-orbit nature of the magnetic dipolar interaction, these two channels are no longer independent but are coupled to each other. Because the Hartree term breaks the rotational symmetry, the hybridization matrices for $J_z = 0, \pm 1$ are different. For the case of $J_z = 0$, it is

$$F_{1^+0} = \begin{pmatrix} F_{1001;1001} & F_{1001;1021} \\ F_{1021;1001} & F_{1021;1021} \end{pmatrix} = \frac{\pi\lambda}{12}\begin{pmatrix} 8 & \sqrt{2} \\ \sqrt{2} & 1 \end{pmatrix}, \tag{7.24}$$

whose two eigenvalues and their associated eigenvectors are

$$\begin{aligned} w_1^{1^+0} &= 0.69\pi\lambda, \quad \psi_1^{1^+0} = (0.98, 0.19)^T, \\ w_2^{1^+0} &= 0.06\pi\lambda, \quad \psi_2^{1^+0} = (-0.19, 0.98)^T. \end{aligned} \tag{7.25}$$

The hybridization is small. For the case of $J_z = \pm 1$, the Landau matrices are the

same as

$$F_{1^+1} = \begin{pmatrix} F_{1101;1101} & F_{1101;1121} \\ F_{1121;1101} & F_{1121;1121} \end{pmatrix} = \frac{\pi\lambda}{12} \begin{pmatrix} -4 & \sqrt{2} \\ \sqrt{2} & 1 \end{pmatrix}. \tag{7.26}$$

Again the hybridization is small as shown in the eigenvalues and their associated eigenvectors

$$\begin{aligned} w_1^{1^+1} &= -0.37\pi\lambda, \quad \psi_1^{1^+1} = (0.97, -0.25)^T, \\ w_2^{1^+1} &= 0.12\pi\lambda, \quad \psi_2^{1^+1} = (0.25, 0.97)^T. \end{aligned} \tag{7.27}$$

Landau parameters, or, matrices, in other high partial-wave channels are neglected, because their magnitudes are significantly smaller than those above.

We need to be cautious on using Eqs. (7.24) and (7.26) in which the Hartree contribution of Eq. 7.6 is taken. However, Eq. (7.6) is valid in the limit $q \ll k_f$ but should be much larger than the inverse of sample size $1/L$. It is valid to use Eqs. (7.24) and (7.26) when studying the collective spin excitations in Sec. 7.5 below. However, when studying thermodynamic properties, say, magnetic susceptibility, under the external magnetic-field uniform at the scale of L, the induced magnetization is also uniform. In this case, the Hartree contribution is suppressed to zero, thus the Landau matrices in the $J = 1^+$ channel are the same for all the values of J_z as

$$\begin{aligned} F_{1^+,thm}(\lambda) &= \begin{pmatrix} F_{1J_z01;1J_z01} & F_{1J_z01;1J_z21} \\ F_{1J_z21;1J_z01} & F_{1J_z21;1J_z21} \end{pmatrix}_{thm} \\ &= \frac{\pi\lambda}{12} \begin{pmatrix} 0 & \sqrt{2} \\ \sqrt{2} & 1 \end{pmatrix}. \end{aligned} \tag{7.28}$$

In this case, the hybridization between these two channels is quite significant. The two eigenvalues and their associated eigenvectors are

$$\begin{aligned} w_1^{1^+} &= -\frac{\pi}{12}\lambda, \quad \psi_1^{1^+} = (\sqrt{\frac{2}{3}}, -\sqrt{\frac{1}{3}})^T, \\ w_2^{1^+} &= \frac{\pi}{6}\lambda, \quad \psi_2^{1^+} = (\sqrt{\frac{1}{3}}, \sqrt{\frac{2}{3}})^T. \end{aligned} \tag{7.29}$$

7.4 Thermodynamic quantities

In this section, we study the renormalizations for thermodynamic properties by the magnetic dipolar interaction and investigate the Pomeranchuk-type Fermi surface instabilities.

7.4.1 Thermodynamics susceptibilities

The change in the ground-state energy with respect to the variation in the Fermi distribution density matrix include the kinetic and interaction parts as

$$\frac{\delta E}{V} = \frac{\delta E_{kin}}{V} + \frac{\delta E_{int}}{V}. \tag{7.30}$$

The kinetic-energy variation is expressed in terms of the angular distribution of $\delta n_{\alpha\alpha'}(\hat{k})$ as

$$\begin{aligned} \frac{\delta E_{kin}}{V} &= \frac{4\pi}{N_0}\sum_{\alpha\alpha'}\int d\hat{k}\delta n_{\alpha\alpha'}(\hat{k})\delta n_{\alpha'\alpha}(\hat{k}) \\ &= \frac{8\pi}{N_0}\sum_{LmSS_z}\delta n^*_{LmSs_z}\delta n_{LmSs_z}, \end{aligned} \tag{7.31}$$

where the units of $\delta n_{Ss_z}(\hat{k})$ and δn_{LmSs_z} are the same as the inverse of the volume. The variation in the interaction energy is

$$\begin{aligned} \frac{\delta E_{int}}{V} &= \frac{1}{2}\sum_{\alpha\alpha'\beta\beta'}\iint d\hat{k}d\hat{k}' f_{\alpha\alpha',\beta\beta'}(\hat{k},\hat{k}')\delta n_{\alpha'\alpha}(\hat{k})\delta n_{\beta'\beta}(\hat{k}') \\ &= 2\sum_{Lms_zL'm's'_z;S}\delta n^*_{LmSs_z} f_{LmSs_z,L'm'Ss'_z}\delta n^*_{L'm'Ss'_z}. \end{aligned} \tag{7.32}$$

Adding them together and changing to the spin-orbit coupled basis, we arrive at

$$\frac{\delta E}{V} = \frac{8\pi}{N_0}\sum_{JJ_z;LL';S}\delta n^*_{JJ_z;LS} M_{JJ_zLS;JJ_zL'S}\delta n_{JJ_z;L'S}, \tag{7.33}$$

where the matrix elements are

$$M_{JJ_zLS;JJ_zL'S} = \delta_{LL'} + F_{JJ_zLS;JJ_zL'S}. \tag{7.34}$$

In the presence of the external field h_{JJ_zLS}, the ground state energy becomes

$$\begin{aligned}\frac{\delta E}{V} &= 16\pi\Big\{\frac{1}{2\chi_0}\sum_{JJ_zLL'S}\delta n^*_{JJ_z;LS}M_{JJ_zLS;JJ_zL'S}\delta n_{JJ_z;L'S} \\ &- \sum_{JJ_zLS}h_{JJ_zLS}\delta n_{JJ_z;LS}\Big\},\end{aligned} \tag{7.35}$$

where $\chi_0 = N_0$ is the Fermi liquid density of states. At the Hartree-Fock level, N_0 receives no renormalization from the magnetic dipolar interaction. The expectation value of δn_{JJ_zLS} is calculated as

$$\delta n_{JJ_zLS} = \chi_0\sum_{L'}(M)^{-1}_{JJ_zLS;JJ_zL'S}h_{JJ_zL'S}. \tag{7.36}$$

For the $J = 1^+$ channel, $M^{-1} \approx I - F_{1^+,thm}(\lambda)$ up to first order of λ in the case of $\lambda \ll 1$. As a result, the external magnetic field $\vec{h}$ along the z axis not only induces the z-component spin polarization, but also induces a spin-nematic order in the channel of $(J^+J_zLS) = (1^+021)$, which is an effective spin-orbit coupling term as

$$\begin{aligned}\delta H &= \frac{\sqrt{2}}{12}\pi\lambda h\sum_k\psi^\dagger_\alpha(\vec{k})\Big\{\big[(k^2-3k_z^2)\sigma_z \\ &- 3k_z(k_x\sigma_x + k_y\sigma_y)\big]\Big\}\psi_\beta(\vec{k}).\end{aligned} \tag{7.37}$$

Apparently, this term breaks time-reversal symmetry, and thus cannot be induced by the relativistic spin-orbit coupling in solid states. This magnetic field induced spin-orbit coupling in magnetic dipolar systems was studied by Fregoso *et al.* [134, 150]

7.4.2 Pomeranchuk instabilities

Even in the absence of external fields, Fermi surfaces can be distorted spontaneously known as Pomeranchuk instabilities [173]. Intuitively, we can imagine the Fermi surface as the elastic membrane in momentum space. The instabilities occur if the surface tension in any of its partial-wave channels becomes negative. In the magnetic dipolar Fermi liquid, the thermodynamic stability condition is equivalent to the fact that all the eigenvalues of the matrix $M_{JJ_zLS;JJ_zL'S}$ are positive.

We next check the negative eigenvalues of the Landau matrix in each partial-wave channel. Due to the absence of external fields, the Pomeranchuk instabilities are allowed to occur as a density wave state with a long wave length $q \to 0$. For the case of $J = 1^+$, it is clear that in the channel of $J_z = \pm 1$, the eigenvalue $w_1^{1^+1}$ in Eq. (7.27) is negative and the largest among all the channels. Thus the leading channel instability is in the $(JJ_z) = (1^+ \pm 1)$ channel, which occurs at $w_1^{1^+1} < -1$, or, equivalently, $\lambda > \lambda_{1^+1}^c = 0.86$. The corresponding eigenvector shows that it is mostly a ferromagnetism order parameter with small hybridization with the ferronematic channel. A repulsive short-range s wave scattering, which we neglected above will enhance ferromagnetism and, thus, will drive $\lambda_{1^+1}^c$ to a smaller value. The wavevector $\vec{q}$ of the spin polarization should be on the order of $1/L$ to minimize the energy cost of twisting spin, thus, essentially exhibiting a domain structure. The spatial configuration of the spin distribution should be complicated by actual boundary conditions. In particular, the three-vector nature of spins implies the rich configurations of spin textures. An interesting result is that the external magnetic field actually weakens the ferromagnetism instability. If the spin polarization is aligned by the external field, the Landau interaction matrix changes to Eq. (7.28). The magnitude of the negative eigenvalue is significantly smaller than that of Eq. (7.26). As a result, an infinitesimal external field cannot align the spin polarization to be uniform but a finite amplitude is needed.

For simplicity, we only consider ferromagnetism with a single plane wave vector $\vec{q}$ along the z axis, then the spin polarization spirals in the xy-plane. Since $q \sim 1/L$, we can still treat a uniform spin polarization over a distance large comparable to the microscopic length scale. Without loss of generality, we set the spin polarization along the x axis. As shown in Ref. [150], ferromagnetism induces ferronematic ordering. The induced ferronematic ordering is also along the x axis, whose spin-orbit coupling can be obtained based on Eq. (7.37) by a permutation among components of $\vec{k}$ as $H'_{so}(\vec{k}) \propto (k^2 - 3k_x^2)\sigma_x - 3k_x(k_y\sigma_y + k_z\sigma_z)$. According to Eq. (7.27), ferromagnetism and ferronematic orders are not strongly hybridized, the energy scale of the ferronematic SO coupling is about 1 order smaller than that of ferromagnetism. An interesting point of this ferromagnetism is that it distorts the spherical shape of the Fermi surface as pointed by Fregoso

and Fradkin [150]. This anisotropy will also affect the propagation of Goldstone modes. Furthermore, spin waves couple to the oscillation of the shape of Fermi surfaces bringing Landau damping to spin waves. This may result in non-Fermi liquid behavior for fermion excitations, and will be studied in a future work. This effect in the nematic symmetry-breaking Fermi liquid state has been extensively studied before in the literature [174, 175, 176, 177, 178, 179].

The next subleading instability is in the $J = 1^-$ channel with $L = 1$ and $S = 1$ as shown in Eq. (7.23), which is a spin-current channel. The generated order parameters are spin-orbit coupled. For the channel of $J_z = 0$, the generated SO coupling at the single-particle level exhibits the three-dimensional (3D) Rashba type as

$$H_{so,1^-} = |n_z| \sum_k \psi^\dagger_\alpha(\vec{k})(k_x\sigma_y - k_y\sigma_x)_{\alpha\beta}\psi_\beta(\vec{k}), \tag{7.38}$$

where $|n_z|$ is the magnitude of the order parameter. The same result was also obtained recently in Ref. [172]. In the absence of spin-orbit coupling, the $L = S = 1$ channel Pomeranchuk instability was studied in Refs. [[180]] and [[181]], which exhibits the unconventional magnetism with both isotropic and anisotropic versions. They are particle-hole channel analogies of the p-wave triplet Cooper pairings of ^{3}He isotropic B and anisotropic A phases, respectively. In the isotropic unconventional magnetic state, the total angular momentum of the order parameter is $J = 0$, which exhibits the $\vec{k} \cdot \vec{\sigma}$-type spin-orbit coupling. This spin-orbit coupling is generated from interactions through a phase transition and, thus, was denoted as the spontaneous generation of spin-orbit coupling. In Eq. (7.38), the spin-orbit coupling that appears at the mean-field single-particle level cannot be denoted as spontaneous because the magnetic dipolar interaction possesses the spin-orbit nature. Interestingly, in the particle-particle channel, the dominant Cooper pairing channel has the same partial-wave property of $L = S = J = 1$ [165].

The instability in the $J = 1^-$ (spin current) channel is weaker than that in the 1^+ (ferromagnetism) channel because the magnitude of Landau parameters is larger in the former case. The 1^- channel instability should occur after the appearance of ferromagnetism. Since spin-current instability breaks parity, whereas, ferromagnetism does not, this transition is a genuine phase transition. For

simplicity, we consider applying an external magnetic field along the z axis in the ferromagnetic state to remove the spin texture structure. Even though the $J = 1^+$ and 1^- channels share the same property under rotation transformation, they do not couple at the quadratic level because of their different parity properties. The leading-order coupling occurs at the quartic order as

$$\delta F = \beta_1(\vec{n}\cdot\vec{n})(\vec{S}\cdot\vec{S}) + \beta_2|\vec{n}\times\vec{S}|^2, \tag{7.39}$$

where $\vec{n}$ and $\vec{S}$ represent the order parameters in the $J = 1^-$ and 1^+ channels, respectively. β_1 needs to be positive to keep the system stable. The sign of β_2 determines the relative orientation between $\vec{n}$ and $\vec{S}$. It cannot be determined purely from the symmetry analysis but depends on microscopic energetics. If $\beta_2 > 0$, it favors $\vec{n} \parallel \vec{S}$, and $\vec{n} \perp \vec{S}$ is favored at $\beta_2 < 0$.

7.5 The spin-orbit coupled collective modes

In this section, we investigate another important feature of the Fermi liquid, the collective modes, which again exhibit the spin-orbit coupled nature.

7.5.1 Spin-orbit coupled Boltzmann equation

We employ the Boltzmann equation to investigate the collective modes in the Fermi liquid state[171]

$$\begin{aligned}&\frac{\partial}{\partial t}n(\vec{r},\vec{k},t) - \frac{i}{\hbar}[\epsilon(\vec{r},\vec{k},t), n(\vec{r},\vec{k},t)] + \frac{1}{2}\sum_i \left\{\frac{\partial\epsilon(\vec{r},\vec{k},t)}{\partial k_i}, \frac{\partial n(\vec{r},\vec{k},t)}{\partial r_i}\right\}\\ &-\frac{1}{2}\sum_i \left\{\frac{\partial\epsilon(\vec{r},\vec{k},t)}{\partial r_i}, \frac{\partial n(\vec{r},\vec{k},t)}{\partial k_i}\right\} = 0,\end{aligned} \tag{7.40}$$

where $n_{\alpha\alpha'}(\vec{r},\vec{k},t)$ and $\epsilon_{\alpha\alpha'}(\vec{r},\vec{k},t)$ are the density and energy matrices for the coordinate $(\vec{r},\vec{k})$ in the phase space and $[,]$ and $\{,\}$ mean the commutator and anticommutator, respectively. Under small variations in $n_{\alpha\alpha'}(\vec{r},\vec{k},t)$ and $\epsilon_{\alpha\alpha'}(\vec{r},\vec{k},t)$,

$$\begin{aligned} n_{\alpha\alpha'}(\vec{r},\vec{k},t) &= n_0(k)\delta_{\alpha\alpha'} + \delta n_{\alpha\alpha'}(\vec{r},\vec{k},t),\\ \epsilon_{\alpha\alpha'}(\vec{r},\vec{k},t) &= \epsilon(k)\delta_{\alpha\alpha'} + \int \frac{d^3k'}{(2\pi)^3} f_{\alpha\alpha',\beta\beta'}(\hat{k},\hat{k}')\\ &\times \delta n_{\beta\beta'}(\hat{k}'). \end{aligned} \tag{7.41}$$

the above Boltzmann equation can be linearized. Plugging the plane-wave solution of

$$\delta n_{\alpha\alpha'}(\vec{r},\vec{k},t)=\sum_{q}\delta n_{\alpha\alpha'}(\vec{k})e^{i(\vec{q}\cdot\vec{r}-\omega t)}, \tag{7.42}$$

we arrive at

$$\begin{aligned}\delta n_{\alpha\alpha'}(\hat{k}) &- \frac{1}{2}\frac{\cos\theta_k}{s-\cos\theta_k}\sum_{\beta\beta'}\int d\Omega_{k'}\frac{N_0}{4\pi}f_{\alpha\alpha',\beta\beta'}(\hat{k},\hat{k}')\\ &\times \delta n_{\beta\beta'}(\hat{k}')=0,\end{aligned} \tag{7.43}$$

where s is the dimensionless parameter $\omega/(v_f q)$. The propagation direction of the wavevector $\vec{q}$ is defined along the z-direction.

In the spin-orbit decoupled basis defined as δn_{LmSs_z} in Sec. 7.3.2, the linearized Boltzmann equation becomes

$$\delta n_{LmSs_z} + \Omega_{LL';m}(s)F_{L'm'Ss_z;L''m''Ss_z''}\delta n_{L''m''Ss_z''}=0, \tag{7.44}$$

where $\Omega_{LL'}(s)$ is equivalent to the particle-hole channel Fermi bubble in the diagrammatic method as

$$\Omega_{LL';m}(s)=-\int d\Omega_{\hat{k}}Y^*_{Lm}(\hat{k})Y_{L'm}(\hat{k})\frac{\cos\theta_k}{s-\cos\theta_k}. \tag{7.45}$$

For later convenience, we present $\Omega_{LL';m}$ in several channels of LL' and m as follows

$$\begin{aligned}\Omega_{00;0}(s) &= 1-\frac{s}{2}\ln|\frac{1+s}{1-s}|+i\frac{\pi}{2}s\Theta(s<1),\\ \Omega_{10;0}(s) &= \Omega_{01;0}=\sqrt{3}s\Omega_{00;0}(s),\\ \Omega_{11;0}(s) &= 1+3s^2\Omega_{00;0}(s),\\ \Omega_{11;1}(s) &= \Omega_{11;-1}(s)=-\frac{1}{2}\Big[1-3(1-s^2)\Omega_{00;0}(s)\Big].\end{aligned} \tag{7.46}$$

Equation (7.44) can be further simplified by using the spin-orbit coupled basis $\delta n_{JJ_z;LS}$ defined in Sec. 7.3.2,

$$\begin{aligned}\delta n_{JJ_z;LS} &+ \sum_{J';LL'}K_{JJ_zLS;J'J_zL'S}(s)F_{J'J_zL'S;J'J_zL''S}\\ &\times \delta n_{J'J_zL''S}=0,\end{aligned} \tag{7.47}$$

where the matrix kernel $K_{JJ_zLS;J'J_zL'S}$ reads

$$\begin{aligned} K_{JJ_zLS;J'J_zL'S}(s) &= \sum_{ms_z} \langle LmSs_z|JJ_z\rangle\langle L'mSs_z|J'J_z\rangle \\ &\times \Omega_{LL';m}(s). \end{aligned} \tag{7.48}$$

7.5.2 The spin-orbit coupled sound modes

Propagating collective modes exist if Landau parameters are positive. In these collective modes, interactions among quasiparticles rather than the hydrodynamic collisions provide the restoring force. Because only the spin channel receives renormalization from the magnetic dipolar interaction, we only consider spin channel collective modes. The largest Landau parameter is in the (1^+001) channel in which the spin oscillates along the direction of $\vec{q}$. The mode in this channel is the longitudinal spin zero sound. On the other hand, due to the spin-orbit coupled nature, the Landau parameters are negative in the transverse spin channels of $(1^+ \pm 1\ \ 0\ \ \pm 1)$, and thus no propagating collective modes exist in these channels. The hybridization between (1^+001) and (1^+021) is small as shown in Eq. (7.25), and the Landau parameter in the (1^+021) channel is small, thus, this channel also is neglected below for simplicity.

Because the propagation wave vector $\vec{q}$ breaks the parity and 3D rotation symmetries, the (1^+001) channel couples to other channels with the same J_z. As shown in Eq. (7.47), the coupling strengths depend on the magnitudes of Landau parameters. We truncate Eq. (7.47) by keeping the orbital partial-wave channels of $L = 0$ and $L = 1$ because Landau parameters with orbital-partial waves $L \geq 2$ are negligible. There are three channels with $L = S = 1$ as (0^-011), (1^-011), and (2^-011). We further check the symmetry properties of these four modes under the reflection with respect to any plane containing $\vec{q}$. The mode of (1^-011) is even and the other three are odd, thus it does not mix with them. The Landau parameter in the (2^-011) channel is calculated as $\frac{\pi}{20}\lambda$, which is 1 order smaller than those in (1^+001) and (1^-001), thus this channel is also neglected. We only keep these two coupled channels (1^+001) and (1^-001) in the study of collective spin excitations.

The solution of the two coupled modes reduces to a 2×2 matrix linear

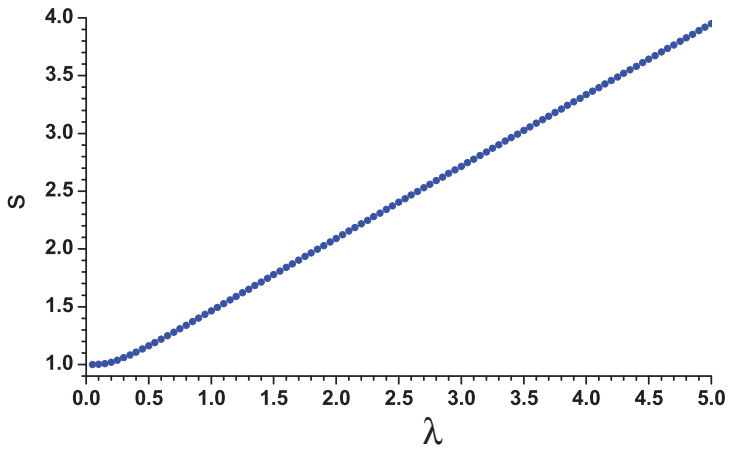

Figure 7.1: The sound velocity s in the unit of v_f v.s. the dipolar coupling strength λ. At $0 < \lambda \ll 1$, $s(\lambda) \approx 1 + 0^+$. On the order of $\lambda \gg 1$, $s(\lambda)$ becomes linear with the slope indicated in Eq. (7.56).

equation as

$$\begin{pmatrix} 1+\Omega_{00;0}(s)F_{1001;1001} & s\Omega_{00;0}(s)F_{0011;0011} \\ s\Omega_{00;0}(s)F_{1001;1001} & 1+\Omega_{00;0}(s)F_{0011;0011} \end{pmatrix} \begin{pmatrix} \delta n_{1001} \\ \delta n_{0011} \end{pmatrix} = 0, \tag{7.49}$$

where the following relations are used

$$\begin{aligned} K_{1001;1001}(s) &= \Omega_{00;0}(s) \\ K_{1001;0011}(s) &= K_{0011;1001}(s) = \langle 0010|10\rangle\langle 1010|00\rangle\Omega_{01;0}(s) = s\Omega_{00;0}(s) \\ K_{0011,0011}(s) &= \sum_m |\langle 1m1-m|00\rangle|^2\Omega_{11;m}(s) = \frac{1}{3}\Omega_{11;0}(s) + \frac{2}{3}\Omega_{11;1}(s) = \Omega_{00;0}(s). \end{aligned} \tag{7.50}$$

The condition of the existence of nonzero solutions of Eq. (7.49) becomes

$$(1-s^2)\Omega_{00;0}^2(s) + 2\Omega_{00;0}(s)\frac{F_+}{F_\times^2} + \frac{1}{F_\times^2} = 0, \tag{7.51}$$

where $F_+ = (F_{1001:1001} + F_{0011;0011})/2$ and $F_\times = \sqrt{F_{1001:1001}F_{0011;0011}}$.

Let us discuss several important analytical properties of its solutions. In order for collective modes to propagate in Fermi liquids, its sound velocity must

satisfy $s > 1$, otherwise it enters the particle-hole continuum and is damped, a mechanism called Landau damping. We can solve Eq. (7.51) as

$$\Omega^{\pm}_{00;0}(s) = \frac{F_+ \pm \sqrt{F_+^2 + (s^2-1)F_\times^2}}{(s^2-1)F_\times^2}. \tag{7.52}$$

Only the expression of the $\Omega^{-}_{00;0}(s)$ is consistent with $s > 1$ and is kept. The other branch has no solution of the propagating collective modes.

Let us analytically check two limits with large and small values of λ, respectively. In the case of $0 < \lambda \ll 1$ such that $s \to 1 + 0^+$, Eq. (7.51) reduces to

$$\Omega_{00;0}(s_{\lambda\ll 1}) \approx 1 - \frac{1}{2}\ln 2 + \frac{1}{2}\ln(s-1) = -\frac{1}{2F_+}. \tag{7.53}$$

Its sound velocity solution is

$$s_{\lambda\ll 1} \;\approx\; 1 + 2e^{-2\left(1+\frac{1}{2F_+}\right)} = 1 + 2e^{-2-\frac{12}{7\pi\lambda}}. \tag{7.54}$$

The eigenvector can be easily obtained as $\frac{1}{\sqrt{2}}(1,1)^T$, which is an equal mixing between these two modes. On the other hand, in the case of $\lambda \gg 1$, we also expect $s \gg 1$, and thus Eq. (7.51) reduces to

$$\Omega_{00;0}(s_{\lambda\gg 1}) \approx -\frac{1}{sF_\times} = -\frac{1}{3s^2}, \tag{7.55}$$

whose solution becomes

$$s_{\lambda\gg 1} \approx \frac{F_\times}{3} = \frac{\pi}{3\sqrt{3}}\lambda. \tag{7.56}$$

In our case, F_{1001} is larger than F_{0011} but is on the same order. The eigenvector can be solved as $\frac{1}{\sqrt{2F_+}}(\sqrt{F_{0011}}, \sqrt{F_{1001}})^T$ in which the weight of the (0011) channel is larger.

The dispersion of the sound velocity s with respect to the dipolar interaction strength λ is solved numerically as presented in Fig. 7.1. Collective sound excitations exist for all the interaction strengths with $s > 1$. In both limits of $0 \ll \lambda \ll 1$ and $\lambda \gg 1$, the numerical solutions agree with the above asymptotic analysis of Eqs. (7.54) and (7.56). In fact, the linear behavior of $s(\lambda)$ already appears at $\lambda \sim 1$, and the slope is around 0.6. For all the interaction strengths, the (1^+001) and (0^-011) modes are strongly hybridized.

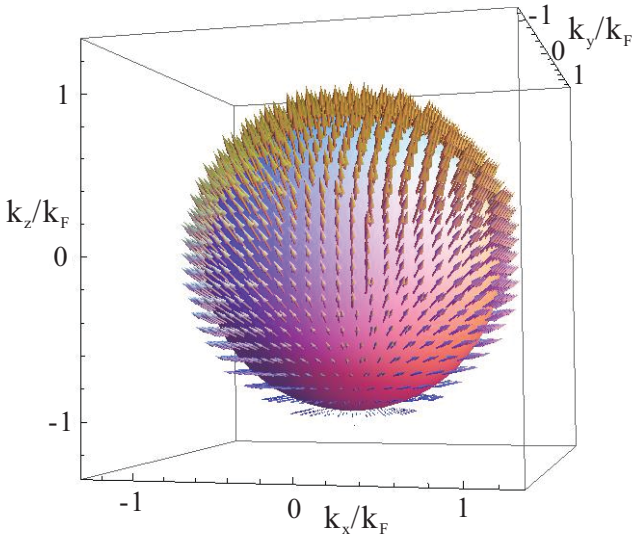

Figure 7.2: The spin configuration [Eq. (7.57)] of the zero-sound mode over the Fermi surface shows hedgehog-type topology at $\lambda = 10$. The common sign of u_1 and u_2 is chosen to be positive, which gives rise to the Pontryagin index $+1$. Although the hedgehog configuration is distorted in the z component, its topology does not change for any values of λ describing the interaction strength.

This mode is an oscillation of spin-orbit coupled Fermi surface distortions. The configuration of the $(0^{-}011)$ mode exhibits an oscillating spin-orbit coupling of the $\vec{k}\cdot\vec{\sigma}$ type. This is the counterpart of the isotropic unconventional magnetism, which spontaneously generates the $\vec{k}\cdot\vec{\sigma}$-type coupling [180, 181]. The difference is that, here, it is a collective excitation rather than an instability. It strongly hybridizes with the longitudinal spin mode. The spin configuration over the Fermi surface can be represented as

$$\vec{s}(\vec{r},\vec{k},t) = \begin{pmatrix} u_2 \sin\theta_{\vec{k}} \cos\phi_{\vec{k}} \\ u_2 \sin\theta_{\vec{k}} \sin\phi_{\vec{k}} \\ u_2 \cos\phi_{\vec{k}} + u_1 \end{pmatrix} e^{i(\vec{q}\cdot\vec{r} - sqv_f t)}, \tag{7.57}$$

where $(u_1, u_2)^T$ is the eigenvector for the collective mode. We have checked that for all the values of λ, $|u_2| > |u_1|$ is satisfied with no change in their relative sign, thus the spin configuration as shown in Fig. 7.2 is topologically non-trivial with the Pontryagin index ± 1 which periodically flips the sign with time and the spatial coordinate along the propagating direction. It can be considered as a topological

zero sound.

7.6 Summary

We have presented a systematic study on the Fermi liquid theory with the magnetic dipolar interaction, emphasizing its intrinsic spin-orbit coupled nature. Although this spin-orbit coupling does not exhibit at the single-particle level, it manifests in various interaction properties. The Landau interaction function is calculated at the Hartree-Fock level and is diagonalized by the total angular momentum and parity quantum numbers. The Pomeranchuk instabilities occur at the strong magnetic dipolar interaction strength generating effective spin-orbit coupling in the single-particle spectrum.

We have also investigated novel collective excitations in the magnetic dipolar Fermi liquid theory. The Boltzmann transport equations are decoupled in the spin-orbit coupled channels. We have found an exotic collective excitation, which exhibits spin-orbit coupled Fermi surface oscillations with a topologically nontrivial spin configuration, which can be considered as a topological zero-sound-like mode.

Acknowledgements: This chapter is in part a reprint of the paper "Spin-orbit coupled Fermi liquid theory with magnetic dipolar interaction", Yi Li and Congjun Wu, *Phys. Rev. B*, 85, 205126 (2012).

Chapter 8

Concluding remarks and outlook

We have already presented several studies on novel states of matter with non-trivial topological properties in both condensed matter and ultra-cold atom systems. Below we summarize the main results in this thesis and discuss open problems for further research.

First, we have constructed Landau levels for both Schrödinger and Dirac fermions in three and four dimensions. This provides a new mechanism for high dimensional topological insulators, which is independent from the well-studied band inversion mechanism. Furthermore, the flat energy spectra of Landau levels are an advantage in which interaction effects are non-perturbative. High dimensional Landau level Hamiltonians and eigen wavefunctions are based on harmonic oscillators, and thus are simple and explicit. The lowest Landau level wavefunctions further exhibit elegant quaternionic analyticity which is a natural extension of the complex analyticity to high dimensions. Generalizations of Landau levels to the Landau-type gauges, Dirac fermions, and parity breaking systems are also systematically performed. Below we present some open questions.

1. The elegant quaternionic analyticity of the three and four dimensional lowest Landau level wavefunctions provides a promising platform for the numeric and analytic studies of fractional topological states. Since the complex analyticity plays an important role in studying fractional quantum Hall effects in 2D, we plan to explicitly construct Laughlin-type wavefunction for fractional topological states based on the quaternionic analytic wavefunctions,

and further study novel fractional excitations and their exotic statistics.

2. Unlike the two-dimensional Landau level systems in which there exists the magnetic translation symmetry, such a symmetry does not exist in our cases in three and four dimensions. The usual calculation method for the Z_2 topological index is based on Bloch-wave band structures associated with translation symmetry, and thus does not apply in our systems. So far, we have used the explicit calculations of surface spectra, whose helical and chiral properties infer their non-trivial bulk topology. Since topological properties should not rely on translational symmetry, an open question is how to define the topological index in an inhomogeneous system. In particular, the harmonic potential is the simplest inhomogeneity, we are interested in constructing a rigorous mathematical formulation in such a system.

3. An important question is experimental realizations of three dimensional Landau level Hamiltonians, including both non-relativistic and relativistic ones in both symmetric and Landau-type gauges. We will seek collaborations with experimentalists in both condensed matter and ultra-cold atom physics for realizations and detections.

Second, we have studied the spin-orbit coupling effects in ultra-cold magnetic dipolar fermion atoms. Magnetic dipolar interactions are rotationally invariant only under simultaneous spin-orbit rotations. Thus different from the conventional spin-orbit coupling which is at the single-particle level, magnetic dipolar interactions generate spin-orbit coupling effects at the interaction level. They exhibit in various aspects in many-body physics with novel topological properties. In particular, it leads to a robust pairing mechanism for the Weyl pairing state in the p-wave spin triplet channel. It is a novel pairing symmetry in which the total spin and orbital angular momentum of the Cooper pair are entangled into the total angular momentum $J = 1$. Such a state is different from both ^{3}He-A and B phases. We are interested in further exploring these systems with following open questions.

1. So far, we have considered a toy model of spin-$\frac{1}{2}$ fermions interacting with magnetic dipolar interactions. However, the energy scale of magnetic dipolar

interactions are usually very week. Thus, in real experimental systems, the magnetic dipole moments are very large in order to enhance the interaction energy scale. We need to generalize our previous study of Cooper pairing to dipolar fermions with large spins. Even richer patterns of unconventional and topological Cooper pairings are expected.

2. We are interested in further exploring non-trivial topological properties of our novel spin triplet Weyl pairing, including the surface modes and topological defects. In particular, we expect a variety of rich topological spin textures, superfluid vortices, and their combined defects. Novel fermion zero modes, such as Majorana fermions, can exhibit around these defects. Such systems will exhibit novel topological properties that do not appear in the superfluid ^{3}He systems.

3. We will actively explore the collaboration opportunity with experimental groups of ultra-cold fermions. The study of dipolar fermions has become a hot research topic in ultra-cold community. Extensive studies have been performed in electric dipolar systems. The research on magnetic dipolar systems is just beginning which provides a large opportunity for exploring novel states.

Bibliography

[1] N. D. Mermin. The topological theory of defects in ordered media. *Rev. Mod. Phys.*, 51:591–648, Jul 1979.

[2] G.E. Volovik. *The Universe in a Helium droplet*. Oxford University Press, USA, 2009.

[3] M. M. Salomaa and G. E. Volovik. Quantized vortices in superfluid ^{3}He. *Rev. Mod. Phys.*, 59:533–613, Jul 1987.

[4] John B. Kogut. An introduction to lattice gauge theory and spin systems. *Rev. Mod. Phys.*, 51:659–713, Oct 1979.

[5] K. Klitzing, G. Dorda, and M. Pepper. New method for high-accuracy determination of the fine-structure constant based on quantized Hall resistance. *Phys. Rev. Lett.*, 45(6):494–497, 1980.

[6] D. C. Tsui, H. L. Stormer, and A. C. Gossard. Two-dimensional magnetotransport in the extreme quantum limit. *Phys. Rev. Lett.*, 48:1559–1562, May 1982.

[7] DJ Thouless, M. Kohmoto, MP Nightingale, and M. Den Nijs. Quantized Hall conductance in a two-dimensional periodic potential. *Phys. Rev. Lett.*, 49(6):405–408, 1982.

[8] F. D. M. Haldane. Model for a quantum hall effect without landau levels: Condensed-matter realization of the "parity anomaly". *Phys. Rev. Lett.*, 61:2015–2018, Oct 1988.

[9] J. E. Avron, R. Seiler, and B. Simon. Homotopy and quantization in condensed matter physics. *Phys. Rev. Lett.*, 51:51–53, Jul 1983.

[10] Q. Niu, D.J. Thouless, and Y.S. Wu. Quantized Hall conductance as a topological invariant. *Phys. Rev. B*, 31(6):3372–3377, 1985.

[11] M. Kohmoto. Topological invariant and the quantization of the Hall conductance. *Ann. Phys.*, 160(2):343–354, 1985.

[12] Joseph E. Avron, Ruedi Seiler, and Barry Simon. Quantum hall effect and the relative index for projections. *Phys. Rev. Lett.*, 65:2185–2188, Oct 1990.

[13] RB Laughlin. Quantized Hall conductivity in two dimensions. *Phys. Rev. B*, 23(10):5632–5633, 1981.

[14] B. I. Halperin. Quantized hall conductance, current-carrying edge states, and the existence of extended states in a two-dimensional disordered potential. *Phys. Rev. B*, 25(4):2185–2190, Feb 1982.

[15] B. A. Bernevig and S. C. Zhang. Quantum spin Hall effect. *Phys. Rev. Lett.*, 96(10):106802, 2006.

[16] CL Kane and EJ Mele. Quantum spin Hall effect in graphene. *Phys. Rev. Lett.*, 95(22):226801, 2005.

[17] C. L. Kane and E. J. Mele. Z_ {2} Topological Order and the Quantum Spin Hall Effect. *Phys. Rev. Lett.*, 95(14):146802, 2005.

[18] L. Fu and CL Kane. Topological insulators with inversion symmetry. *Phys. Rev. B*, 76(4):45302, 2007.

[19] L. Fu, C. L. Kane, and E. J. Mele. Topological insulators in three dimensions. *Phys. Rev. Lett.*, 98(10):106803, 2007.

[20] JE Moore and L. Balents. Topological invariants of time-reversal-invariant band structures. *Phys. Rev. B*, 75(12):121306, 2007.

[21] B. A. Bernevig, T. L. Hughes, and S. C. Zhang. Quantum spin Hall effect and topological phase transition in HgTe quantum wells. *Science*, 314(5806):1757, 2006.

[22] X.L. Qi, T.L. Hughes, and S.C. Zhang. Topological field theory of time-reversal invariant insulators. *Phys. Rev. B*, 78(19):195424, 2008.

[23] R. Roy. Topological phases and the quantum spin Hall effect in three dimensions. *Phys. Rev. B*, 79(19):195322, 2009.

[24] R. Roy. Characterization of three-dimensional topological insulators by two-dimensional invariants. *New J. Phys.*, 12:065009, 2010.

[25] M.Z. Hasan and C.L. Kane. Colloquium: Topological insulators. *Rev. Mod. Phys.*, 82(4):3045–3067, 2010.

[26] Xiao-Liang Qi and Shou-Cheng Zhang. Topological insulators and superconductors. *Rev. Mod. Phys.*, 83:1057–1110, Oct 2011.

[27] M. König, S. Wiedmann, C. Brüne, A. Roth, H. Buhmann, L. W. Molenkamp, X.-L. Qi, and S.-C. Zhang. Quantum spin hall insulator state in hgte quantum wells. *Science*, 318:766, 2007.

[28] Dong-Xia Qu, Y. S. Hor, Jun Xiong, R. J. Cava, and N. P. Ong. Quantum Oscillations and Hall Anomaly of Surface States in the Topological Insulator Bi2Te3. *Science*, 329(5993):821–824, 2010.

[29] Jun Xiong, Yongkang Luo, YueHaw Khoo, Shuang Jia, R. J. Cava, and N. P. Ong. High-field Shubnikov˘de Haas oscillations in the topological insulator Bi_2Te_2Se. *Phys. Rev. B*, 86:045314, Jul 2012.

[30] P. Roushan, J. Seo, C.V. Parker, YS Hor, D. Hsieh, D. Qian, A. Richardella, MZ Hasan, RJ Cava, and A. Yazdani. Topological surface states protected from backscattering by chiral spin texture. *Nature*, 460(7259):1106–1109, 2009.

[31] D. Hsieh, D. Qian, L. Wray, Y. Xia, YS Hor, RJ Cava, and MZ Hasan. A topological Dirac insulator in a quantum spin Hall phase. *Nature*, 452(7190):970–974, 2008.

[32] D. Hsieh, Y. Xia, D. Qian, L. Wray, J. H. Dil, F. Meier, J. Osterwalder, L. Patthey, J. G. Checkelsky, N. P. Ong, A. V. Fedorov, H. Lin, A. Bansil, D. Grauer, Y. S. Hor, R. J. Cava, and M. Z. Hasan. A tunable topological insulator in the spin helical Dirac transport regime. *Nature*, 460(7259):1101–1105, 2009.

[33] Y. Xia, D. Qian, D. Hsieh, L. Wray, A. Pal, H. Lin, A. Bansil, D. Grauer, Y. S. Hor, R. J. Cava, and M. Z. Hasan. Observation of a large-gap topological-insulator class with a single Dirac cone on the surface. *Nature Physics*, 5(6):398–402, 2009.

[34] Y. L. Chen, J. G. Analytis, J.-H. Chu, Z. K. Liu, S.-K. Mo, X. L. Qi, H. J. Zhang, D. H. Lu, X. Dai, Z. Fang, S. C. Zhang, I. R. Fisher, Z. Hussain, and Z.-X. Shen. Experimental realization of a three-dimensional topological insulator, bi2te3. *Science*, 325(5937):178–181, 2009.

[35] Z. Alpichshev, JG Analytis, JH Chu, IR Fisher, YL Chen, ZX Shen, A. Fang, and A. Kapitulnik. STM Imaging of Electronic Waves on the Surface of Bi_{2} Te_{3}: Topologically Protected Surface States and Hexagonal Warping Effects. *Phys. Rev. Lett.*, 104(1):16401, 2010.

[36] Tong Zhang, Peng Cheng, Xi Chen, Jin-Feng Jia, Xucun Ma, Ke He, Lili Wang, Haijun Zhang, Xi Dai, Zhong Fang, Xincheng Xie, and Qi-Kun Xue. Experimental demonstration of topological surface states protected by time-reversal symmetry. *Phys. Rev. Lett.*, 103:266803, Dec 2009.

[37] S.M. Girvin. The quantum hall effect: Novel excitations and broken symmetries. In A. Comtet, T. Jolicur, S. Ouvry, and F. David, editors, *Aspects topologiques de la physique en basse dimension. Topological aspects of low dimensional systems*, volume 69 of *Les Houches - Ecole dte de Physique Theorique*, pages 53–175. Springer Berlin Heidelberg, 1999.

[38] D. P. Arovas, J. R. Schrieffer, and F. Wilczek. Fractional statistics and the quantum hall effect. *Phys. Rev. Lett.*, 53:722–723, Aug 1984.

[39] N. Read and D. Green. Paired states of fermions in two dimensions with breaking of parity and time-reversal symmetries and the fractional quantum Hall effect. *Phys. Rev. B*, 61(15):10267–10297, 2000.

[40] A.Y. Kitaev. Unpaired Majorana fermions in quantum wires. *Physics-Uspekhi*, 44:131, 2001.

[41] S. Ryu, A.P. Schnyder, A. Furusaki, and A.W.W. Ludwig. Topological insulators and superconductors: tenfold way and dimensional hierarchy. *New J. Phys.*, 12:065010, 2010.

[42] R.B. Laughlin. Anomalous quantum Hall effect: an incompressible quantum fluid with fractionally charged excitations. *Phys. Rev. Lett.*, 50(18):1395–1398, 1983.

[43] F.D.M. Haldane. Fractional quantization of the hall effect: a hierarchy of incompressible quantum fluid states. *Phys. Rev. Lett.*, 51(7):605–608, 1983.

[44] B. I. Halperin. Statistics of quasiparticles and the hierarchy of fractional quantized Hall states. *Phys. Rev. Lett.*, 52(18):1583–1586, 1984.

[45] SM Girvin and T. Jach. Formalism for the quantum hall effect: Hilbert space of analytic functions. *Phys. Rev. B*, 29(10):5617, 1984.

[46] F. D. M. Haldane and E. H. Rezayi. Finite-size studies of the incompressible state of the fractionally quantized hall effect and its excitations. *Phys. Rev. Lett.*, 54:237–240, Jan 1985.

[47] SM Girvin and AH MacDonald. Off-diagonal long-range order, oblique confinement, and the fractional quantum hall effect. *Phys. Rev. Lett.*, 58(12):1252–1255, 1987.

[48] J. K. Jain. Composite-fermion approach for the fractional quantum hall effect. *Phys. Rev. Lett.*, 63:199–202, Jul 1989.

[49] Jainendra K Jain. *Composite fermions*. Cambridge University Press, 2007.

[50] SC Zhang, TH Hansson, and S. Kivelson. Effective-field-theory model for the fractional quantum Hall effect. *Phys. Rev. Lett.*, 62(1):82–85, 1989.

[51] Gregory Moore and Nicholas Read. Nonabelions in the fractional quantum hall effect. *Nucl. Phys. B*, 360(23):362 – 396, 1991.

[52] XG Wen and A. Zee. Classification of Abelian quantum Hall states and matrix formulation of topological fluids. *Phys. Rev. B*, 46(4):2290–2301, 1992.

[53] SL Sondhi, A. Karlhede, SA Kivelson, and EH Rezayi. Skyrmions and the crossover from the integer to fractional quantum hall effect at small zeeman energies. *Phys. Rev. B*, 47(24):16419, 1993.

[54] Ganpathy Murthy and R. Shankar. Hamiltonian theories of the fractional quantum hall effect. *Rev. Mod. Phys.*, 75:1101–1158, Oct 2003.

[55] S. Das Sarma, M. Freedman, and C. Nayak. Topologically protected qubits from a possible non-Abelian fractional quantum Hall state. *Phys. Rev. Lett.*, 94(16):166802, 2005.

[56] S. Das Sarma and Aron Pinczuk. *Perspectives in quantum Hall effects*. Wiley-VCH, 2008.

[57] S.C. Zhang and J. Hu. A four-dimensional generalization of the quantum Hall effect. *Science*, 294(5543):823, 2001.

[58] B. A. Bernevig, C. H. Chern, J. P. Hu, N. Toumbas, and S. C. Zhang. Effective field theory description of the higher dimensional quantum Hall liquid. *Ann. Phys.*, 300(2):185–207, 2002.

[59] H. Elvang and J. Polchinski. The quantum Hall effect on. *Comptes Rendus Physique*, 4(3):405–417, 2003.

[60] M. Fabinger. Higher-dimensional quantum Hall effect in string theory. *JHEP*, 2002:037, 2002.

[61] B. A. Bernevig, J. Hu, N. Toumbas, and S. C. Zhang. Eight-Dimensional Quantum Hall Effect and"Octonions". *Phys. Rev. Lett.*, 91(23):236803, 2003.

[62] K. Hasebe. Hopf Maps, Lowest Landau Level, and Fuzzy Spheres. *Symmetry, Integrability and Geometry: Methods and Applications*, 6(071), 2010.

[63] B.K. Bagchi. *Supersymmetry in quantum and classical mechanics*. Chapman & Hall/CRC, 2001.

[64] J. E. Hirsch. Electrodynamics of spin currents in superconductors. *Annalen der Physik*, 17(6):380–409, 2008.

[65] J. E. Hirsch. Spin meissner effect in superconductors and the origin of the meissner effect. *Europhys. Lett.*, 81:67003, 2008.

[66] J. E. Hirsch. Meissner effect, spin meissner effect and charge expulsion in superconductors. *private communication; Journal of Superconductivity and Novel Magnetism*, 26:2239, 2013.

[67] A. V. Balatsky. Quaternion generalization of the laughlin state and the three dimensional fractional qhe. *arXiv:cond-mat/9205006*, 1992.

[68] S.L. Adler. *Quaternionic quantum mechanics and quantum fields*, volume 88. Oxford University Press, USA, 1995.

[69] Yi Li, Shou-Cheng Zhang, and Congjun Wu. Topological insulators with su (2) landau levels. *arXiv preprint arXiv:1208.1562*, 2012.

[70] A. Sudbery. Quaternionic analysis. *Math. Proc. Cambridge Philos. Soc*, 85(2):199–224, 1979.

[71] N. Gemelke, E. Sarajlic, and S. Chu. Rotating few-body atomic systems in the fractional quantum hall regime. *arXiv preprint arXiv:1007.2677*, 2010.

[72] Y. J. Lin, K. Jiménez-García, and I. B. Spielman. Spin-orbit-coupled bose-einstein condensates. *Nature*, 471(7336):83–86, 2011.

[73] Jean Dalibard, Fabrice Gerbier, Gediminas Juzeliūnas, and Patrik Öhberg. *Colloquium* : Artificial gauge potentials for neutral atoms. *Rev. Mod. Phys.*, 83:1523–1543, Nov 2011.

[74] X. Zhou, Y. Li, and C. Wu. in preparation.

[75] S. C. Zhang. private communication.

[76] X.L. Qi and S.C. Zhang. The quantum spin Hall effect and topological insulators. *Phys. Today*, 63(1):33, 2010.

[77] H. Zhang, C.X. Liu, X.L. Qi, X. Dai, Z. Fang, and S.C. Zhang. Topological insulators in Bi2Se3, Bi2Te3 and Sb2Te3 with a single Dirac cone on the surface. *Nature Phys.*, 5(6):438–442, 2009.

[78] X.L. Qi, R. Li, J. Zang, and S.C. Zhang. Inducing a magnetic monopole with topological surface states. *Science*, 323(5918):1184, 2009.

[79] A. Kitaev. Periodic table for topological insulators and superconductors. In *American Institute of Physics Conference Series*, volume 1134, pages 22–30, 2009.

[80] D. Karabali and VP Nair. Quantum Hall effect in higher dimensions. *Nucl. Phys. B*, 641(3):533–546, 2002.

[81] J. M. Edge, J. Tworzydlo, and C. W. J. Beenakker. Metallic phase of the quantum Hall effect in four-dimensional space. *Arxiv preprint arXiv:1206.0099*, 2012.

[82] Yi Li and Congjun Wu. High-dimensional topological insulators with quaternionic analytic landau levels. *Phys. Rev. Lett.*, 110:216802, May 2013.

[83] Yi Li, Kenneth Intriligator, Yue Yu, and Congjun Wu. Isotropic landau levels of dirac fermions in high dimensions. *Phys. Rev. B*, 85:085132, Feb 2012.

[84] Yi Li and Congjun Wu. Spin-orbit coupled fermi liquid theory of ultracold magnetic dipolar fermions. *Phys. Rev. B*, 85:205126, May 2012.

[85] R. Jackiw and C. Rebbi. Solitons with fermion number 1/2. *Phys. Rev. D*, 13:3398–3409, Jun 1976.

[86] A.J. Niemi and G.W. Semenoff. Fermion number fractionization in quantum field theory. *Physics Reports*, 135(3):99 – 193, 1986.

[87] E. H. Rezayi and F. D. M. Haldane. Laughlin state on stretched and squeezed cylinders and edge excitations in the quantum Hall efFect. *Phys. Rev. B*, 50:17199, 1994.

[88] M. Zahid Hasan and Joel E. Moore. Three-dimensional topological insulators. *Annual Review of Condensed Matter Physics*, 2(1):55–78, 2011.

[89] KS Novoselov, AK Geim, SV Morozov, D. Jiang, M.I.K.I.V. Grigorieva, SV Dubonos, and AA Firsov. Two-dimensional gas of massless dirac fermions in graphene. *Nature*, 438(7065):197–200, 2005.

[90] Y. B. Zhang, Y. W. Tan, H. L. Stormer, and P. Kim. Experimental observation of the quantum hall effect and berry's phase in graphene. *Nature*, 438(7065):201–204, 2005. Times Cited: 3174.

[91] A. H. Castro Neto, F. Guinea, N. M. R. Peres, K. S. Novoselov, and A. K. Geim. The electronic properties of graphene. *Rev. Mod. Phys.*, 81:109–162, Jan 2009.

[92] A. J. Niemi and G. W. Semenoff. Axial-anomaly-induced fermion fractionization and effective gauge-theory actions in odd-dimensional space-times. *Phys. Rev. Lett.*, 51:2077–2080, Dec 1983.

[93] R. Jackiw. Fractional charge and zero modes for planar systems in a magnetic field. *Phys. Rev. D*, 29:2375–2377, May 1984.

[94] A. N. Redlich. Parity violation and gauge noninvariance of the effective gauge field action in three dimensions. *Phys. Rev. D*, 29:2366–2374, May 1984.

[95] G.W. Semenoff. Condensed-matter simulation of a three-dimensional anomaly. *Phys. Rev. Lett.*, 53(26):2449–2452, 1984.

[96] EI Rashba. Properties of semiconductors with an extremum loop. 1. cyclotron and combinational resonance in a magnetic field perpendicular to the plane of the loop. *Sov. Phys. Solid State*, 2:1109–1122, 1960.

[97] Christian R. Ast, Jürgen Henk, Arthur Ernst, Luca Moreschini, Mihaela C. Falub, Daniela Pacilé, Patrick Bruno, Klaus Kern, and Marco Grioni. Giant spin splitting through surface alloying. *Phys. Rev. Lett.*, 98:186807, May 2007.

[98] Erez Berg, Mark S. Rudner, and Steven A. Kivelson. Electronic liquid crystalline phases in a spin-orbit coupled two-dimensional electron gas. *Phys. Rev. B*, 85:035116, Jan 2012.

[99] Cong-Jun Wu, Mondragon-Shem Ian, and Xiang-Fa Zhou. Unconventional bose-einstein condensations from spin-orbit coupling. *Chinese Physics Letters*, 28(9):097102, 2011.

[100] Tin-Lun Ho and Shizhong Zhang. Bose-einstein condensates with spin-orbit interaction. *Phys. Rev. Lett.*, 107:150403, Oct 2011.

[101] Z. Wang, X.L. Qi, and S.C. Zhang. Equivalent topological invariants of topological insulators. *New J. Phys.*, 12:065007, 2010.

[102] Hui Hu, B. Ramachandhran, Han Pu, and Xia-Ji Liu. Spin-orbit coupled weakly interacting bose-einstein condensates in harmonic traps. *Phys. Rev. Lett.*, 108:010402, Jan 2012.

[103] Sudeep Kumar Ghosh, Jayantha P. Vyasanakere, and Vijay B. Shenoy. Trapped fermions in a synthetic non-abelian gauge field. *Phys. Rev. A*, 84:053629, Nov 2011.

[104] Subhasis Sinha, Rejish Nath, and Luis Santos. Trapped two-dimensional condensates with synthetic spin-orbit coupling. *Phys. Rev. Lett.*, 107:270401, Dec 2011.

[105] Xiang-Fa Zhou, Jing Zhou, and Congjun Wu. Vortex structures of rotating spin-orbit-coupled bose-einstein condensates. *Phys. Rev. A*, 84:063624, Dec 2011.

[106] C. Wu. Orbital Analogue of the Quantum Anomalous Hall Effect in p-Band Systems. *Phys. Rev. Lett.*, 101(18):186807, 2008.

[107] D. Xiao, M.C. Chang, and Q. Niu. Berry phase effects on electronic properties. *Rev. Mod. Phys.*, 82:1959–2007, 2010.

[108] Dung-Hai Lee. Surface states of topological insulators: The dirac fermion in curved two-dimensional spaces. *Phys. Rev. Lett.*, 103:196804, Nov 2009.

[109] V. Parente, P. Lucignano, P. Vitale, A. Tagliacozzo, and F. Guinea. Spin connection and boundary states in a topological insulator. *Phys. Rev. B*, 83:075424, Feb 2011.

[110] G. Juzeliunas, J. Ruseckas, D. L. Campbell, and I. B. Spielman. Engineering dresselhaus spin-orbit coupling for cold atoms in a double tripod configuration. pages 79500M–79500M–7, 2011.

[111] J. Ruseckas, G. Juzeliūnas, P. Öhberg, and M. Fleischhauer. Non-abelian gauge potentials for ultracold atoms with degenerate dark states. *Phys. Rev. Lett.*, 95:010404, Jun 2005.

[112] VP Nair and S. Randjbar-Daemi. Quantum Hall effect on S3, edge states and fuzzy S3/Z2. *Nucl. Phys. B*, 679(3):447–463, 2004.

[113] A. N. Redlich. Gauge noninvariance and parity nonconservation of three-dimensional fermions. *Phys. Rev. Lett.*, 52:18–21, Jan 1984.

[114] Eduardo Fradkin, Elbio Dagotto, and Daniel Boyanovsky. Physical realization of the parity anomaly in condensed matter physics. *Phys. Rev. Lett.*, 57:2967–2970, Dec 1986.

[115] A. J. Heeger, S. Kivelson, J. R. Schrieffer, and W. P. Su. Solitons in conducting polymers. *Rev. Mod. Phys.*, 60:781–850, Jul 1988.

[116] M. O. Goerbig. Electronic properties of graphene in a strong magnetic field. *Rev. Mod. Phys.*, 83:1193–1243, Nov 2011.

[117] M Moshinsky and A Szczepaniak. The dirac oscillator. *Journal of Physics A: Mathematical and General*, 22(17):L817, 1989.

[118] J. Bentez, R. P. Martnez y Romero, H. N. Núez-Yépez, and A. L. Salas-Brito. Solution and hidden supersymmetry of a dirac oscillator. *Phys. Rev. Lett.*, 64:1643–1645, Apr 1990.

[119] N. Levy, S. A. Burke, K. L. Meaker, M. Panlasigui, A. Zettl, F. Guinea, A. H. Castro Neto, and M. F. Crommie. Strain-induced pseudomagnetic fields greater than 300 tesla in graphene nanobubbles. *Science*, 329(5991):544–547, 2010.

[120] Morton Hamermesh. *Group theory and its application to physical problems*. Courier Dover Publications, 1962.

[121] S. Ospelkaus, K.K. Ni, MHG de Miranda, B. Neyenhuis, D. Wang, S. Kotochigova, PS Julienne, DS Jin, and J. Ye. Ultracold polar molecules near quantum degeneracy. *arXiv:0811.4618*, 2008.

[122] K.K. Ni, S. Ospelkaus, MHG De Miranda, A. Pe'er, B. Neyenhuis, JJ Zirbel, S. Kotochigova, PS Julienne, DS Jin, and J. Ye. A high phase-space-density gas of polar molecules. *Science*, 322(5899):231, 2008.

[123] A. Griesmaier, J. Werner, S. Hensler, J. Stuhler, and T. Pfau. Bose-einstein condensation of chromium. *Phys. Rev. Lett.*, 94(16):160401, 2005.

[124] JJ McClelland and JL Hanssen. Laser cooling without repumping: a magneto-optical trap for erbium atoms. *Phys. Rev. Lett.*, 96(14):143005, 2006.

[125] M. Lu, S.H. Youn, and B.L. Lev. Trapping ultracold dysprosium: a highly magnetic gas for dipolar physics. *Phys. Rev. Lett.*, 104(6):63001, 2010.

[126] Seo Ho Youn, Mingwu Lu, Ushnish Ray, and Benjamin L. Lev. Dysprosium magneto-optical traps. *Phys. Rev. A*, 82:043425, Oct 2010.

[127] K. Aikawa, A. Frisch, M. Mark, S. Baier, A. Rietzler, R. Grimm, and F. Ferlaino. Bose-einstein condensation of erbium. *Phys. Rev. Lett.*, 108:210401, May 2012.

[128] T. Koch, T. Lahaye, J. Metz, B. Fröhlich, A. Griesmaier, and T. Pfau. Stabilization of a purely dipolar quantum gas against collapse. *Nat. Phys.*, 4(3):218–222, 2008.

[129] T. Lahaye, C. Menotti, L. Santos, M. Lewenstein, and T. Pfau. The physics of dipolar bosonic quantum gases. *Rep. Prog. Phys.*, 72:126401, 2009.

[130] T. Lahaye, J. Metz, T. Koch, B. Fröhlich, A. Griesmaier, and T. Pfau. A purely dipolar quantum gas. In *21st International Conference on Atomic Physics*, page 160. World Scientific Pub Co Inc, 2009.

[131] C. Menotti, M. Lewenstein, T. Lahaye, and T. Pfau. Dipolar interaction in ultra-cold atomic gases. In *Dynamics and Thermodynamics of Systems with Long Range Interactions: Theory and Experiments*, volume 970, pages 332–361, 2008.

[132] T. Sogo, L. He, T. Miyakawa, S. Yi, H. Lu, and H. Pu. Dynamical properties of dipolar fermi gases. *New J. Phys.*, 11:055017, 2009.

[133] T. Miyakawa, T. Sogo, and H. Pu. Phase-space deformation of a trapped dipolar fermi gas. *Phys. Rev. A*, 77(6):061603, 2008.

[134] B.M. Fregoso and E. Fradkin. Ferronematic ground state of the dilute dipolar fermi gas. *Phys. Rev. Lett.*, 103(20):205301, 2009.

[135] Shai Ronen and John L. Bohn. Zero sound in dipolar fermi gases. *Phys. Rev. A*, 81:033601, Mar 2010.

[136] C.K. Chan, C. Wu, W.C. Lee, and S.D. Sarma. Anisotropic-fermi-liquid theory of ultracold fermionic polar molecules: Landau parameters and collective modes. *Phys. Rev. A*, 81(2):023602, 2010.

[137] C. Lin, E. Zhao, and W.V. Liu. Liquid crystal phases of ultracold dipolar fermions on a lattice. *Phys. Rev. B*, 81(4):045115, 2010.

[138] M. A. Baranov, M. S. Mar'enko, Val. S. Rychkov, and G. V. Shlyapnikov. Superfluid pairing in a polarized dipolar fermi gas. *Phys. Rev. A*, 66:013606, Jul 2002.

[139] MA Baranov, Ł. Dobrek, and M. Lewenstein. Superfluidity of trapped dipolar fermi gases. *Phys. Rev. Lett.*, 92(25):250403, 2004.

[140] M.A. Baranov. Theoretical progress in many-body physics with ultracold dipolar gases. *Physics Reports*, 464(3):71–111, 2008.

[141] L. You and M. Marinescu. Prospects for p-wave paired bardeen-cooper-schrieffer states of fermionic atoms. *Phys. Rev. A*, 60(3):2324, 1999.

[142] G.M. Bruun and E. Taylor. Quantum phases of a two-dimensional dipolar fermi gas. *Phys. Rev. Lett.*, 101(24):245301, 2008.

[143] J. Levinsen, N. R. Cooper, and G. V. Shlyapnikov. Topological $p_x + ip_y$ superfluid phase of fermionic polar molecules. *Phys. Rev. A*, 84:013603, Jul 2011.

[144] Andrew C. Potter, Erez Berg, Daw-Wei Wang, Bertrand I. Halperin, and Eugene Demler. Superfluidity and dimerization in a multilayered system of fermionic polar molecules. *Phys. Rev. Lett.*, 105:220406, Nov 2010.

[145] Roman M. Lutchyn, Enrico Rossi, and S. Das Sarma. Spontaneous interlayer superfluidity in bilayer systems of cold polar molecules. *Phys. Rev. A*, 82:061604, Dec 2010.

[146] KV Samokhin and MS Mar'Enko. Nonuniform mixed-parity superfluid state in fermi gases. *Phys. Rev. Lett.*, 97(19):197003, 2006.

[147] C. Wu and JE Hirsch. Mixed triplet and singlet pairing in ultracold multicomponent fermion systems with dipolar interactions. *Phys. Rev. B*, 81(2):020508, 2010.

[148] T. Shi, J.N. Zhang, C.P. Sun, and S. Yi. Singlet and triplet bcs pairs in a gas of two-species fermionic polar molecules. *arXiv: 0910.4051*, 2009.

[149] B. Kain and H.Y. Ling. Singlet and triplet superfluid competition in a mixture of two-component fermi and one-component dipolar bose gases. *Phys. Rev. A*, 83(6):061603, 2011.

[150] B.M. Fregoso and E. Fradkin. Unconventional magnetism in imbalanced fermi systems with magnetic dipolar interactions. *Phys. Rev. B*, 81(21):214443, 2010.

[151] B.M. Fregoso, K. Sun, E. Fradkin, and B.L. Lev. Biaxial nematic phases in ultracold dipolar fermi gases. *New J. Phys.*, 11:103003, 2009.

[152] PW Anderson and P. Morel. Generalized bardeen-cooper-schrieffer states and the proposed low-temperature phase of liquid he^{3}. *Phys. Rev.*, 123(6):1911, 1961.

[153] R. Balian and NR Werthamer. Superconductivity with pairs in a relative p wave. *Phys. Rev.*, 131(4):1553, 1963.

[154] WF Brinkman, JW Serene, and PW Anderson. Spin-fluctuation stabilization of anisotropic superfluid states. *Phys. Rev. A*, 10(6):2386, 1974.

[155] Anthony J. Leggett. A theoretical description of the new phases of liquid ^{3}He. *Rev. Mod. Phys.*, 47:331–414, Apr 1975.

[156] Tetsuo OhMi and Kazushige MaChiDa. Bose-einstein condensation with internal degrees of freedom in alkali atom gases. *Journal of the Physical Society of Japan*, 67(6), 1998.

[157] T.L. Ho. Spinor bose condensates in optical traps. *Phys. Rev. Lett.*, 81(4):742–745, 1998.

[158] F. Zhou. Quantum spin nematic states in bose einstein condensates. *Int. J. Mod. Phys. B*, 17:2643–2698, 2003.

[159] E. Demler and F. Zhou. Spinor bosonic atoms in optical lattices: symmetry breaking and fractionalization. *Phys. Rev. Lett.*, 88(16):163001, 2002.

[160] M. Cheng, K. Sun, V. Galitski, and S.D. Sarma. Stable topological superconductivity in a family of two-dimensional fermion models. *Phys. Rev. B*, 81(2):024504, 2010.

[161] Mingwu Lu, Nathaniel Q. Burdick, and Benjamin L. Lev. Quantum degenerate dipolar fermi gas. *Phys. Rev. Lett.*, 108:215301, May 2012.

[162] Amodsen Chotia, Brian Neyenhuis, Steven A. Moses, Bo Yan, Jacob P. Covey, Michael Foss-Feig, Ana Maria Rey, Deborah S. Jin, and Jun Ye. Long-lived dipolar molecules and feshbach molecules in a 3d optical lattice. *Phys. Rev. Lett.*, 108:080405, Feb 2012.

[163] Kai Sun, Congjun Wu, and S. Das Sarma. Spontaneous inhomogeneous phases in ultracold dipolar fermi gases. *Phys. Rev. B*, 82:075105, Aug 2010.

[164] Yasuhiro Yamaguchi, Takaaki Sogo, Toru Ito, and Takahiko Miyakawa. Density-wave instability in a two-dimensional dipolar fermi gas. *Phys. Rev. A*, 82:013643, Jul 2010.

[165] Yi Li and Congjun Wu. The j-triplet cooper pairing with magnetic dipolar interactions. *Scientific reports*, 2, 2012.

[166] Chi-Ming Chang, Wei-Chao Shen, Chen-Yen Lai, Pochung Chen, and Daw-Wei Wang. Interaction-induced first-order correlation between spatially separated one-dimensional dipolar fermions. *Phys. Rev. A*, 79:053630, May 2009.

[167] J. Zhang and T.L. Ho. Spontaneous vortex lattices in quasi 2d dipolar spinor condensates. *J. Low Temp. Phys.*, pages 1–9, 2010.

[168] Y-J Lin, Rob L Compton, K Jimenez-Garcia, James V Porto, and Ian B Spielman. Synthetic magnetic fields for ultracold neutral atoms. *Nature*, 462(7273):628–632, 2009.

[169] Mingwu Lu, Nathaniel Q. Burdick, Seo Ho Youn, and Benjamin L. Lev. Strongly dipolar bose-einstein condensate of dysprosium. *Phys. Rev. Lett.*, 107:190401, Oct 2011.

[170] Jorge Quintanilla, Sam T. Carr, and Joseph J. Betouras. Metanematic, smectic, and crystalline phases of dipolar fermions in an optical lattice. *Phys. Rev. A*, 79:031601, Mar 2009.

[171] John W Negele and Henri Orland. *Quantum many-particle systems*, volume 200. Addison-Wesley New York, 1988.

[172] T. Sogo, M. Urban, P. Schuck, and T. Miyakawa. Spontaneous generation of spin-orbit coupling in magnetic dipolar fermi gases. *Phys. Rev. A*, 85:031601, Mar 2012.

[173] I Ja Pomeranchuk. On the stability of a fermi liquid. *Zh. Eksp. Teor. Fiz*, 35:524, 1958.

[174] Vadim Oganesyan, Steven A. Kivelson, and Eduardo Fradkin. Quantum theory of a nematic fermi fluid. *Phys. Rev. B*, 64:195109, Oct 2001.

[175] Markus Garst and Andrey V. Chubukov. Electron self-energy near a nematic quantum critical point. *Phys. Rev. B*, 81:235105, Jun 2010.

[176] Max A. Metlitski and Subir Sachdev. Quantum phase transitions of metals in two spatial dimensions. i. ising-nematic order. *Phys. Rev. B*, 82:075127, Aug 2010.

[177] P. Woelfle and A. Rosch. Fermi liquid near a quantum critical point. *Journal of Low Temperature Physics*, 147(3-4):165–177, 2007.

[178] C. A. Lamas, D. C. Cabra, and N. Grandi. Generalized pomeranchuk instabilities in graphene. *Phys. Rev. B*, 80:075108, Aug 2009.

[179] C. A. LAMAS, D. C. CABRA, and N. E. GRANDI. Pomeranchuk instabilities in multicomponent lattice systems at finite temperature. *International Journal of Modern Physics B*, 25(27):3539–3554, 2011.

[180] C. Wu and S.C. Zhang. Dynamic Generation of Spin-Orbit Coupling. *Phys. Rev. Lett.*, 93(3):36403, 2004.

[181] Congjun Wu, Kai Sun, Eduardo Fradkin, and Shou-Cheng Zhang. Fermi liquid instabilities in the spin channel. *Phys. Rev. B*, 75:115103, Mar 2007.